



Topological Modifications Of Graphene Under Periodic Kicking

Master Thesis In Physics

Anurag Pallaprolu
2012B5A3405P

December 6, 2016

Advisors: Dr. Tapomoy G. Sarkar
Department of Physics, BITS Pilani

Abstract

The present thesis deals with the quantum mechanical study of Graphene when subjected to "single" and "double kicking". These terms refer to the special kind of perturbations that are applied to the "unkicked" Graphene Hamiltonian. The idea stems from the paper [AGA], in which the band structures of the singly kicked Graphene Hamiltonian are studied. However, the approach to study kicked Graphene taken in this work is different and is topological in nature.

Important ideas are taken from Floquet Theory [SHA] which reduce the seemingly complicated *periodic* kicked Hamiltonian to a *time independent* stroboscopic one in momentum space. In doing so one can compare this stroboscopic Hamiltonian to that of a standard two state system such as the spin half particle in a magnetic field example. Once this comparison is done it is only a matter of analogy that leads to the computation of the Berry curvature tensor which brings the topological nature of Graphene in the spotlight. An analytic expression for the mass term and the curvature tensor are derived for the singly kicked case and an approximate expression for the mass term is derived for the doubly kicked one. These expressions are verified using computer assisted proving with Mathematica and important phase transitions are noted.

The material in the thesis is divided into five sections:

1 A Quick Introduction To Graphene

2 Topological Interlude and The Berry Curvature

3 Singly Kicked Graphene

4 Doubly Kicked Graphene

5 Appendices on the Quantum Hall Effect, FEM methods for Graphene and Mathematica notebooks for the simulations.

Acknowledgements

I would like to thank Dr. Tapomoy Sarkar for providing me with this opportunity to do research on an exciting topic in current day physics. I would like to thank Rajath Shashidhara for his support throughout the duration of the thesis and Tridev Mishra for his excellent analytic calculations, without which this work would have no meaning. I would like to thank my friends at BITS Pilani (a special shout-out to Aarzoo Sharma) for taking care of me. Finally, I would like to thank my parents for being supportive throughout my journey in college.

A. Pallaprolu
Pilani, Rajasthan

DECLARATION

I, Anurag Pallaprolu, 2012B5A3405P, declare that this thesis titled, "Topological Modifications Of Graphene Under Periodic Kicking", and the work presented in it is my original work. I affirm that all references are clearly attributed and any collaboration with others has been duly acknowledged.

(Signature)

Date: 6th December, 2016

CERTIFICATE

This is to certify that the thesis titled, "Topological Modifications Of Graphene Under Periodic Kicking", and submitted by Anurag Pallaprolu, 2012B5A3405P, in partial fulfillment of the requirements of BITS F421T embodies the work done by him under my supervision.

(Signature of Supervisor)

Dr. Tapomoy G. Sarkar
Department of Physics,
Birla Institute of Technology and Science, Pilani,

Date: 6th December, 2016

Contents

Contents	v
List of Figures	vi
1 Graphene	1
1.1 The Structure	1
1.2 The Tight Binding Approximation	4
1.3 The Band Structure	6
2 The Machinery	9
2.1 The Berry Phase	9
2.2 Topology	12
2.3 Two Level System	21
2.4 Floquet Theory	23
3 Singly Kicked Graphene	27
3.1 Analysis	27
3.2 More Analysis	32
3.3 Simulation and Computer Assisted Proof	36
4 Doubly Kicked Graphene	45
4.1 Clarifications	45
4.2 Analysis	47
4.3 Simulation and Computer Assisted Proof	50
5 Epilogue	67
A Analytic derivation of the Singly Kicked Berry Field	69
B The Hall Effect	73
B.1 Classical Hall Effect	73

B.2	Quantum Hall Effect	75
B.2.1	Introduction	75
B.2.2	The Landau Problem (Landau Gauge)	76
B.2.3	The Landau Problem (Symmetric Gauge)	79
B.2.4	The Landau Problem (Center Of Mass Coordinates)	81
B.3	The Phenomenon	83
B.3.1	Spectral Flow	83
B.3.2	Conduction	84
B.3.3	Conduction Revisited	86
B.4	The Landau Problem in Graphene with an Electric Field	87
B.4.1	Mathematical Solution	87
B.4.2	The Finite Element Method	96
C	Mathematica Notebooks	113
Bibliography		123

List of Figures

1.1	Honeycomb lattice of Graphene. Taken from [7]	2
1.2	Single hexagonal cell. Taken from [LEG]	3
1.3	First Brillouin Zone Γ . Taken from [LEG]	4
1.4	Nearest neighbor hopping of the electron cloud on the linear lattice. Taken from [9]	5
1.5	Band Structure : View 1. Not To Scale	7
1.6	Band Structure : View 2. Not To Scale	8
2.1	The infinitesimal triangle considered by Mukunda and Simon . .	16
2.2	The curvilinear triangle considered by A. M. Legendre	19
3.1	γT is taken to as 1. Purely y-kicking. This is a semi-Dirac dispersion. Refer to Agarwala et al. for discussion.	30
3.2	Purely x-kicking. Notice the dispersionless lines. Refer to Agarwala et al. for discussion.	31

3.3 Purely z-kicking. Probably the only kicking which retains the unkicked Graphene band structure. Notice that the central peak becomes more prominent.	32
3.4 The Berry field versus the magnitude of the wave-vector. Δ is taken to be 2. Not to scale.	36
3.5 The Berry field over the square area of $(-6\pi, 6\pi) \times (-6\pi, 6\pi)$ and $\alpha_z = 5\sqrt{3}$. γT is assumed to be 1. Notice the three prominent peaks and the three prominent valleys. Compare this with Fig 3.7.	37
3.6 The top view of the Berry field for the same square area in the FBZ as Fig 3.5 and $\alpha_z = -5\sqrt{3}$. The hexagonal shape of the FBZ is clearly visible here. It is also clear that the only interesting features of the Berry field happen at the Dirac points, and they look somewhat Lorentzian.	38
3.7 The Berry field for the same initial parameters as that of Fig. 3.6 but $\alpha_z = -5\sqrt{3}$. According to theoretical calculations because the mass term and hence the Berry field depends on α_z as a sinusoid, it should definitely behave like an odd function. And it clearly does. The hills have become the valleys and vice versa. This is a typical topological insulator-like transition with the point of transition being the origin.	39
3.8 The variation of the Chern number with α_z near the Dirac points as computed by Mathematica. Figure 3.9 gives a closer look at the structure of this function.	40
3.9 A closer look at Figure 3.8. Notice the irregularities. These are due to the power series approximations that Mathematica makes to simplify symbolic math.	40
3.10 Plot of the function $-f(\alpha_z)$	41
3.11 The machine computed Berry tensor at the point $(1, 1)$ in the Brillouin Zone.	41
3.12 The analytically computed Berry tensor field at the point $(1, 1)$ in the Brillouin Zone. Note the scale shift but the retention of the structure.	42
3.13 Comparison of Figures 3.11 and 3.12. The scale shift is much more apparent here. The zeros however coincide, not surprisingly at multiples of π	42
3.14 The machine computed Berry tensor at the point $(2, 2)$ in the Brillouin Zone.	43
3.15 Comparison of the machine computed function and the analytic expression at $(2, 2)$. The plots are much more similar in this case.	43
3.16 The "near Dirac point" Berry field computed from the analytic expression. Notice that the expression actually diverges and Mathematica cuts it off for the sake of representation.	44

LIST OF FIGURES

3.17	The "near Dirac point" Berry field computed by the machine. Notice that the expression <i>converges</i> instead and this is mostly due to the power series approximations.	44
4.1	Singly kicked system. The arrows represent Dirac delta spikes normalized to $\bar{\alpha} \cdot \bar{\sigma}$	45
4.2	Doubly kicked system. The arrows represent Dirac delta spikes normalized to $\bar{\alpha}_1 \cdot \bar{\sigma}$ and $\bar{\alpha}_2 \cdot \bar{\sigma}$	46
4.3	The anomalous case of double kicking no longer being periodic of $\delta t > \frac{T}{2}$. Note that the first cycle has a kick, gap, kick. The second cycle has kick, small gap, kick, large gap, kick. This is unlike Figure 4.2 where it was truly periodic.	46
4.4	The Mathematica code snippet from the file doubly-kicked-1.nb provided in the appendices. Note: α_z^2 is not the square of α_z . . .	49
4.5	The band structure for purely doubly z-kicked Graphene for $\alpha_z^2 = 2\sqrt{3}$	50
4.6	The band structure for purely doubly z-kicked Graphene for $\alpha_z^2 = 10\sqrt{3}$. Note the shift in the scale and the fact that the curvature becomes more prominent.	51
4.7	The upper half plane band structures for $\alpha_z^2 = 2\sqrt{3}$ in yellow, $\alpha_z^2 = 3\sqrt{3}$ in blue and $\alpha_z^2 = 4\sqrt{3}$ in red. The band comes close to the zero plane and then moves away.	51
4.8	The upper half plane band structures for $\alpha_z^2 = 4\sqrt{3}$ in yellow, $\alpha_z^2 = 5\sqrt{3}$ in blue and $\alpha_z^2 = 6\sqrt{3}$ in green. The bands show reverse polarity before coming closer to the zero plane again. . .	52
4.9	The Berry field for the purely doubly z-kicked Graphene when $\alpha_z^2 = \sqrt{3}$. This was taken as the base case for further comparisons. Note that the Lorentzian nature of the Dirac cones is very stark. Just as a reminder, the FWHM of the Lorentzian is a rule-of-thumb indicator of the band gap.	52
4.10	The Berry field for the purely doubly z-kicked Graphene when $\alpha_z^2 = 2\sqrt{3}$. The peaks and the valleys become smoother and the Lorentzian approximation turns out to be almost exact. So far there was no phase transition related to the Berry field flipping was noted.	53
4.11	The Berry field for the purely doubly z-kicked Graphene when $\alpha_z^2 = 2.6\sqrt{3}$. The peaks and the valleys become sharp and distinct Dirac spikes start forming around the FBZ. This also implies the band gap lowering, refer Figure 4.7.	54
4.12	The Berry field for the purely doubly z-kicked Graphene when $\alpha_z^2 = 2.7\sqrt{3}$. The peaks and the valleys become wide and almost rectangular. This is probably the limit of the machine precision and it shows an incoming phase flip point.	55

4.13 The Berry field for the purely doubly z-kicked Graphene when $\alpha_z^2 = 2.9\sqrt{3}$. The peaks and the valleys surprisingly become smooth once again. An initial naive guess would be that we already passed the phase transition point but the Berry field has hardly flipped.	56
4.14 The Berry field for the purely doubly z-kicked Graphene when $\alpha_z^2 = 3\sqrt{3}$. The transition has occurred! The peaks and valleys have flipped completely.	57
4.15 The Berry field for the purely doubly z-kicked Graphene when $\alpha_z^2 = 5\sqrt{3}$. Another transition has occurred! The peaks and valleys have flipped once again. Notice that this is similar to Figure 4.9 and the Lorentzian Dirac cones have resurfaced.	58
4.16 The Berry field for the purely doubly z-kicked Graphene when $\alpha_z^2 = 10\sqrt{3}$. This is a flip away from the previous image and thus the doubly kicked system has gone through another topological transition.	59
4.17 The variation of the mass term with δt when $\alpha_z^2 = 2\sqrt{3}$ as computed by the machine. Notice that it decreases for increasing δt but saturates at a value. It is to be seen as to how well this trend performs with the analytic expression stated in the text.	60
4.18 The variation of the mass term with δt when $\alpha_z^2 = 2\sqrt{3}$ as computed by the approximate analytic expression. Notice that it decreases for increasing δt but saturates at a different value than the machine, probably due to the same scaling issue encountered in singly kicked system. However it has remarkably the same behavior as the machine computed result.	61
4.19 The variation of the mass term with δt when $\alpha_z^2 = 3\sqrt{3}$ as computed by the machine. Notice that it increases for increasing δt but saturates at a value. The transition has occurred signified by the change in the trend.	62
4.20 The variation of the mass term with δt when $\alpha_z^2 = 3\sqrt{3}$ as computed by the approximate analytic expression. Notice that it increases monotonically but saturates at a different value yet again. The transition has been verified by this.	63
4.21 The variation of the mass term with δt when $\alpha_z^2 = 5\sqrt{3}$ as computed by the machine. Notice that it decreases once again for increasing δt but saturates at a value. The transition has occurred signified by the change in the trend once again.	64
4.22 The variation of the mass term with δt when $\alpha_z^2 = 5\sqrt{3}$ as computed by the approximate analytic expression. Notice that it decreases monotonically. The transition has been verified yet again by this.	65

LIST OF FIGURES

Chapter 1

Graphene

In this preliminary section, I discuss the solid state aspects of Graphene and I derive the Graphene Hamiltonian in k-space from the tight binding approximation on the hexagonal lattice. This section is by no means a complete primer on the nature of Graphene and references such as [NET] and [GEI] are probably better standard general references. Most of the material in this section is adapted from the lectures due to Anthony Leggett at the University of Waterloo in the Summer of 2010 [LEG].

1.1 The Structure

Graphene is an allotrope of carbon and belongs to the family of allotropes formed due to the four valence electron freedom of carbon. Other examples of allotropes include fullerenes, nanotubes, Diamond and finally Graphite, which is nothing but many sheets of Graphene stacked one on top of the other. Graphene is the most primitive allotrope of carbon and consists of sp^2 hybridized carbon atoms in a plane, much like Benzene but with the hydrogens replaced by covalently bonded carbon atoms. One can, in principle, construct carbon nanotubes and fullerenes by stitching a Graphene sheet cylindrically and spherically respectively (the subject of nanotube physics will not be discussed in this section or the thesis, and the interested reader is referred to [LEO] for an excellent introduction).

Until the year 2004, Graphene was only a subject of theoretical interest and the material was considered to be unstable at temperatures above 0 K primarily due to its high amount of "two dimensionality" which prevents it from existing stably in accordance with the Mermin-Wagner-Coleman theorem of field theory (see [COL], [HOH], [MER]). It was in 2004 that Andre K. Geim and Konstantin Novoselov made the breakthrough discovery and extracted the very first sample of monolayer Graphene and studied it using optical

1. GRAPHENE

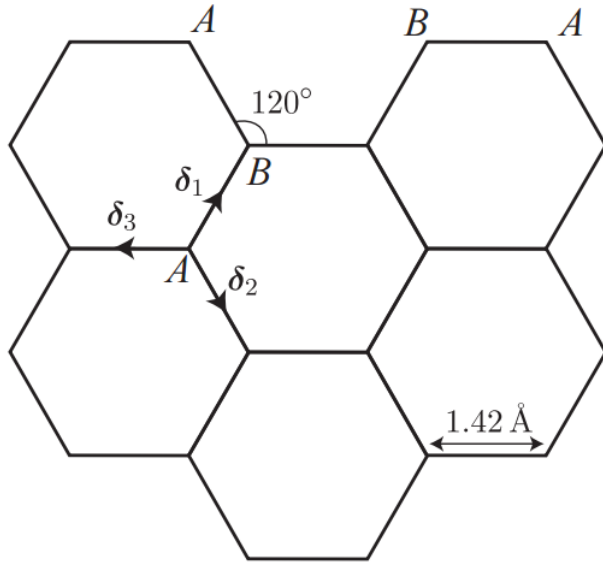


Figure 1.1: Honeycomb lattice of Graphene. Taken from [7]

microscopy on a silicon substrate at the University of Manchester. This led to a flurry of research (according to the statistics in [LEG], the number of papers on Graphene in the last decade is over 3000) and Graphene became the central figure in condensed matter research.

In Figure 1.1 we can see the arrangement of the carbon atoms in Graphene in the now well known honeycomb pattern. The solid state analysis of Graphite rather was done first by P. R. Wallace in 1947 [WAL], and the same technique is used to study the properties of Graphene which leads to certain remarkable conclusions. To start from scratch we can see that carbon having four valence orbitals free leads to either of the two arrangements, four sp^3 hybridized orbitals which leads to a very stable structure, notably that of diamond (which therefore is a very good electronic insulator) or three sp^2 hybridized orbitals with one electron left in the π cloud (which projects out of the plane), which leads to Graphene (and hence a semi-metal type behaviour). It has been spectroscopically determined that the nearest neighbor spacing in this honeycomb lattice is 0.14 nm.

It turns out that the honeycomb lattice can be seen as the combination of two inequivalent triangular sublattices labeled A and B respectively in Figure 1.1. The description of the honeycomb lattice can be given by stating

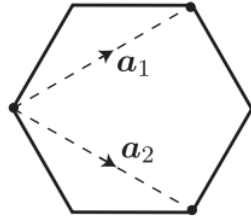


Figure 1.2: Single hexagonal cell. Taken from [LEG]

the three nearest neighbor vectors for either of the two unequal sublattice points, in this case for A labelled as $\delta_1, \delta_2, \delta_3$ given by

$$\delta_1 = \frac{a}{2}(1, \sqrt{3})$$

$$\delta_2 = \frac{a}{2}(1, -\sqrt{3})$$

$$\delta_3 = -a(1, 0)$$

In Figure 1.2, I focus on one single hexagonal cell where it is clear that the two primitive vectors for the translation on the triangular A sublattice are given by

$$\bar{a}_1 = \frac{a}{2}(3, \sqrt{3})$$

$$\bar{a}_2 = \frac{a}{2}(3, -\sqrt{3})$$

Using the idea of the reciprocal lattice, we can construct the equivalent translation vectors in the first Brillouin zone (indicated as FBZ henceforth) using the reciprocal relation $\bar{a}_i \cdot \bar{b}_j = 2\pi\delta_{ij}$ as

$$\bar{b}_1 = \frac{2\pi}{3a}(1, \sqrt{3})$$

$$\bar{b}_2 = \frac{2\pi}{3a}(1, -\sqrt{3})$$

One can in essence repeat the same process for the triangular B sublattice. The complete FBZ of the honeycomb lattice can be seen as the intersection of the two triangular FBZ of A and B sublattices, as shown in Figure 1.3. Just as in the actual lattice, in the FBZ there are two unequal points which have the momentum space representation of

$$\bar{K} = \frac{2\pi}{3a}(1, \frac{1}{\sqrt{3}})$$

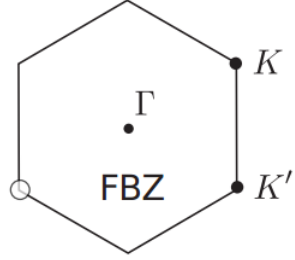


Figure 1.3: First Brillouin Zone Γ . Taken from [LEG]

$$\bar{K}' = \frac{2\pi}{3a} \left(1, -\frac{1}{\sqrt{3}}\right)$$

It is suggested that (see [7]) sometimes taking the Brillouin lattice point marked with the open circle in Figure 1.3 is more useful as a second sublattice point for it is not connected by any visible k space vector and it simplifies calculations related to the tight binding Hamiltonian, which I now turn to.

1.2 The Tight Binding Approximation

The core idea behind the Tight Binding Approximation, called henceforth as TBA is to focus only on the nearest neighbor interactions on the lattice. In order to simplify the discussion I will use the linear chain of atoms as an example lattice. This is borrowed from Richard Feynman's classic text [FEY] and is a nice way to see how band structures arise from the Schrodinger equation. The base assumption of the approximation is the idea that the electron has interaction limited to the nearest neighbor atoms. For the linear lattice, one can write the following series of Schrodinger differential equations, assuming the electron has equal amplitude to move to $|n-1\rangle$ and $|n+1\rangle$.

$$\begin{aligned} i\hbar \frac{dC_{n-1}}{dt} &= E_0 C_{n-1} - AC_{n-2} - AC_n \\ i\hbar \frac{dC_n}{dt} &= E_0 C_n - AC_{n-1} - AC_{n+1} \\ i\hbar \frac{dC_{n+1}}{dt} &= E_0 C_{n+1} - AC_n - AC_{n+2} \end{aligned}$$

These can be solved, either iteratively (requires a computer), or using an *ansatz* solution for one of the three differential equations. The latter approach leads us to writing

$$C_n = e^{i(kx_n - \frac{Et}{\hbar})}$$

1.2. The Tight Binding Approximation

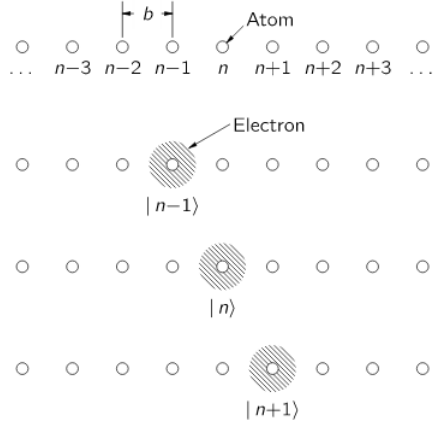


Figure 1.4: Nearest neighbor hopping of the electron cloud on the linear lattice. Taken from [9]

Although these approximations look naive, for a first guess, this is the best a human could do. Now, plugging this into the second of the three I've stated before, it is easy to see that the dispersion relation turns out to be sinusoidal and, to be a bit more precise, of the form

$$E(k) = E_0 - 2A \cos(kb)$$

This can be easily verified with the fact that $x_{n+1} = x_n + b$ and $x_{n-1} = x_n - b$. Extending this argument to the honeycomb lattice of Graphene, it becomes clear that the electron cloud which "hops" around is just the free π electron available for each sp^2 hybridized carbon atom and thus, using the language of second quantization, the tight binding Hamiltonian can be written down with the following notation. The electron being a spin half Fermion can be labeled with a spin index σ and a lattice index i . For instance, if the p_i electron hops to one atom of the A sublattice with index j from the nearest neighbor atom of the B sublattice, we can write the amplitude for this process as being proportional to the term $a_{i,\sigma}^\dagger b_{j,\sigma}$ assuming that the spin remains the same during the hop. Therefore, it is only a matter of accounting for all possible nearest neighbor hopping processes to get the final tight binding Hamiltonian and this is given by

$$\mathcal{H}_{TB} = -\gamma \sum_{i,j,\sigma} (a_{i,\sigma}^\dagger b_{j,\sigma} + b_{j,\sigma}^\dagger a_{i,\sigma})$$

The parameter γ is the proportionality constant for the process amplitude and is called the hopping constant. It is experimentally verified to be around 2.8eV. A much more useful form of the tight binding Hamiltonian is obtained when one Fourier transforms the position space representation given above into the momentum space operators, or equivalently, we could look at the

1. GRAPHENE

tight binding picture in the FBZ. The latter is easier to understand and writing down the expression is yet again accounting for all possible processes. Let us assume that the electron cloud is on some site i which belongs to some unknown sublattice. There are only three possible ways out for the electron. It does not hop, it hops to the A sublattice in the FBZ or it hops to the B sublattice in the FBZ. If the electron is labeled by the wave vector \bar{k} instead, we can account for all the three ways by writing the first off diagonal term as

$$\mathcal{H}_{TB,1,2} = 1 + e^{i\bar{k}\cdot\bar{K}} + e^{i\bar{k}\cdot\bar{K}'}$$

where \bar{K} and \bar{K}' are defined in the previous section. Since the Hamiltonian must be Hermitian, the other off diagonal term is also fixed. The on diagonal terms turn out to be zero for we do not consider hopping on the same point in the lattice. This fact has significance when we discuss the implications of the band structure. Therefore, writing the tight binding Hamiltonian in the FBZ completely, we have

$$\mathcal{H}_{TB,\bar{k}} = -\gamma \begin{bmatrix} 0 & 1 + e^{i\bar{k}\cdot\bar{K}} + e^{i\bar{k}\cdot\bar{K}'} \\ 1 + e^{-i\bar{k}\cdot\bar{K}} + e^{-i\bar{k}\cdot\bar{K}'} & 0 \end{bmatrix}$$

It turns out that by using the De Moivre expansion for the complex exponential and writing the cosine and sine terms separately for the Hamiltonian above, it can be written neatly in the basis for the Pauli matrices. Thence, we have the following representation of the tight binding Hamiltonian

$$\mathcal{H}_{\bar{k}} = -\gamma(G(\bar{k})\sigma^x - H(\bar{k})\sigma^y)$$

$$G(\bar{k}) = 1 + \cos(\bar{k}\cdot\bar{K}) + \cos(\bar{k}\cdot\bar{K}')$$

$$H(\bar{k}) = \sin(\bar{k}\cdot\bar{K}) + \sin(\bar{k}\cdot\bar{K}')$$

The advantage of writing it in the Pauli basis is that the eigenvalues, and thus the band structure are easy to compute. The eigenvalues are nothing but

$$E(\bar{k}) = \pm\gamma\sqrt{G(\bar{k})^2 + H(\bar{k})^2}$$

1.3 The Band Structure

The knowledge of the Pauli basis representation made the computation of the band structure easier but it need not be the only way to get there if you have a Computer Algebra System available at hand. However, the direct computation of eigenvalues is time consuming as shall be seen in future sections. I have attached the Mathematica notebook `band.nb` in the appendices for reference. The band structure of Graphene looks as follows. The band structure shows a nice quadratic dispersion everywhere except six points (in

1.3. The Band Structure

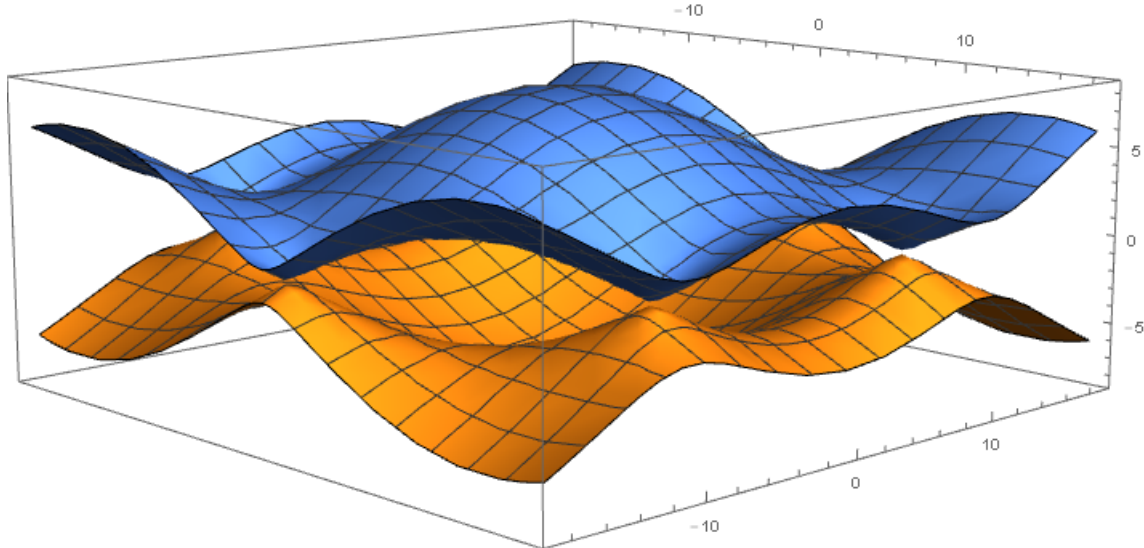


Figure 1.5: Band Structure : View 1. Not To Scale

the figures displayed) where it abruptly goes to zero. These are the points when the conduction and the valence band touch, but only just. This clarifies the semi-metal type behavior of Graphene and these points are called Dirac points. Again, excepting the six points, Graphene behaves like a semiconductor with a well defined band-gap depending on the \vec{k} values chosen. As promised before, if we include a non-zero probability for the electron to hop on the same site, we would essentially be creating a gap between the Dirac points in the conduction and valence bands and this corroborates with the fact that the so called "mass term" is zero in the present Hamiltonian (more on this later).

The band structure in essence describes the dispersion relation of the Fermions in the scenario, that is, the relation between the energy and the wave vector of the quantum mechanical specie. The oddity in the Graphene band structure is that the dispersion relation is linear when near the Dirac points and this leads one to conclude that the electrons, which are known to be mas-

1. GRAPHENE

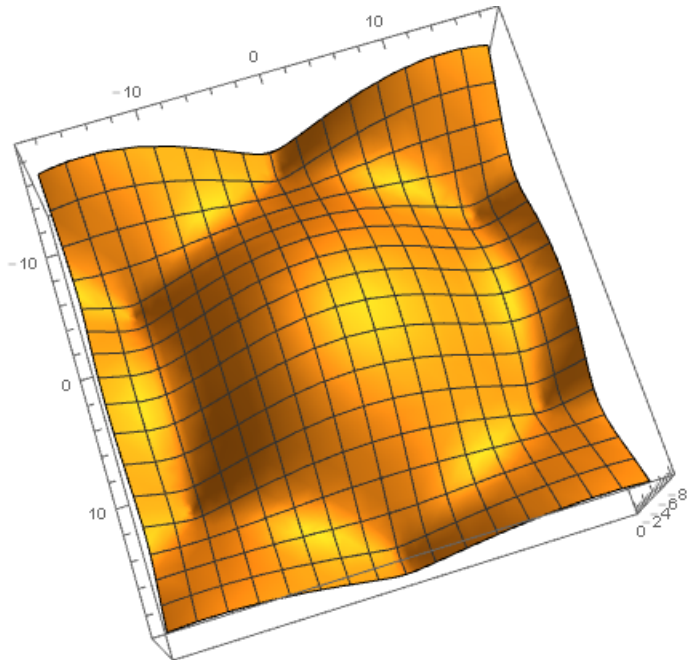


Figure 1.6: Band Structure : View 2. Not To Scale

sive Fermions, seemingly become massless and take the linear dispersion relation at the Dirac points. The reason for calling these points so is because in this neighborhood they obey the linear dispersion picture, that of the massless Fermions obeying the Dirac equation. This does *not* imply that the electrons lose mass, but it can be related to a much more deeper idea about the collective phenomenon of electrons interacting with each other (which we have neglected so far in the study) to create such an effect. I will not digress much into the implications as this is not the subject of the thesis, but I have a suspicion that the Fermion modes form some sort of composite Goldstone modes which lead to the Dirac points and the behavior just described.

With this I conclude the quick introduction to Graphene and its properties and I move on to the qualitative discussion about the Berry Phase and the topology of quantum mechanics, along with some mathematical ideas from Floquet theory which will be sufficient for the exposition of my work.

Chapter 2

The Machinery

With the basics of Graphene out of the way, I will require some machinery which will be useful for analyzing the behavior under the influence of different perturbations. The first of the two topics, Berry Phase, is an independent topic in itself and I borrow a certain ideas from this to establish a qualitative way to observe the phase transitions in singly and doubly kicked Graphene in the upcoming chapters. The section can be skipped by a confident reader.

2.1 The Berry Phase

General references: [WIL], [MUK], [AHA], [TON]

This is like a fast food introduction to calculating what is known as the Geometric Phase or the Berry Phase (to be more pedantic, the Pancharatnam-Berry Phase [BER], [PAN]), and this is by no means the complete description of this exotic effect. A more general (gauge invariant) approach has been developed sequentially by V. Bargmann, Y. Aharonov and J. Anandan [AHA1], and finally a much more complete approach was given by N. Mukunda and R. Simon [SIM]. A chronological introduction to the subject can be found in the collection of papers titled *Geometric Phases In Physics* by Frank Wilczek and Alfred Shapere.

Mathematically, what Michael Berry discovered is known as a holonomy in the world of differential geometry. In essence, we are planning on working out the features of the Hilbert space when a metric is defined on it. That is, we would be able to see effects such as curvature, parallel transport et cetera even in the Hilbert space but the vectors we deal with here are the state vectors of the quantum mechanical system and hence necessary care has to be taken as to what one is ultimately interpreting from this formalism.

2. THE MACHINERY

With the prelude out of the way, let us get straight to the issue. We have a time dependent Hamiltonian $\mathcal{H}(\lambda)$ where λ 's are the *parameters* of the quantum system we are dealing with. These parameters might themselves be time varying or there could be an explicit time dependence, we do not care. Writing the Schrodinger equation for a given configuration $\lambda(t)$ we have

$$i\hbar \frac{\partial |\psi\rangle}{\partial t} = \mathcal{H}(\lambda(t))|\psi\rangle$$

The point here is to remember something from the Adiabatic Theorem, we change the λ s in such a way that the system goes through a cycle and comes back to $\mathcal{H}(\lambda(0))$. For every change we make to the configuration parameters, we have to assign some states $|n(\lambda)\rangle$ such that we have a representation of ψ at every point in the path. But, if we do this slowly enough, then using the adiabatic theorem we can say that we have the following relationship

$$|\psi(t)\rangle = U(t)|n(\lambda)\rangle$$

where U is a time dependent phase factor which does not disturb the probability distribution or the expectation values, thereby keeping the things the same underneath. This we fancily call as the adiabatic ansatz, and then we take the inner product $\langle \psi | \dot{\psi} \rangle$ and see what turns out (the actual idea comes from the standard Rayleigh Schrodinger perturbation theory for a time dependent Hamiltonian where this term is computed (a review of the RS and BW perturbation theory will be given later)). We assume for the sake of discussion that the states $|n\rangle$ are all ground states for a given set of configuration parameters. We also set the ground state energies to zero (these arbitrary choices are made because the result would just have to be shifted by a constant factor to the right hand sides of the equations henceforth, the implications are far more subtle) Taking the inner product, we see that we have the following, from the ansatz

$$\langle \psi | \dot{\psi} \rangle = \dot{U} \tilde{U} + \langle n | \dot{n} \rangle = 0$$

Now, it is a matter of simple convention to solve for U using the above equality as a differential equation. This would essentially give the complete Schrodinger evolution of the situation

$$\begin{aligned} \implies U^* \dot{U} &= - \langle n | \dot{n} \rangle \\ \implies U^* \dot{U} &= - \langle n | \frac{\partial}{\partial \lambda^i} |n\rangle \lambda^i \\ \implies \dot{U} &= - \langle n | \frac{\partial}{\partial \lambda^i} |n\rangle \lambda^i U \end{aligned}$$

2.1. The Berry Phase

$$\implies U(t) = e^{-i \oint_{path} \mathcal{A}_i(\lambda) \lambda^i dt}$$

where $\mathcal{A}_i(\lambda)$ has a geometric significance known as the *connection* on the space, or as it is known colloquially as the *Berry connection*.

$$\mathcal{A}_i(\lambda) = -i \langle n | \frac{\partial}{\partial \lambda_i} | n \rangle$$

So the first step is to understand your parameter space and then compute the Berry connection for the corresponding degree of freedom. Now, there is a reason why the symbol looks like A. It is because the Berry connection on the Hilbert space has properties similar to the four vector potential in electromagnetism. For a more legit reason, one has to go through the derivation of the gauge invariant formalism of the Berry phase to realise that it is simply because both electromagnetism and the Hilbert space of quantum mechanical state vectors share some similar geometric structure. Just as how the electromagnetic four vector potential is gauge invariant under U(1) like transformations, even state vectors have something similar to this.

If you were observant, you would have probably felt a bit uneasy when we set the state vectors to always have a representation which had the basis vectors as some ground state vectors at every point in configuration space. In a more general scenario, let us assume that the basis vectors are ground state vectors but are shifted by a *configuration dependent phase*. Mathematically speaking, we have

$$|n'(\lambda)\rangle = e^{i\omega(\lambda)} |n(\lambda)\rangle$$

With this modification, if we compute the new connection, we will see the following

$$\mathcal{A}'_i = -i \langle n' | \frac{\partial}{\partial \lambda^i} | n' \rangle = \mathcal{A}_i + \frac{\partial \omega}{\partial \lambda^i}$$

Now, the equation for the gauge transformation for the four vector potential by ω is

$$A'_\mu = A_\mu + \frac{\partial \omega}{\partial x^\mu}$$

This is the symmetry we will be exploiting like anything. The Faraday tensor in electromagnetism is the one mathematical quantity from which we can extract almost anything required for a configuration, and we would want to explore what the same tensor in the quantum mechanical space looks like and hence construct a (somewhat gauge invariant) second rank tensor, calling it the *Berry curvature tensor*.

$$\mathcal{F}_{\mu\nu}(\lambda) = \frac{\partial \mathcal{A}_\mu}{\partial \lambda^\nu} - \frac{\partial \mathcal{A}_\nu}{\partial \lambda^\mu}$$

Using n-dimensional Stokes' theorem, we can see the following equality

$$\oint_C \mathcal{A}_i(\lambda) d\lambda^i = \int_S \mathcal{F}_{\mu\nu} dS^{\mu\nu}$$

The quantities can be exactly seen as vectors and tensors, but mathematicians will use fancy language and call them one-forms and two-forms in literature. This is pretty much there is to computing geometric phases. You set up your Hilbert space, compute the Berry curvature tensor and integrate to get the phase component. Therefore, the net Berry phase in a cyclic path c is given by

$$e^{i\gamma} = e^{-i \int_S \mathcal{F}_{\mu\nu} dS^{\mu\nu}}$$

There is however another nagging issue. What if the ground states, whose condition we have dealt with when they vary by a phase, are now degenerate? The issue with the degenerate ground state condition turns out to change the mathematical structure of the connection over the space, and eventually leads to the Berry curvature tensor to have an extra commutator term added to it. For each degree of freedom λ_i , we will now have the connection to be a matrix valued quantity $\mathcal{A}_{\mu\nu}$. The adiabatic hypothesis only assures the pinning of the spectrum in this case, it is unable to tell us which of the degenerate kets it pins on to. With this structure of the connection, one could still salvage some form of gauge invariance and this turns out to be the exact form of Yang-Mills extensions to electromagnetism (non-abelian gauge group) and just as the Faraday tensor is corrected with the commutator in the Yang-Mills case, the Berry tensor is also appended with a similar form. And this leads to the well known concept of *non abelian Hall states* and so on. The Berry phase has a similar form of computation except that one has to account for the commutator by doing path integrals and all that.

In conclusion, if you have a system then you realise that the Hilbert space of the quantum mechanical treatment of the system has some geometric structure and you would like to characterize systems based on the topology of the Hilbert space. This is the most general idea of the Berry phase (and this is not how Michael Berry started out) known as the gauge invariant formalism. How does one go about classifying systems based on the topology? It turns out that the integral of the Berry tensor over a solid angle of the Hilbert space is always an integral multiple of 2π and the integer is known as the *Chern number*. The idea of the Chern number is closely tied to a few mathematical theorems in topology, which we turn to now.

2.2 Topology

It would be prudent to continue the discussion by showing a way to establish a metric on the Hilbert space as one could then use the metric tensor to

compute quantities such as curvatures et cetera using machinery developed in differential geometry (something similar to general relativity). Given a Hilbert space \mathcal{H} and a basis defined $|\psi\rangle$, you can state that any $|\varphi\rangle$ belongs to the equivalence class of $[\alpha, \psi]$ (the brackets are notational and do not define any commutator) if

$$|\varphi\rangle = |\psi\rangle e^{i\alpha}$$

The geometric consequence of this fact is that the invariant which is directly visible is the adjoint (outer) product of the space, that is, all elements of the class $[\alpha, \psi]$ have the same outer product, or equivalently

$$|\varphi\rangle \langle \varphi| = |\psi\rangle \langle \psi|$$

This idea can be encapsulated by defining a projection operator which takes a φ in the space \mathcal{H} and then "projects" it onto the so called *ray space* by taking the outer product. That is, π can be defined as follows

$$\pi(\varphi) \rightarrow \varphi\varphi^\dagger \in \mathcal{R}_0$$

where \mathcal{R} is the ray space, which can be somewhat rigorously defined as follows. Call \mathcal{N}_0 as the subspace of \mathcal{H} which contains all vectors that are normalized to *unity*. Then

$$\mathcal{N}_0/\mathcal{U}(1) \cong \mathcal{R}_0$$

The ray space can be imagined to be a sheet and the equivalence class defines a *bundle* which projects every $|\varphi\rangle$ on it to a point on the sheet characterized by the invariant outer product. For this geometry, one defines what is known as a Fubini-Study metric on the Hilbert space as follows. For any two kets $|\psi_1\rangle$ and $|\psi_2\rangle$, one could define a "well defined distance" (normalization is fixed to unity)

$$ds^2(\psi_1, \psi_2) = 1 - ||\langle \psi_1 | \psi_2 \rangle||^2 = 1 - Tr(\rho_{\psi_1} \rho_{\psi_2})$$

where ρ_ψ is the von Neumann density matrix. It is only a matter of mathematical computation to get the structure of the metric tensor on \mathcal{H} and it is made easier in the density matrix formulation. To make things look more edible, we would start labelling the state kets in the Hilbert space by actual vectors \bar{x} and thus we could remove the ket subscripts on the density operators and write them directly as $\rho(\bar{x})$. The dimension of the vector \bar{x} is derived from the fact that it must lie either on the ray space sheet or on one of the bundles and is constrained by two arguments, the normalization and the projection operator mapping it to a point on the ray space sheet if it lies on one of the bundles. We assume for the sake of discussion that the eigen-spectrum is discrete and countably finite of dimension N . For an arbitrary $|\varphi\rangle$, we have

$$|\varphi\rangle = \sum_n z_n |n\rangle$$

2. THE MACHINERY

and the two conditions lead to

$$\sum_n ||z_n||^2 = 1$$

$$|\varphi><\varphi| = (\sum_n z_n |n>)(\sum_n <n|z_n^*) = \pi(\varphi)$$

Without the constraints, we would expect the total number of *real* degrees of freedom to be $2N$ for every complex ket has two real components. But the two constraints imposed now cut down the total degrees of freedom to $2N - 2$ and this is the dimension of the vector prescription \bar{x} . With this out of the way, we have the ray space sheet essentially containing matrices (outer products) which have bundles hanging out at each point with respect to a given equivalence class and each point in this space is characterized by a $2N - 2$ dimensional vector.

Rewriting the metric for two vectors separated infinitesimally, that is, for two vectors \bar{x} and $\bar{x} + \delta\bar{x}$, we have

$$ds^2(\bar{x}, \bar{x} + \delta\bar{x}) = 1 - Tr(\rho(\bar{x})\rho(\bar{x} + \delta\bar{x})) = 1 - Tr(\rho(\bar{x})[\rho(\bar{x}) + \frac{\partial\rho}{\partial x^a}\delta x^a + \frac{1}{2}\frac{\partial^2\rho}{\partial x^a\partial x^b}\delta x^a\delta x^b + ..])$$

The Taylor expansion is restricted upto the quadratic term in accordance with the field theoretic harmonic paradigm. The following identities for the density matrices will come in handy when expanding the trace for the product

$$\begin{aligned} Tr(\rho^2) &= 1 \\ \implies Tr(\rho \frac{\partial\rho}{\partial x^a}) &= 0 \\ \implies Tr(\frac{\partial\rho}{\partial x^b} \frac{\partial\rho}{\partial x^a}) + Tr(\rho \frac{\partial^2\rho}{\partial x^a\partial x^b}) &= 0 \end{aligned}$$

Expanding the product inside the trace and using the above identities one ends up with a few cancellations and the structure for the space \mathcal{H} surprisingly looks like any Gaussian metric definition (that is, a quadratic Riemannian manifold)

$$ds^2(\bar{x}, \bar{x} + \delta\bar{x}) = \frac{1}{2} \frac{\partial\rho}{\partial x^a} \frac{\partial\rho}{\partial x^b} \delta x^a \delta x^b = g_{ab} \delta x^a \delta x^b$$

where the metric tensor g_{ab} contains the information regarding the curvature of the space \mathcal{H} which is in turn encapsulated by the derivatives of the density matrices with respect to the state vectors.

Differential geometry tells us that there is a definitive procedure to construct both the analogues of the one form (the Berry connection, the vector potential) and the corresponding curvature two form (the Berry curvature tensor,

the Faraday tensor) from the metric tensor and this will not be discussed here (refer standard texts such as [SPI] or [KOB]). The actual extension to computing the curvature two form involves introducing higher dimensional invariants in the Hilbert space. We have already seen the case for two vectors which appears in the Fubini-Study metric, the product of the two outer products, or, equivalently the product of the corresponding density matrices. How does one construct a $\mathcal{U}(1)$ invariant mathematical structure for three vectors? Denoting the *inner* product by the notation (ψ_1, ψ_2) one could construct

$$\mathcal{B}(\psi_1, \psi_2, \psi_3) = (\psi_1, \psi_2)(\psi_2, \psi_3)(\psi_3, \psi_1)$$

And you can see that if the three vectors varied under independent $\mathcal{U}(1)$ transformations, or equivalently the system went through a $\mathcal{U}(1) \times \mathcal{U}(1) \times \mathcal{U}(1)$ transformation, we would have the quantity \mathcal{B} invariant. Structures such as this and the higher order generalizations are known as *Bargmann Invariants* after Valentin Bargmann who worked on these in 1964 [BAR] with reference to the Wigner theorem. The true mathematical nature of the Hilbert space would need a separate document in itself for an explanation, and wonderful references already exist to clarify certain details. It turns out that the so called ray space is actually isomorphic to the *complex projective space* in $N - 1$ dimensions and the Berry connection turns out to be a valid one form in this space and using the generalized Stokes theorem it can be argued that a curvature two form must exist. Added to this is the whole rich mathematics of Kahler manifolds and the Riemann curvature tensor naturally follows with the definition of the Christoffel symbols on the manifold.

One interesting derivation, due to N. Mukunda and R. Simon [MUK], is that of the curvature tensor from the von Neumann density matrix formulation. This is not surprising as we have already derived the metric tensor on the Hilbert space in the same formulation and this is just an upgrade to that computation. The idea is to use the fact that Bargmann invariants have a nice representation using ρ 's. In Figure 2.1 on the next page, I consider an infinitesimal triangle partitioned into two by another vertex labeled as 4. Just as a reminder, I am still working in the Hilbert space and the vertices here are really wave functions and the distances are defined using the metric tensor g_{ab} given by

$$g_{ab} = \frac{1}{2} \text{Tr}(\partial_a \rho \partial_b \rho)$$

Before I proceed into the complete derivation of the curvature two form/tensor, I must emphasize that the Berry phase is the *argument* of the Bargmann invariant. This leads to the additive nature of the invariants and thus one can say in principle that

$$\mathcal{B}(\psi_1, \psi_2, \psi_3) = \mathcal{B}(\psi_1, \psi_2, \psi_4) + \mathcal{B}(\psi_3, \psi_4, \psi_2)$$

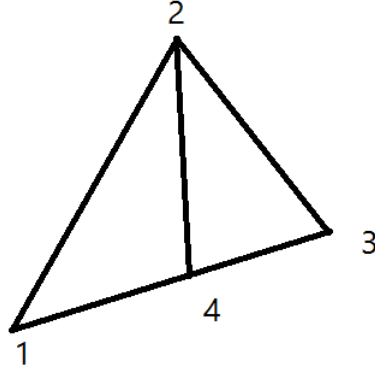


Figure 2.1: The infinitesimal triangle considered by Mukunda and Simon

This fact is essential for inductively computing the Berry phase over a full contour by triangulating the area inside the contour and applying the additivity rule all over it. Thus, it will suffice if I discuss about the curvature tensor on the infinitesimal triangle and then I just call the triangulation and induction routines to generalize it over the larger section. The vertices named 1, 2, and 3 correspond to the wave functions $\psi(x), \psi(x + \delta x_1), \psi(x + \delta x_2)$ respectively where x is the position variable and x_1, x_2 are two arbitrary directions chosen for the sake of discussion. Now the Bargmann invariant for the triangle going clockwise is given by

$$\mathcal{B}(1, 2, 3) = |1\rangle\langle 1|2\rangle\langle 2|3\rangle\langle 3| = \langle 1|2\rangle\langle 2|3\rangle\langle 3|1\rangle = \text{Tr}(\rho(x)\rho(x + \delta x_1)\rho(x + \delta x_2))$$

The invariant for the counterclockwise rotation is given by

$$\mathcal{B}(1, 3, 2) = |1\rangle\langle 1|3\rangle\langle 3|2\rangle\langle 2| = \langle 1|3\rangle\langle 3|2\rangle\langle 2|1\rangle = \text{Tr}(\rho(x)\rho(x + \delta x_2)\rho(x + \delta x_1))$$

I use the fact that the state vectors are all unit modulus and thus one can write the following equality

$$\mathcal{B}(1, 2, 3) = e^{i\Omega_{123}}$$

where Ω_{123} is the Berry phase picked up around the infinitesimal triangle. The anticlockwise Bargmann invariant will similarly equal $e^{i\Omega_{132}}$ and this is $e^{-i\Omega_{123}}$ due to the phase behaving additively as the argument. Thus the ratio of the clockwise and the counterclockwise Bargmann invariants is nothing but

$$\frac{\mathcal{B}(1, 2, 3)}{\mathcal{B}(1, 3, 2)} = e^{2i\Omega_{123}}$$

2.2. Topology

Using the basic Taylor expansion of $e^x \approx 1 + x$ I can write the following

$$\frac{\mathcal{B}(1,2,3)}{\mathcal{B}(1,3,2)} = 1 + 2i\Omega_{123} = 1 + (1 + i\Omega_{123}) - (1 - i\Omega_{123})$$

Ignoring the leading constant, the expression can be seen to be the difference of the two Bargmann invariants' approximate Taylor expansions

$$\begin{aligned} (1 + i\Omega_{123}) - (1 - i\Omega_{123}) &= (1 + i\Omega_{123}) - (1 + i\Omega_{132}) \\ \implies \mathcal{B}(1,2,3) - \mathcal{B}(1,3,2) &= \text{Tr}(\rho(x)\rho(x + \delta x_1)\rho(x + \delta x_2)) - \text{Tr}(\rho(x)\rho(x + \delta x_2)\rho(x + \delta x_1)) \\ \implies \mathcal{B}(1,2,3) - \mathcal{B}(1,3,2) &= \text{Tr}(\rho(x)[\rho(x + \delta x_1), \rho(x + \delta x_2)]) \end{aligned}$$

The next few steps are similar in spirit to the derivation of the metric tensor. We expand the density matrices around the points x_1, x_2

$$\begin{aligned} \rho(x + \delta x_1) &= \rho(\bar{x}) + \frac{\partial \rho}{\partial x_1^\mu} \delta x_1^\mu + \frac{1}{2} \frac{\partial^2 \rho}{\partial x_1^\mu \partial x_1^\nu} \delta x_1^\mu \delta x_1^\nu + \dots \\ \rho(x + \delta x_2) &= \rho(\bar{x}) + \frac{\partial \rho}{\partial x_2^\mu} \delta x_2^\mu + \frac{1}{2} \frac{\partial^2 \rho}{\partial x_2^\mu \partial x_2^\nu} \delta x_2^\mu \delta x_2^\nu + \dots \end{aligned}$$

Plugging this into the commutator, one can see that the zeroth order terms cancel out to zero because they are nothing but $\text{Tr}(\rho[\rho, \rho])$ and thus, neglecting the third and higher order terms in the *final* expansion we have the following

$$\text{Tr}(\rho(x)[\rho(x + \delta x_1), \rho(x + \delta x_2)]) = \text{Tr}(\rho(\frac{\partial \rho}{\partial x_1^\mu} \frac{\partial \rho}{\partial x_2^\nu} \delta x_1^\mu \delta x_2^\nu - \frac{\partial \rho}{\partial x_2^\nu} \frac{\partial \rho}{\partial x_1^\mu} \delta x_2^\nu \delta x_1^\mu))$$

It can be shown by simple algebraic manipulation that the right hand side equals the expression supplied below which is probably the last step in the derivation

$$\text{Tr}(\rho(x)[\rho(x + \delta x_1), \rho(x + \delta x_2)]) = \text{Tr}(\rho[\frac{\partial \rho}{\partial x_1^\mu} \frac{\partial \rho}{\partial x_2^\nu} - \frac{\partial \rho}{\partial x_2^\nu} \frac{\partial \rho}{\partial x_1^\mu}]) (\delta x_1^\mu * \delta x_2^\nu)$$

where $*$ is the wedge product. Dividing this expression by $2i$ I end up with the Berry phase picked up after going around an infinitesimal triangulation. Integrating this over the surface bounded by a specified contour I get the total Berry phase as

$$\Omega = \int_S \frac{1}{2i} \text{Tr}(\rho[\frac{\partial \rho}{\partial x_1^\mu} \frac{\partial \rho}{\partial x_2^\nu} - \frac{\partial \rho}{\partial x_2^\nu} \frac{\partial \rho}{\partial x_1^\mu}]) (\delta x_1^\mu * \delta x_2^\nu)$$

Thus, the conclusion is that the curvature two form is nothing but the expression in front of the wedge product infinitesimals. That is,

$$\mathcal{F}_{\mu\nu} = \frac{1}{2i} \text{Tr}(\rho[\partial_\mu \rho, \partial_\nu \rho])$$

2. THE MACHINERY

The question as to how the integral of the connection one form or the curvature two form over a surface gives 2π times an integer is a deeper one and we would like to address this. The idea is to relate the integral of the curvature to something that is fundamental about the surface, and this relation comes from the work of Carl Gauss in what is now known as the Gauss-Bonnet theorem [HAZ]. Added to this, the extension of the said idea leads to another Theorema Egregium (literally, remarkable theorem) due to Gauss [GAU] which proves that any continuous deformation does not change the curvature or the integral over the surface. The integer which is multiplied by 2π (the result of the Gauss-Bonnet theorem) is nothing but the Euler characteristic of the surface $\chi(S)$, also known to algebraic geometers as the first Chern number due to the relationship of such manifolds with Chern classes.

Assuming that it is understood how the curvature two form/the Berry curvature tensor can be constructed for a given path C enclosing a section of a surface of the manifold (either from the fast food explanation in the last section or the rigorous steps laid out in the previous paragraph, just to be pedantic, from the Maurer-Cartan one forms), it has been demonstrated in many ways how the Stokes integral turns out the way it is. First, we define the Euler characteristic for polyhedra (why polyhedra? One of the many versions of the Gauss-Bonnet theorem involves triangulations of the surface for its proof, refer [SPI] or [STR], I present a proof on the same lines).

$$\chi(S) = V - E + F$$

(For a profound and thought provoking discussion on the formula and its elementary proof for polyhedra, refer [LAK]). Here, V, E, F are respectively the number of vertices, edges and faces of the polyhedron. The formula can be extended to Riemann manifolds by calling for the *genus* of the surface denoted by $g(S)$ and the Euler characteristic is denoted by

$$\chi(S) = 2 - 2g(S)$$

The next result is from Adrien-Marie Legendre (refer Figure 2.2 and [ARM]) which gives the area of a curvilinear triangle on S^2 , the three dimensional sphere. Take three non collinear points A, B, C on a sphere and join them along their great arcs to form a curvilinear triangle ΔABC . The Legendre theorem states that the area of the triangle, denoted henceforth wherever clear by Δ is related to the local angles made by the arcs at the vertices and the radius of the sphere

$$\Delta = (\alpha + \beta + \gamma - \pi) \times R^2$$

The proof for this statement can be done using calculus (integrate pieces) or could be argued heuristically from the symmetries of S^2 . Either way, we take

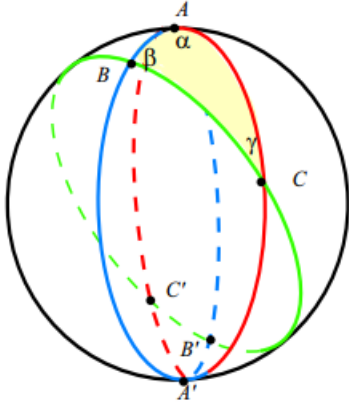


Figure 2.2: The curvilinear triangle considered by A. M. Legendre

this as a lemma in the proof of the actual result. Now, how do we quantify curvature, if at all we wanted to as a basic element of geometry? One way to do this is to introduce the idea of *parallel transport*. Take a vector \bar{x} which is tangent to A on the sphere and then move it along the curvilinear triangle in counter-clockwise orientation to B, then to C and back to A. Even if one does an approximate computation with a pencil and ruler, one can see that the vector will not be parallel to the initial direction, and in fact, the difference in the direction is exactly $\alpha + \beta + \gamma - \pi$ in the counter-clockwise direction. This should actually give us an insight into an induction like proof of the Gauss-Bonnet theorem using the lemma all over a given surface. This is because one could, in a sufficiently local frame approximate a surface to a curvilinear triangle on S^2 . The change in the angle of a vector when parallel transported around a closed path is known traditionally as the *holonomy* (and thence the terminology of the *Berry holonomy*).

First, some more fancy language. The *angle defect* of a curvilinear polygon on S^2 is defined as the amount of deviation the polygon takes from that drawn on R^2 . Deviation here refers to the total angle sum of the vertex angles of the polygon on the curvilinear surface.

$$\delta(A_1, A_2, \dots, A_n) = (\theta_1 + \theta_2 + \theta_3 + \dots + \theta_n) - (n - 2)\pi$$

It is straightforward to see (angles are linearly additive thankfully) that if I now deal with a $n + 1$ curvilinear polygon, the angle defect is also linearly additive

$$\delta(A_1, A_2, A_3, A_4, \dots, A_{n+1}) = \delta(A_1, A_2, \dots, A_n) + (\theta_1 + \theta_n + \theta_{n+1} - \pi) = \delta(A_1, A_2, \dots, A_n) + \delta(A_1, A_n, A_{n+1})$$

If the induction isn't already kicking in, then this step should probably clarify. Just as we do in calculus, we see that there is this thing known as the

2. THE MACHINERY

angle defect which can be defined for large polygons using elementary triangulations. Thus, if we are given an *oriented* area on a surface, we could essentially use the limiting process of a curvilinear polygon to cover the area. Then, we could triangulate the limiting curvilinear polygon to get the net angle defect, and hence some *measure* of the Gaussian curvature enclosed in the area (the word "measure" plays an important role in what is to be stated now, in the theory of measures, this is known as the Radon-Nikodym form). That is, we could say that in the limiting process

$$\delta(S) = \mathcal{F} \times \text{Area}$$

where \mathcal{F} is some function which encapsulates the curvature and this turns out to be, not surprisingly, the Gaussian curvature which is itself defined in a limiting process as the ratio of the angle defect of S to the actual area of S as S is contracted to a point on the surface. Mathematically, that is, define a manifold Σ and a point on the area S on Σ as z .

$$\kappa(z) = \lim_{S \rightarrow z} \frac{\delta(S)}{A(S)}$$

Inverting this, we have the definition of the angle defect as a surface (Stokes) integration

$$\delta(S) = \int_S \kappa(z) dA(z)$$

where the continuous integration can be replaced by a discrete summation where the curvature can be extracted for the centroid of the individual triangle element and the infinitesimal area in the summation can be taken as the area of the infinitesimal triangle. Just to make sure things make sense, notice that you can never find a flat sheet of paper which perfectly covers S^2 for the angle defect for any oriented area on the flat sheet is zero (the sum of angles of a triangle is exactly π) and the same becomes non zero on S^2 and this applied to all triangulations shows that the two angle defects do not match.

Now for the theorem due to Gauss, improved upon by Bonnet, this version which is due to Chern himself [CHE]. Let us take a Riemann manifold M with a well defined quadratic metric tensor g_{ab} . The manifold is triangulated as explained before by going really close to M and seeing individual slices as oriented areas on S^2 . Let us have a limiting process of triangles, labelled unto F . That is, we have F countably many triangles on M . Then, there is a straightforward relationship between F and the total number of edges E post triangulation.

$$E = \frac{3F}{2}$$

This comes from the fact that if you have F number of triangles then the number of edges is $3F$ with overcounting because each edge is exactly a part

of two triangles at most (the boundary ones are the ones with one) and by halving the number of overcounted edges we obtain the correct number of (internal) edges. With this fact out of the way, the proof is quite succinct. Note that with the above equality, the Euler characteristic is now a function of two variables.

$$\chi(S) = V - \frac{F}{2}$$

Now, for an infinitesimal triangulation, the angle defect can be written as

$$\delta(\Delta_k) = \theta_{1k} + \theta_{2k} + \theta_{3k} - \pi$$

Summing over all triangulations, we obtain the net angle defect for the limiting polygon on the manifold as

$$\delta(S) = \sum_k \delta(\Delta_k) = \sum_k (\theta_{1k} + \theta_{2k} + \theta_{3k}) - F\pi$$

The total sum of angles can be seen as sum of angles around each vertex in the triangulation multiplied by the number of vertices in the actual triangulation, that is V . Thus, the summation becomes

$$\delta(S) = 2\pi V - F\pi = 2\pi(V - \frac{F}{2}) = 2\pi\chi(S)$$

Thus, it can be proved from the earlier discussion that, the integral of the curvature form on the surface is equal to an integral multiple of 2π , and this number is the Euler characteristic or the Chern number.

$$\int_S \kappa(z) dA(z) = 2\pi\chi(S)$$

This ends the proof of the Gauss-Bonnet theorem, due to Chern. The Chern number plays an important role in classifying materials based on the topological invariant of the Hilber space. The Gauss-Bonnet theorem finds greater use when coupled with the Theorema Egregium due to Gauss. The remarkable theorem states that the characteristic does not change with topologically valid transformations of the Riemann manifold and hence the process of classification becomes even more widely spanned.

2.3 Two Level System

It would be nice to conclude with the first phase of the machinery if I am able to test out the formalism on an example and the best crash test dummy in quantum mechanics is the two state system. Not surprisingly, as it so happens many times, the very same examples actually simplify many real life scenarios when an analogy is drawn to them, and in my case it was more or less direct as the density matrix structure of kicked Graphene was similar to

2. THE MACHINERY

that of the two level system which I am going to describe now.

As the name suggests, you have two state vectors in your basis, $|0\rangle$ and $|1\rangle$. You can then express any ket as the linear combination of these two kets, with the conditions imposed below

$$|\psi\rangle = \alpha|0\rangle + \beta|1\rangle$$

$$||\alpha||^2 + ||\beta||^2 = 1$$

Thus, the most general parametrization for α and β is the polar form $re^{i\theta}$. It turns out that the Hilbert space spanned by all such ψ 's is a well known manifold known as the Bloch sphere. The parametrization which suits this manifold structure is that given below

$$|z_1, z_2\rangle = \begin{bmatrix} \cos\frac{\theta}{2} \\ \sin\frac{\theta}{2}e^{i\varphi} \end{bmatrix}$$

Again, some algebraic manipulation can show that the density matrix for the present spherical polar basis is given by the following simple formula, once again, in the Pauli basis.

$$|z_1, z_2\rangle \langle z_1, z_2| = \frac{1}{2}(1 + \hat{n} \cdot \vec{\sigma})$$

$$\hat{n} = \sin\theta \cos\varphi \hat{x} + \sin\theta \sin\varphi \hat{y} + \cos\theta \hat{z}$$

A real life example of such a situation is the spin half particle placed in a magnetic field where the Hamiltonian is given by

$$\mathcal{H} = \mu ||B|| \vec{\sigma} \cdot \hat{n}$$

where μ is the magnetic moment of the particle and B is the magnetic field intensity. Taking the derivative of \hat{n} with respect to θ and φ it is obvious that

$$\partial_\theta \hat{n} = \cos\theta \cos\varphi \hat{x} + \cos\theta \sin\varphi \hat{y} - \sin\theta \hat{z}$$

$$\partial_\varphi \hat{n} = -\sin\theta \sin\varphi \hat{x} + \sin\theta \cos\varphi \hat{y}$$

I have two independent coordinates and therefore I have a metric tensor which is of order 2. The terms of the metric tensor can be computed using the formula derived in this section and it looks like

$$g = \begin{bmatrix} 1 & 0 \\ 0 & \sin^2\theta \end{bmatrix}$$

It can also be written in the differential form as follows

$$ds^2 = \frac{1}{4}(d\theta^2 + \sin^2\theta d\varphi^2)$$

Continuing the example I can also calculate the Berry tensor and it too turns out to have a simple algebraic structure

$$\begin{aligned}\mathcal{F}_{\theta\varphi} &= \frac{1}{2} \text{Tr}(\rho[\partial_\theta\rho, \partial_\varphi\rho]) = \frac{1}{16} n^i \partial_\theta n^j \partial_\varphi n^k \times 4\epsilon^{ijk} \\ \implies \mathcal{F}_{\theta\varphi} &= \frac{1}{4} \hat{n} \cdot (\partial_\theta \hat{n} \times \partial_\varphi \hat{n})\end{aligned}$$

Simplifying this expression with the derivatives which I readily have, I see that the Berry curvature tensor for the $\theta\varphi$ orientation turns out to be

$$\mathcal{F}_{\theta\varphi} = \frac{1}{4} \sin\theta$$

To compute the Berry phase, I choose a curvilinear triangle on the Bloch sphere (much like the one chosen by Legendre) and I see that the surface integral directly depends upon the area of the triangle. The final expression for the Berry phase in this case is the following

$$\Omega = \frac{1}{2}(\Delta_{123} \pm 4\pi) \bmod 2\pi = \frac{1}{2}\Delta_{123}$$

In the next section I will briefly talk about some important ideas from Floquet theory and then my repertoire of tools needed for discussing the singly and doubly kicked cases will be complete. The entire idea of kicking and how periodic systems can be represented in a much more simplified manner without the use of perturbation theory is what is called Floquet-Abel theory. The section is more mathematical and can be skipped by an experienced reader.

2.4 Floquet Theory

General references: [ECKI], [SHI], [TGS], [DAL], [SHA]

Floquet theory is a branch of the theory of ordinary differential equations which deals with solutions of the system

$$\dot{\bar{x}} = \hat{A}(t)\bar{x}$$

where the time dependent coefficient matrix \hat{A} is periodic and piecewise continuous at the worst. The fundamental theorem which forms the basis for much of the discussion, known as the Floquet-Abel theorem exposites the structure of the solutions of such systems of differential equations and states that the solutions look like

$$\bar{x} = e^{\mu t} \bar{p}(t)$$

2. THE MACHINERY

where $\bar{p}(t)$ is periodic with the same period as that of \hat{A} , say T . Infact, if the dimension of \hat{A} is n then there exist $\mu_1, \mu_2, \mu_3, \dots, \mu_n$ such that

$$e^{\mu_1 T} e^{\mu_2 T} e^{\mu_3 T} \dots e^{\mu_n T} = \exp\left(\int_0^T \text{Tr}(\hat{A}(z)) dz\right)$$

Let us say we have a system with a Hamiltonian running with a time dependent perturbation

$$\mathcal{H} = \mathcal{H}_0 + V(t)$$

The concept of time dependent perturbation theory is useful only when V is small. But what if V is large and moreover periodic? If periodicity is assured, the magnitude of V is immaterial and the problem can be attacked using Floquet theory. The idea is to find a special *unitary* transformation which takes me from the set of all eigenvectors of the time dependent Hamiltonian \mathcal{H} to a new set whose eigenmatrix is time *independent*. That is, is it possible to find a \mathcal{U} such that

$$\begin{aligned} |\varphi(t)\rangle &= \mathcal{U}|\psi(t)\rangle \\ i\frac{\partial|\varphi(t)\rangle}{\partial t} &= \mathcal{H}_e|\varphi(t)\rangle \end{aligned}$$

The answer is positive and the proof is sketched below. What we have, to start with, is the Schrodinger equation for the initial basis,

$$i\frac{\partial\psi}{\partial t} = \mathcal{H}\psi$$

Now, for the Schrodinger equation in the transformed basis, I have

$$i\frac{\partial\mathcal{U}\psi}{\partial t} = \mathcal{H}_e\mathcal{U}\psi$$

A guess solution for \mathcal{U} is made which looks like

$$\mathcal{U} = e^{i\mathcal{F}(t)}$$

and plugging this *ansatz* into the transformed Schrodinger equation

$$i\frac{\partial}{\partial t}e^{i\mathcal{F}(t)}\psi = \mathcal{H}_e e^{i\mathcal{F}(t)}\psi$$

$$ie^{i\mathcal{F}(t)}\frac{\partial\psi}{\partial t} + i\psi\frac{\partial e^{i\mathcal{F}(t)}}{\partial t} = \mathcal{H}_e e^{i\mathcal{F}(t)}\psi$$

Simplifying this and making \mathcal{H}_e the subject we have

$$\mathcal{H}_e = e^{i\mathcal{F}(t)}\mathcal{H}e^{-i\mathcal{F}(t)} + i\frac{\partial}{\partial t}e^{i\mathcal{F}(t)}e^{-i\mathcal{F}(t)}$$

Now, for a time evolution from t_i to t_f I can write the following in the transformed basis

$$|\varphi(t_f)\rangle = e^{-i\mathcal{H}(t_f-t_i)}|\varphi(t_i)\rangle$$

But we know that

$$\begin{aligned} |\varphi(t_f)\rangle &= e^{i\mathcal{F}(t_f)}|\psi(t_f)\rangle \\ |\varphi(t_i)\rangle &= e^{i\mathcal{F}(t_i)}|\psi(t_i)\rangle \\ \implies e^{i\mathcal{F}(t_f)}|\psi(t_f)\rangle &= e^{-i\mathcal{H}(t_f-t_i)}e^{i\mathcal{F}(t_i)}|\psi(t_i)\rangle \\ \implies |\psi(t_f)\rangle &= e^{-i\mathcal{F}(t_f)}e^{-i\mathcal{H}(t_f-t_i)}e^{i\mathcal{F}(t_i)}|\psi(t_i)\rangle \end{aligned}$$

Et Volia! I have arrived at the evolution operator for the old basis represented in terms of three distinct quantities, two kicks at t_i and t_f and one time independent evolution for the period between the kicks. The advantage of this formalism will be directly visible when we deal with the kicked systems in the next two sections. The kick operators are not easily derivable in most cases but for simplified periodic models such as the Dirac comb one can write a nicer (probably Fourier represented) kick operator than go through the hassle of time dependent perturbation theory which might not be even valid in some situations.

Chapter 3

Singly Kicked Graphene

The discussion in this chapter follows naturally from the paper due to Agarwala et al. and forms the basis of much of the discussion in the next chapter. The mode of discussion would be exploratory and the theoretical details will be supplied before the simulations are presented (the full Mathematica notebooks are available in the appendix) and analyzed. It is to be stressed throughout these two chapters that the simulations are only approximate to a certain order and are not to scale, the reason being that the symbolic math evaluation and handling becomes too complicated if one has to do the calculations rigorously.

3.1 Analysis

To recapitulate, we start with an undriven Graphene system defined by the following Hamiltonian representation in k-space.

$$\mathcal{H}_{TB,\bar{k}} = -\gamma \begin{bmatrix} 0 & 1 + e^{i\bar{k}\cdot\bar{K}} + e^{i\bar{k}\cdot\bar{K}'} \\ 1 + e^{-i\bar{k}\cdot\bar{K}} + e^{-i\bar{k}\cdot\bar{K}'} & 0 \end{bmatrix}$$

It was also stated that a more succinct way of expressing the same was in the Pauli basis and this looks like

$$\mathcal{H}(k) = -\gamma(G(k)\sigma^x - H(k)\sigma^y)$$

If this is not clear then the reader is suggested to go through the first chapter again. The eigenenergies are given in full below

$$E(\bar{k}) = \pm \gamma \sqrt{3 + 2\cos(\sqrt{3}k_y a) + 4\cos(\frac{\sqrt{3}k_y a}{2})\cos(\frac{3k_x a}{2})}$$

Now I add a perturbation which looks like the following

$$\mathcal{H}_{kick}(t) = \sum_{\bar{n}} (\alpha_x \sigma^x + \alpha_y \sigma^y + \alpha_z \sigma^z) \sum_{m=-\infty}^{m=\infty} \delta(t - mT)$$

3. SINGLY KICKED GRAPHENE

This term requires some explanation. The outer summation is on \bar{n} which is the lattice displacement vector from a chosen origin. Therefore we are performing a summation over one unit cell, and thus has the same periodicity as the lattice. The parameters $\alpha_x, \alpha_y, \alpha_z$ which will be collectively called as $\bar{\alpha}$ henceforth, are independent sources in the three coordinate directions which perform the "kicking". They are operated in the Pauli basis. So in k-space, when this expression is Fourier transformed, we lose the outer summation because we are only working in one unit cell, and it looks like the following

$$\mathcal{H}_{kick}(t) = (\alpha_x \sigma^x + \alpha_y \sigma^y + \alpha_z \sigma^z) \sum_{m=-\infty}^{m=\infty} \delta(t - mT)$$

Now this term is a periodic perturbation (of period T, clearly). From section 2.4, we can clearly use Floquet-Abel theorem to reduce this (seemingly complicated) time dependent Hamiltonian to a combination of a time independent part and a "kick" (refer to the operator \mathcal{F} in 2.4). This structure is colloquially known as the Floquet stroboscopic picture. I construct a new unitary evolution operator known as U_{XYZ} (the notation is borrowed partly from Adhip Agarawala et al.,) which looks somewhat like

$$U_{XYZ} = U_{kick} U_{static} = e^{-i\bar{\alpha} \cdot \vec{\sigma}} e^{-i\mathcal{H}(k)T}$$

and from the definition of a unitary evolution operator, I have, for the whole time period T

$$U_{XYZ} = e^{-i\mathcal{H}_{XYZ}T}$$

Thus, I can write from the above two equations that

$$e^{-i\bar{\alpha} \cdot \vec{\sigma}} e^{-i\mathcal{H}(k)T} = e^{-i\mathcal{H}_{XYZ}T}$$

The idea is to extract an expression for \mathcal{H}_{XYZ} from the above equality and this is done using a remarkable identity involving the Pauli matrices. Given two unit vectors \hat{n}, \hat{m} and constants a, b , then one can find a constant c and a unit vector \hat{k} (this is not to be confused by the unit wave vector) such that

$$e^{ia(\hat{n} \cdot \vec{\sigma})} e^{ib(\hat{m} \cdot \vec{\sigma})} = e^{ic(\hat{k} \cdot \vec{\sigma})}$$

and they are given by

$$c = \text{ArcCos}(\text{Cos}(a)\text{Cos}(b) - \hat{n} \cdot \hat{m} \text{Sin}(a)\text{Sin}(b))$$

$$\hat{k} = \frac{1}{\text{Sin}(c)} (\hat{n} \text{Sin}(a)\text{Cos}(b) + \hat{m} \text{Sin}(b)\text{Cos}(a) - \hat{n} \times \hat{m} \text{Sin}(a)\text{Sin}(b))$$

To use this identity for our purpose, I need to map the exponents of the Floquet stroboscopic operator to the exponential structure shown in the above

3.1. Analysis

identity. This is simple algebra and we end up with the following equality involving \mathcal{H}_{XYZ}

$$U_{XYZ} = e^{-i\sqrt{\alpha_x^2 + \alpha_y^2 + \alpha_z^2}(\hat{\alpha} \cdot \sigma)} e^{-iE(k)(\hat{\beta} \cdot \sigma)T} = e^{-i\mathcal{H}_{XYZ}T}$$

where

$$\begin{aligned} a &\rightarrow -\sqrt{\alpha_x^2 + \alpha_y^2 + \alpha_z^2} = -||\bar{\alpha}|| \\ b &\rightarrow -E(k)T \\ \hat{n} &\rightarrow \hat{\alpha} = \frac{1}{\sqrt{\alpha_x^2 + \alpha_y^2 + \alpha_z^2}}(\alpha_x, \alpha_y, \alpha_z) \\ \hat{m} &\rightarrow \hat{\beta} = \frac{1}{\sqrt{G(k)^2 + H(k)^2}}(G(k), -H(k), 0) \end{aligned}$$

With these correspondences clear, I can claim that my effective time independent Hamiltonian is given by

$$\mathcal{H}_{XYZ} = -\frac{1}{T}c(\hat{k} \cdot \bar{\sigma})$$

The algebra is slightly involved but if carefully done, one ends up with

$$\frac{-c}{T} = -\frac{1}{T} \text{ArcCos}(\text{Cos}||\alpha||\text{Cos}(E(k)T) + \frac{\gamma}{||\alpha||E(k)}(\alpha_x G(k) - \alpha_y H(k))\text{Sin}||\alpha||\text{Sin}(E(k)T))$$

and $\hat{k} \cdot \bar{\sigma}$ is computed with the two unique matrix elements written separately to avoid cluttering (the other two can be determined easily enough to make the entire matrix Hermitian)

$$\begin{aligned} (\hat{k} \cdot \bar{\sigma})_{1,1} &= \frac{1}{\text{Sin}(c)}\left(-\frac{\alpha_z}{||\alpha||}\right)\text{Sin}||\alpha||\text{Cos}(E(k)T) - \frac{1}{||\alpha||}\frac{\gamma}{E(k)}\alpha_x H(k)\text{Sin}||\alpha||\text{Sin}(E(k)T) \\ &\quad - \frac{1}{||\alpha||}\frac{\gamma}{E(k)}\alpha_y G(k)\text{Sin}||\alpha||\text{Sin}(E(k)T) \\ (\hat{k} \cdot \bar{\sigma})_{1,2} &= \frac{1}{\text{Sin}(c)}\left(-\frac{\alpha_x}{||\alpha||}\right)\text{Sin}||\alpha||\text{Cos}(E(k)T) + \frac{\gamma}{E(k)}G(k)\text{Cos}||\alpha||\text{Sin}(E(k)T) \\ &\quad + \frac{\gamma}{||\alpha||E(k)}\alpha_z H(k)\text{Sin}||\alpha||\text{Sin}(E(k)T) - \frac{i}{\text{Sin}(c)}\left(-\frac{\alpha_y}{||\alpha||}\right)\text{Sin}||\alpha||\text{Cos}(E(k)T) - \\ &\quad \frac{\gamma}{E(k)}H(k)\text{Cos}||\alpha||\text{Sin}(E(k)T) + \frac{1}{||\alpha||}\frac{\gamma}{E(k)}\alpha_z G(k)\text{Sin}||\alpha||\text{Sin}(E(k)T) \end{aligned}$$

Before I proceed to further calculations, I would like to demonstrate the band structures derived from the eigenvalues of the effective Hamiltonian \mathcal{H}_{XYZ} . The plots were done in Mathematica and both the plotting script and the main notebook are provided in the appendices (band-2.nb and

3. SINGLY KICKED GRAPHENE

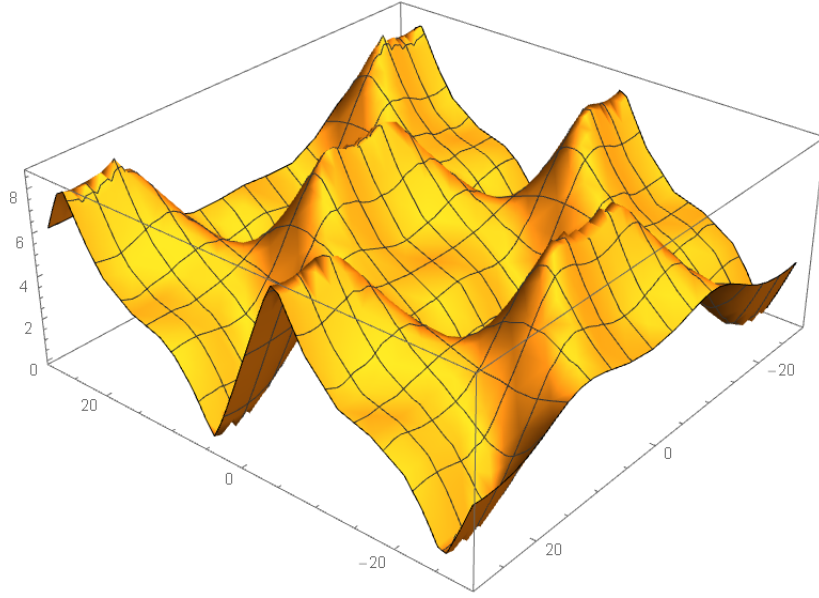


Figure 3.1: γT is taken to be 1. Purely y-kicking. This is a semi-Dirac dispersion. Refer to Agarwala et al. for discussion.

singly-kicked.nb to be precise). Figures 3.1, 3.2 and 3.3 are the three forms of kicking that are possible in each of the directions of the three coordinate axes. For furthering the analytic calculations, I simplify the situation by taking $\alpha_x, \alpha_y = 0$ and $\alpha_z \neq 0$. This reduces the eigenvalues to the following simple expression

$$\varepsilon_{XYZ} = \frac{1}{T} \cos^{-1}(\cos(\alpha_z) \cos(E(k)T))$$

It can be noted that when the band structure approaches the Dirac points (technically, the points where $E(k)$ is zero) there is a non zero band gap because the eigenvalue is still non-zero from the above expression, it is $\frac{\alpha_z}{T}$. This opening up of the band gap is one of the effects of kicking on the Dirac points. Infact, working in the infrared regime, that is $E(k)$ is very small, the following approximations can be made

$$\begin{aligned} \cos(c) &= \cos(\alpha_z) \cos(E(k)T) \approx \cos(\alpha_z) \left(1 - \frac{E(k)^2 T^2}{2}\right) \\ \implies \sin(c) &\approx \sqrt{1 - \cos^2(\alpha_z)(1 - E(k)^2 T^2)} \end{aligned}$$

3.1. Analysis

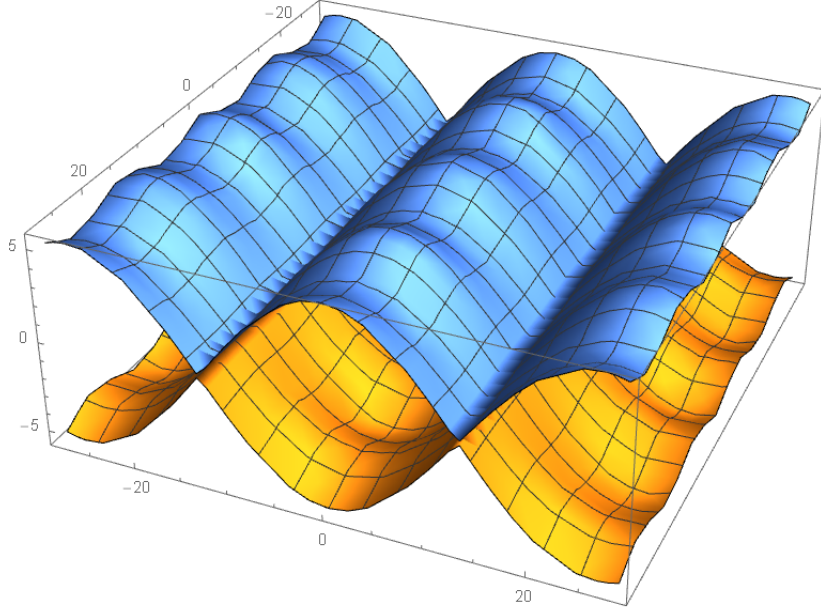


Figure 3.2: Purely x-kicking. Notice the dispersionless lines. Refer to Agarwala et al. for discussion.

The unit vector \hat{k} then becomes the following after this approximation is made

$$\begin{aligned}\hat{k} = & \frac{1}{\sqrt{1 - \cos^2(\alpha_z)(1 - E(k)^2 T^2)}} (\gamma T G(k) \cos(\alpha_z) + \alpha_z \gamma T H(k) \sin(\alpha_z)) \hat{x} + \\ & \frac{1}{\sqrt{1 - \cos^2(\alpha_z)(1 - E(k)^2 T^2)}} (-\gamma T H(k) \cos(\alpha_z) + \alpha_z \gamma T G(k) \sin(\alpha_z)) \hat{y} \\ & + \frac{1}{\sqrt{1 - \cos^2(\alpha_z)(1 - E(k)^2 T^2)}} (-\sin(\alpha_z)(1 - \frac{E(k)^2 T^2}{2})) \hat{z}\end{aligned}$$

There is one more approximation which makes computation easier when one is considering the infrared regime, or, the FBZ around the Dirac points, and it is known as the linearization approach as given below

$$G(k_x, k_y) = -\frac{3a}{2} k_y$$

$$H(k_x, k_y) = \frac{3a}{2} k_x$$

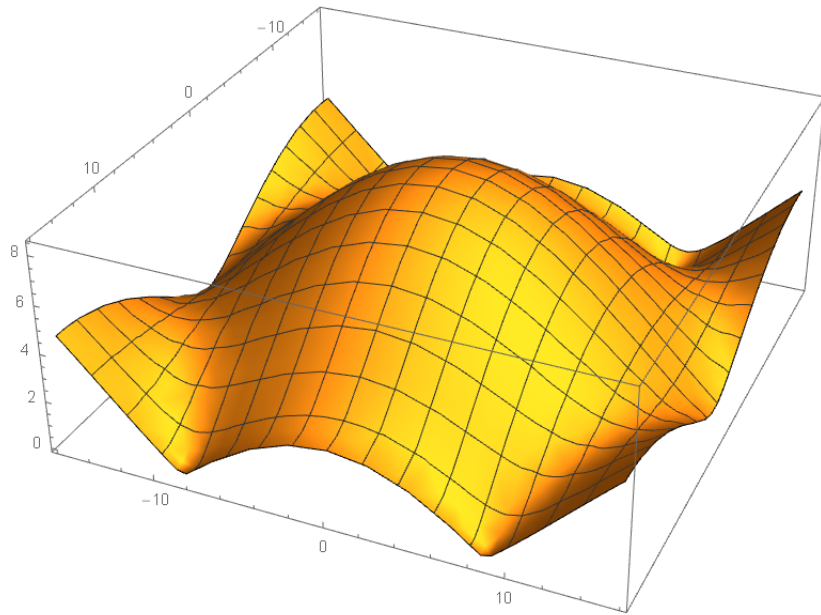


Figure 3.3: Purely z-kicking. Probably the only kicking which retains the unkicked Graphene band structure. Notice that the central peak becomes more prominent.

$$\implies E(k_x, k_y) = \frac{3\gamma}{2} \sqrt{k_x^2 + k_y^2}$$

It is time to now start working towards calculating the mass term, the density matrix, the Berry field and finally the Chern number for the given system. Once the density matrix is figured out (which is done via an analogy with our old friend, the two level system), the rest of the components follow directly from the formalism derived in the last chapter.

3.2 More Analysis

The analogy that will be drawn is with respect to the situation of a spin half particle in a magnetic field. As explained in section 2.3, the Hamiltonian for such a system is given by

$$\mathcal{H} = \mu ||B|| \vec{\sigma} \cdot \hat{n}$$

In the present case, the effective Hamiltonian has a similar structure

$$\mathcal{H}_{XYZ} = -\frac{c}{T} \hat{k} \cdot \bar{\sigma}$$

The analogy that is to be noted is that due to the structure of the first Hamiltonian and the fact that the eigenvalue of the spin half particle in a magnetic field is given by $\mu||B||$ I can construct the density matrix, which, for the two level system was derived to be

$$\rho = \frac{1 + \hat{n} \cdot \bar{\sigma}}{2}$$

can now be written down for the singly kicked effective Hamiltonian to be

$$\rho = \frac{1 - \hat{k} \cdot \bar{\sigma}}{2}$$

since the positive eigenvalue for the same is given by $\frac{c}{T}$ as explained in the previous section. The entire idea behind the legitimacy of the analogy lies in the fact that to get anywhere close to calculating the Chern number I need to find a representation of the density matrix as a function of k-space coordinates which is also invariant under $U(1)$ gauge transformations and which is a good ray space quantity. Using the definition of the curvature tensor (notation not to be confused with the unitary kick operator) as a function of the density matrix

$$\mathcal{F}_{\alpha\beta} = \frac{1}{2i} \text{Tr}(\rho[\partial_\alpha \rho, \partial_\beta \rho])$$

Plugging the density matrix expression and after a bit of algebra, the curvature tensor looks like

$$\mathcal{F}_{k_x k_y} = \frac{i}{8} \text{Tr}(\hat{k} \cdot \bar{\sigma} [\partial_{k_x} \hat{k} \cdot \bar{\sigma}, \partial_{k_y} \hat{k} \cdot \bar{\sigma}])$$

Before evaluating this expression it is a good idea to keep track of how the matrix $\hat{k} \cdot \bar{\sigma}$ changes after the approximations introduced in the previous section and the two unique matrix elements are now given as

$$\begin{aligned} (\hat{k} \cdot \bar{\sigma})_{1,1} &= \frac{1}{\sqrt{1 - (1 - T^2 \gamma^2 \frac{9a^2}{4} (k_x^2 + k_y^2)) \cos^2 \alpha_z}} - \sin \alpha_z (1 - T^2 \gamma^2 \frac{9a^2}{8} (k_x^2 + k_y^2)) \\ (\hat{k} \cdot \bar{\sigma})_{1,2} &= \frac{1}{\sqrt{1 - (1 - T^2 \gamma^2 \frac{9a^2}{4} (k_x^2 + k_y^2)) \cos^2 \alpha_z}} ((-\frac{3a\gamma T}{2} k_y \cos \alpha_z + \frac{3a}{2} \alpha_z k_x \gamma T \sin \alpha_z) + \\ &\quad i(\frac{3a}{2} k_x \gamma T \cos \alpha_z + \frac{3a}{2} \gamma T k_y \alpha_z \sin \alpha_z)) \end{aligned}$$

If recollected correctly, in the last section of Chapter 1 it was mentioned that the gapless-ness and hence the semi-metal like behavior of unkicked Graphene was due to the $(1, 1)$ element of the Hamiltonian matrix being zero. This element is known as the "mass term" and it is called so because

3. SINGLY KICKED GRAPHENE

it is the effective mass that the Fermion sees in the lattice. In this case of purely z-kicking, the mass term is non zero and varies sinusoidally with α_z (a claim which is verified by simulation later on). For the sake of clarity, it is restated here without the obvious constants

$$\Delta = -\text{Sin}\alpha_z \left(\frac{2}{3a\gamma T} - \frac{3a\gamma T}{4} (k_x^2 + k_y^2) \right)$$

Now that we know how the $\hat{k}\bar{\sigma}$ matrix looks like, it is a mere matter of substitution into the formula for the Berry tensor or the Berry field to get the final expression. I have taken the approach of doing this using Mathematica as my computational engine to give me a closed form final expression for the tensor or if that is not possible, at the least an approximate plot for the Taylor expanded computation of the commutator. I was fortunate to know Tridev Mishra, who has actually computed the entire commutator by hand and derived an analytic closed form expression for the Berry field. It is a computational tour de force exhibited by him and the details are too large to be included in this section and they are available in the appendix A for the interested reader. I only state the final expression which he arrived at, and it is surprisingly not very complicated

$$\mathcal{F}_{k_x k_y} = -\frac{1}{2} \frac{\omega^4 \text{Sin}(\alpha_z)(k_x^2 + k_y^2)(\alpha_z^2 \text{Sin}^2(\alpha_z) + \text{Cos}^2(\alpha_z))}{(1 - [1 - \omega^2(k_x^2 + k_y^2)] \text{Cos}^2(\alpha_z))^{\frac{3}{2}}}$$

where

$$\omega = \frac{3a\gamma T}{2}$$

It is to be understood that this expression is valid for the linearization approximation which restricts us to only those parts of the FBZ which are near the Dirac points. The exact computation at the Dirac points gives indeterminate eigenvalues as the matrix elements diverge. The Chern number computation involves integrating the *whole* Berry tensor around the hexagonal FBZ or this approximate reduced Berry tensor around a suitable (probably circular) domain around the Dirac points. Analytic integration of this expression might look cumbersome but before I move on to discussions regarding simulations and computer assisted proof of the above expression, a nice calculation can be done to give some qualitative indications as to how the Berry field and the Chern number behave.

The expression for the density matrix can be rewritten in terms of the effective Hamiltonian matrix \mathcal{H}_{XYZ} and its eigenvalue $\epsilon = \pm \frac{c}{T}$

$$\rho = \frac{1}{2} \left(1 \mp \frac{\mathcal{H}_{XYZ}}{\epsilon} \right)$$

Plugging this into the initial expression for the Berry field in terms of the density matrix, we evaluate it to the following simplified expression

$$\mathcal{F}_{k_x k_y} = \frac{i}{8\varepsilon^3} \text{Tr}(\mathcal{H}_{XYZ} [\partial_{k_x} \mathcal{H}_{XYZ}, \partial_{k_y} \mathcal{H}_{XYZ}])$$

Near the Dirac points the eigenvalues can be written down as a function of the mass term and the wave vector components, and this fact is obvious from the $\bar{\sigma}$ basis representation of the effective Hamiltonian

$$\varepsilon = \pm \sqrt{\Delta^2 + k^2}$$

To clarify this, I need to go back right to the first chapter when there was another representation of the unkicked Graphene Hamiltonian using the three displacement vectors $\delta_1, \delta_2, \delta_3$ instead of the two triangular sublattice picture. The upgrade from this unkicked Graphene form to the singly kicked Graphene is the non zero mass term (atleast for the purely z-kicked system) and the Hamiltonian now looks like

$$\mathcal{H} = \Delta\alpha_0 + \bar{\alpha} \cdot \bar{\pi}(k)$$

where

$$\alpha_0 = \begin{bmatrix} 1 & 0 \\ 0 & -1 \end{bmatrix} \quad \alpha_1 = \begin{bmatrix} 0 & 1 \\ 1 & 0 \end{bmatrix} \quad \alpha_2 = \begin{bmatrix} 0 & -i \\ i & 0 \end{bmatrix}$$

This is the complete kicked Hamiltonian and the near Dirac point approximation now makes the structure of the eigenvalues all the more obvious

$$\mathcal{H} = \Delta\alpha_0 + k^x\alpha_1 + k^y\alpha_2$$

Using this as the expression for the effective Hamiltonian in the Berry tensor equality the following Lorentzian profiled function results

$$\mathcal{F}_{k_x k_y}(\bar{k}) = -\frac{1}{2} \frac{\Delta}{(k^2 + \Delta^2)^{\frac{3}{2}}}$$

It is encouraging to see that the actual analytic expression looks similar to this one, and is exact to dimensions (refer Fig. 3.4). The computation of the Chern number near the Dirac point is done over a circular contour. With a CAS like Mathematica, one would not have to put any upper limits on the integration and one can end up with an analytic expression for the Chern number. However, to go ahead with the hand calculation, we set the upper limit to be $\frac{\Lambda}{\Delta}$ where Λ is known as the regulator (the terminology is borrowed from field theory) and this process is called regularization.

$$C = \frac{1}{4\pi} \int_0^{\frac{\Lambda}{\Delta}} \frac{\Delta}{(k^2 + \Delta^2)^{\frac{3}{2}}} 2\pi k dk$$

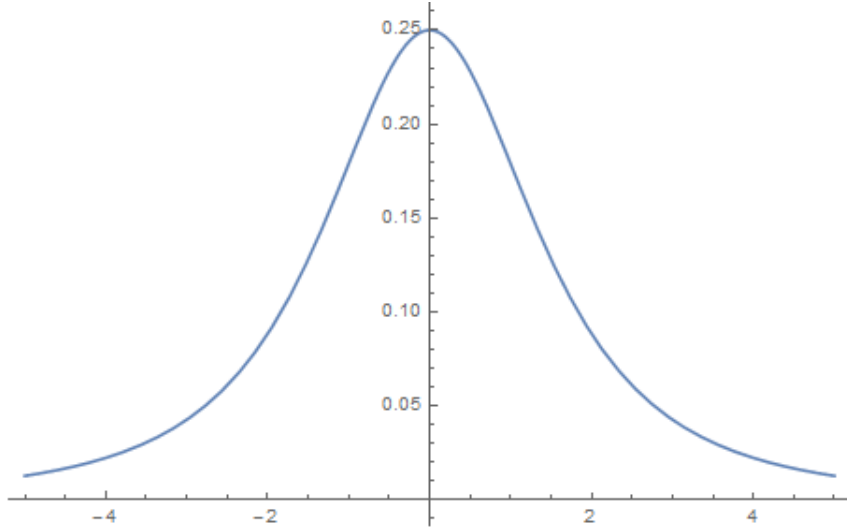


Figure 3.4: The Berry field versus the magnitude of the wave-vector. Δ is taken to be 2. Not to scale.

$$\begin{aligned} \Rightarrow \mathcal{C} &= \frac{\Delta}{||\Delta||} \times \int_0^{\frac{\Delta}{\Delta}} \frac{k'}{(k'^2 + 1)^{\frac{3}{2}}} dk' \\ \Rightarrow \mathcal{C} &= Sgn(\Delta) \left(1 - \frac{1}{\sqrt{1 - \frac{\Delta^2}{\Delta^2}}} \right) \end{aligned}$$

The clear conclusion from the expression above is that the Chern number would flip signs for negative and positive mass terms. This implies that the Chern number would flip signs *sinusoidally* with α_z as the mass term depends on the kicking parameter sinusoidally. These claims will be verified by simulation which I move to now.

3.3 Simulation and Computer Assisted Proof

The idea of using Mathematica as a tool to verify the analytic calculation was actually an offshoot of a more general idea that I was working on long before I started working on this thesis, and it involved using computers to prove logic theorems in mathematics. In this case, the initial parameters are set and the computation is listed as mathematical statements to Mathematica and it chugs the derivatives in Appendix A and prints the final expression. It would be nice if it could print the exact analytic computation but the computer being classical can only do approximate symbolic manipulation and hence shows some distortion in the results. Added to this the parameters and the dimensionless constants have been ignored all over the place and hence there would be, at the most, an issue with the scaling. First off, the

3.3. Simulation and Computer Assisted Proof

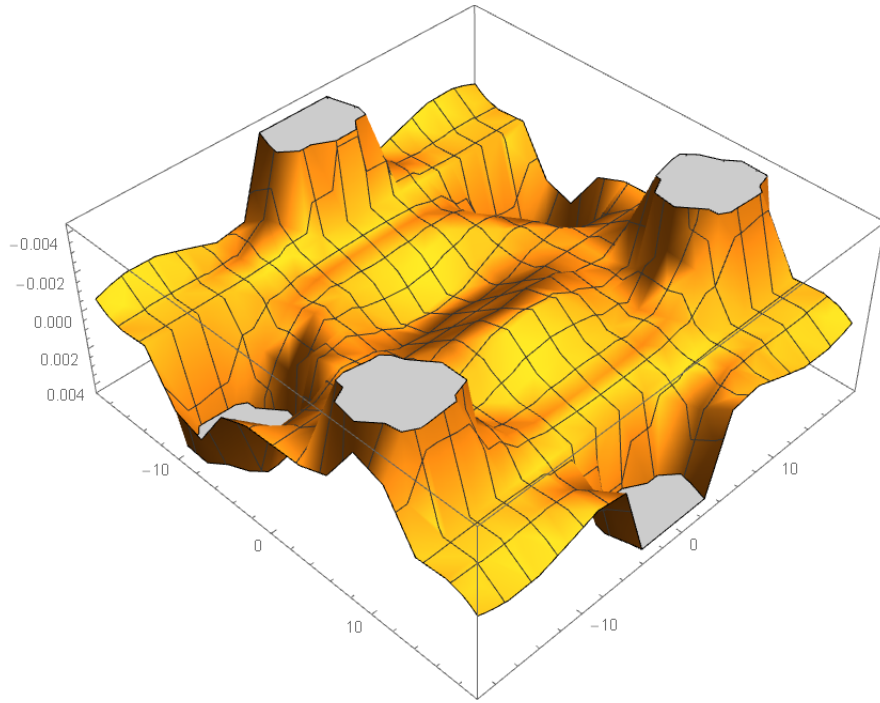


Figure 3.5: The Berry field over the square area of $(-6\pi, 6\pi) \times (-6\pi, 6\pi)$ and $\alpha_z = 5\sqrt{3}$. γT is assumed to be 1. Notice the three prominent peaks and the three prominent valleys. Compare this with Fig 3.7.

plot of the Berry field for a fixed value of α_z is shown in Figures 3.5, 3.6 and 3.7. This is made up of six Dirac point like Lorentzian approximations for the Berry field derived in the previous section (the Lorentzian structure might not be very apparent or accurate, but in the doubly kicked case it is almost exact), but three of them pointing upwards and the other three pointing downwards alternating with each other. Figure 3.6 is the top view of Fig. 3.7 and it shows the hexagonal nature of Graphene is retained even under z-kicking.

The most interesting aspect of discussion is the comparison between Fig. 3.5 and Fig. 3.7. The only difference in these two configurations is that I have flipped the sign of α_z . Lo and behold, I notice that the entire Berry field has flipped as if the analytic expression churned out by the machine is an odd function as expected. This is also a phase transition and what we have just encountered is Graphene behaving as a *Chern insulator* with the topological transitions happening around the origin. This also shows the correspondence between the Berry field $\mathcal{F}_{k_x k_y}$ and the mass term Δ .

Due to the intricate symmetry in the Berry field structures shown above

3. SINGLY KICKED GRAPHENE

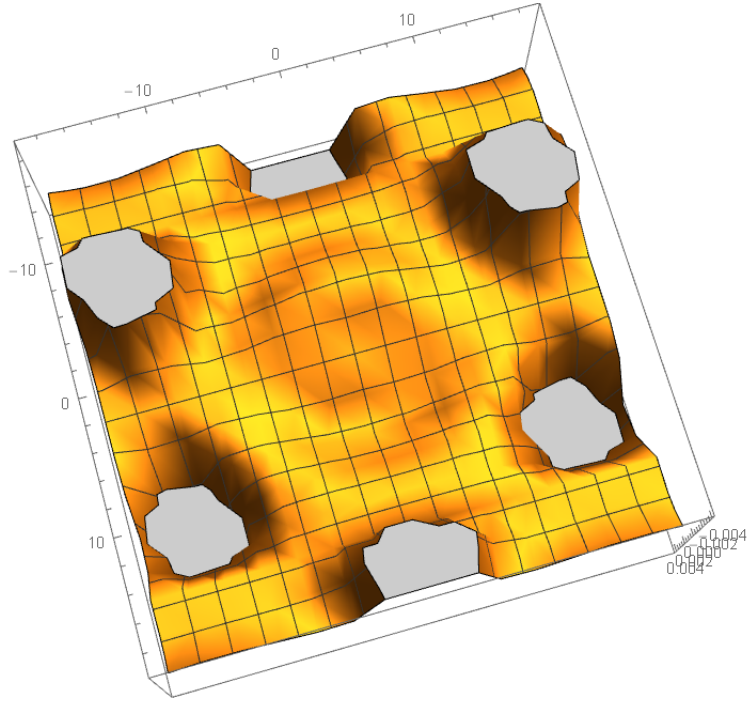


Figure 3.6: The top view of the Berry field for the same square area in the FBZ as Fig 3.5 and $\alpha_z = -5\sqrt{3}$. The hexagonal shape of the FBZ is clearly visible here. It is also clear that the only interesting features of the Berry field happen at the Dirac points, and they look somewhat Lorentzian.

it can be concluded that the integral of the tensor over any symmetric FBZ domain will render a 0 Chern number and this can be checked by integrating the expression for the Berry field derived by Mathematica over a *circular* contour instead of a hexagonal one (which is rather difficult to describe to the machine) and the answer for the integration turns out to be the order of 10^{-18} which can safely be assumed to be zero as we are still working with dimensionless units. However, the integral over a circular domain enclosing an individual Dirac Lorentzian need not be zero. Moreover it is dependent on α_z in a complex way. To recapitulate, the analytic expression for the Berry field around a Dirac point is given by

$$\mathcal{F}_{k_x k_y} = -\frac{1}{2} \frac{\omega^4 \sin(\alpha_z)(k_x^2 + k_y^2)(\alpha_z^2 \sin^2(\alpha_z) + \cos^2(\alpha_z))}{(1 - [1 - \omega^2(k_x^2 + k_y^2)] \cos^2(\alpha_z))^{\frac{3}{2}}}$$

Integrating this over k_x, k_y would effectively entail pulling out all the non k dependent terms outside the integral. One clear expression which is a function of α_z which is also independent of k_x and k_y is the part

$$f(\alpha_z) = \alpha_z^2 \sin^3(\alpha_z) + \cos^2(\alpha_z) \sin(\alpha_z)$$

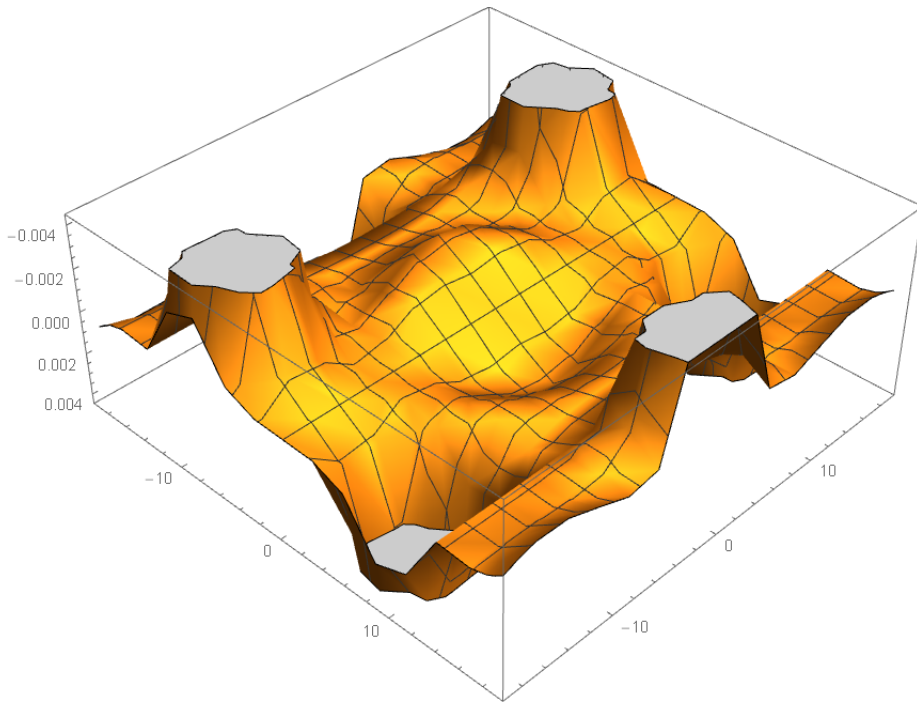


Figure 3.7: The Berry field for the same initial parameters as that of Fig. 3.6 but $\alpha_z = -5\sqrt{3}$. According to theoretical calculations because the mass term and hence the Berry field depends on α_z as a sinusoid, it should definitely behave like an odd function. And it clearly does. The hills have become the valleys and vice versa. This is a typical topological insulator-like transition with the point of transition being the origin.

The verification comes from plotting this function as an approximate trend for the actual integral performed by Mathematica with an `AccuracyGoal` of 6. The two expressions remarkably match in the structure and are approximate to a scale (might include a sign flip too, but then that is like a negative scale (Figure 3.10)). It is not correct to compare these two expressions for a perfect mismatch as I am obviously ignoring the $\text{Cos}\alpha_z$ term sitting in the denominator which cannot be separated from the k_x, k_y integration variables). Figure 3.8, 3.9 and 3.10 are the three plots under comparison. The data sets for the plots are provided in the appendices.

The decisive justification comes from comparing the analytic expression for the Berry field directly with the Berry tensor computed by Mathematica. Again, apart from a scale factor, the behavior is similar and becomes almost exact as one moves away from the center of the Dirac cone. The plots in Figures 3.11 thru 3.15 show the appropriate comparisons between the machine computed Berry tensor's behavior and the analytic Berry field expression at the points (1,1) and (2,2) in the FBZ. Note that (0,0) here refers to the

3. SINGLY KICKED GRAPHENE

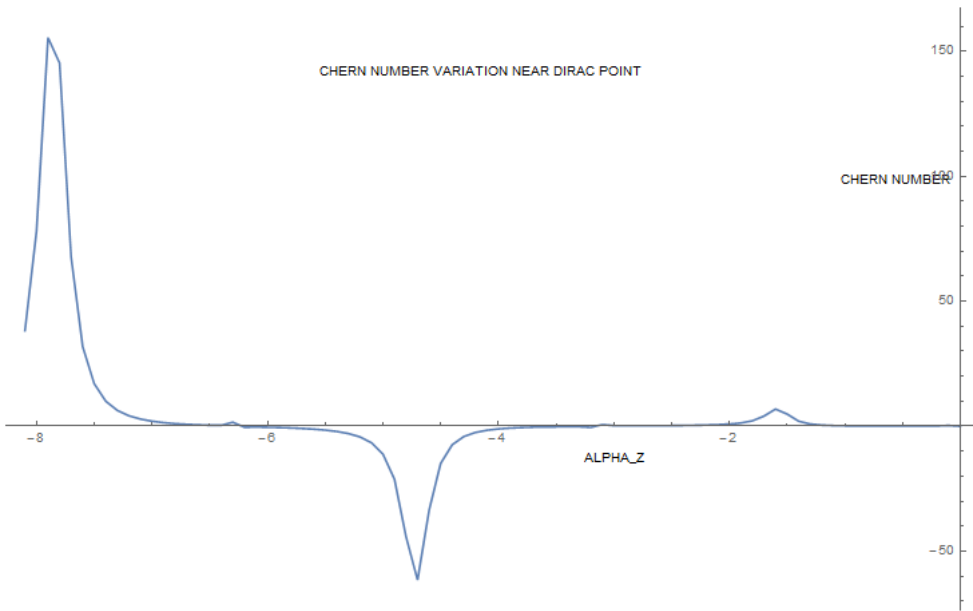


Figure 3.8: The variation of the Chern number with α_z near the Dirac points as computed by Mathematica. Figure 3.9 gives a closer look at the structure of this function.

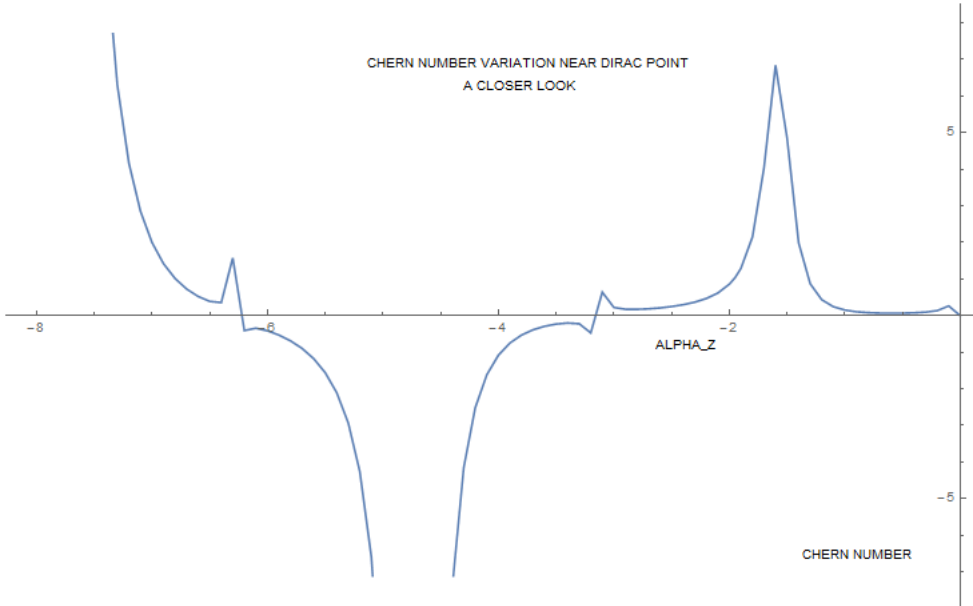


Figure 3.9: A closer look at Figure 3.8. Notice the irregularities. These are due to the power series approximations that Mathematica makes to simplify symbolic math.

3.3. Simulation and Computer Assisted Proof

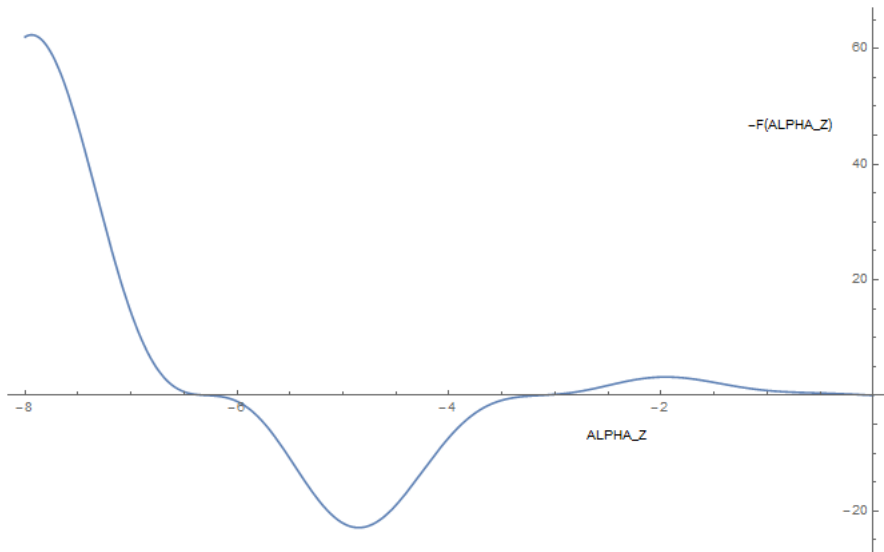


Figure 3.10: Plot of the function $-f(\alpha_z)$.

center of the Dirac cone, which is precisely at the Dirac point, where the computation diverges.

The “near Dirac cone” plots for the Berry field are given in Figures

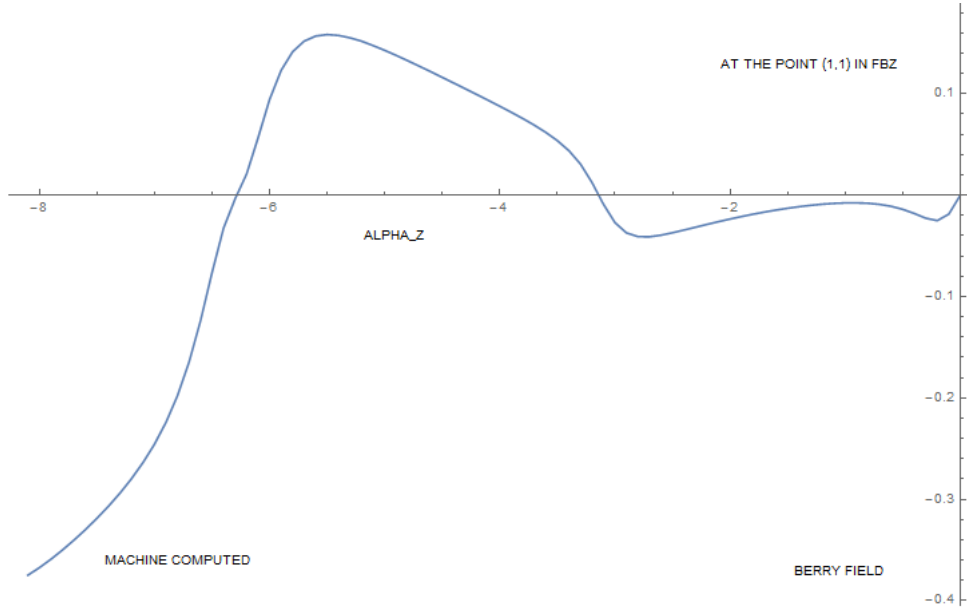


Figure 3.11: The machine computed Berry tensor at the point $(1,1)$ in the Brillouin Zone.

3. SINGLY KICKED GRAPHENE

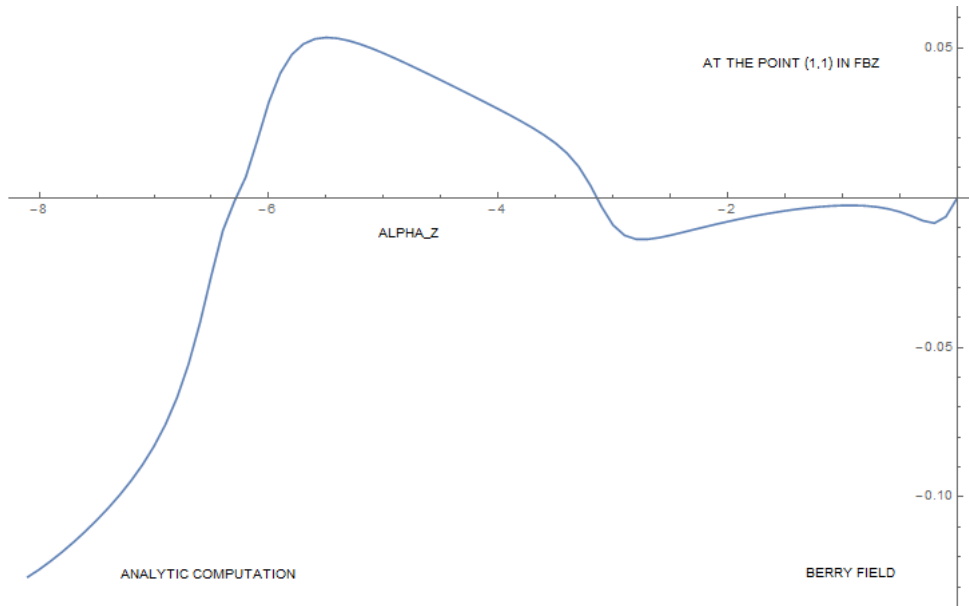


Figure 3.12: The analytically computed Berry tensor field at the point $(1,1)$ in the Brillouin Zone. Note the scale shift but the retention of the structure.

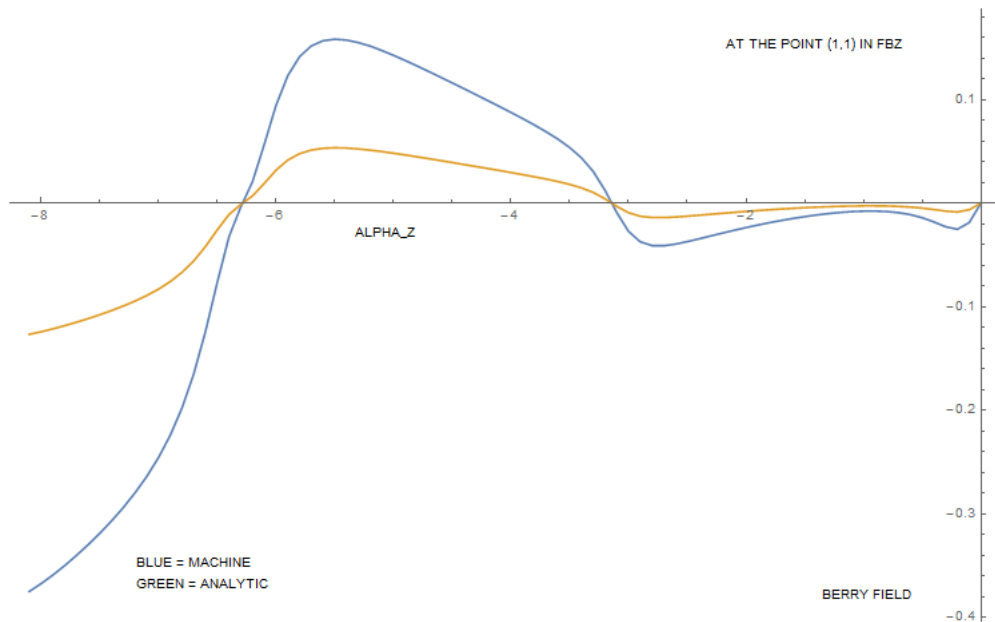


Figure 3.13: Comparison of Figures 3.11 and 3.12. The scale shift is much more apparent here. The zeros however coincide, not surprisingly at multiples of π .

3.3. Simulation and Computer Assisted Proof

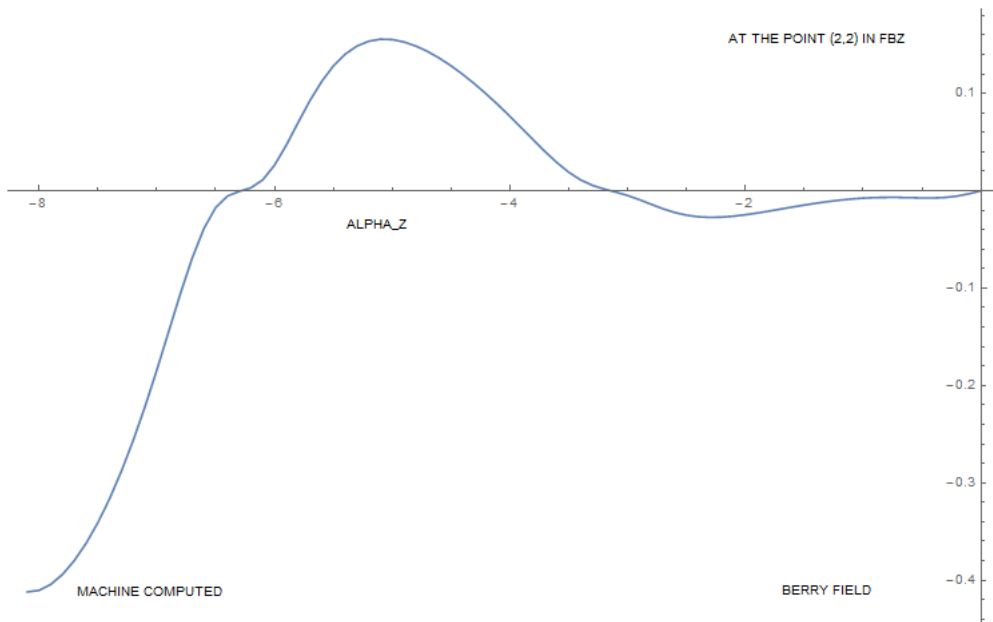


Figure 3.14: The machine computed Berry tensor at the point $(2,2)$ in the Brillouin Zone.

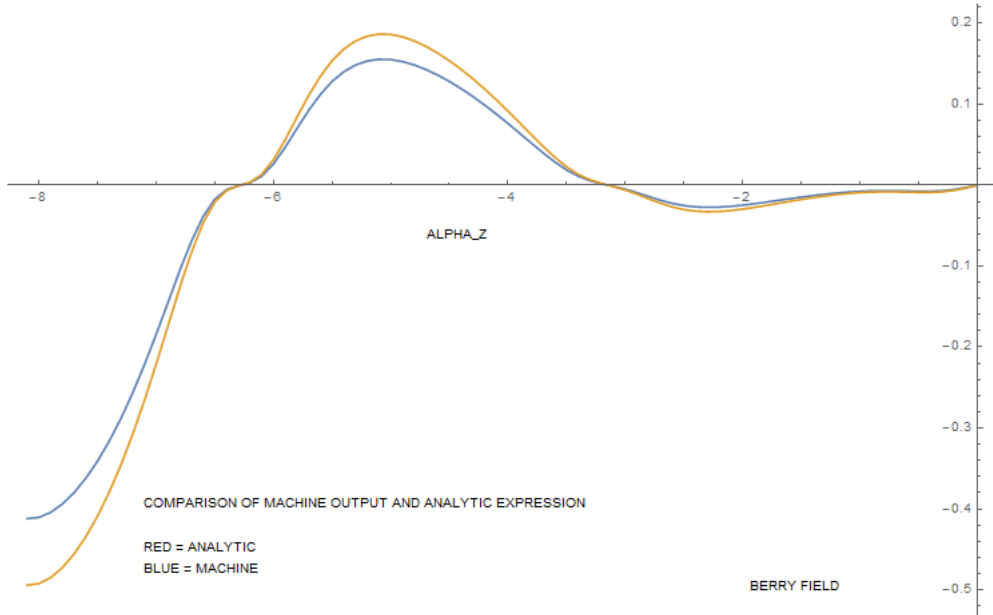


Figure 3.15: Comparison of the machine computed function and the analytic expression at $(2,2)$. The plots are much more similar in this case.

3.16 and 3.17. With this I conclude the section on the singly kicked system and move on to the more exotic doubly kicked Graphene system. It was the

3. SINGLY KICKED GRAPHENE

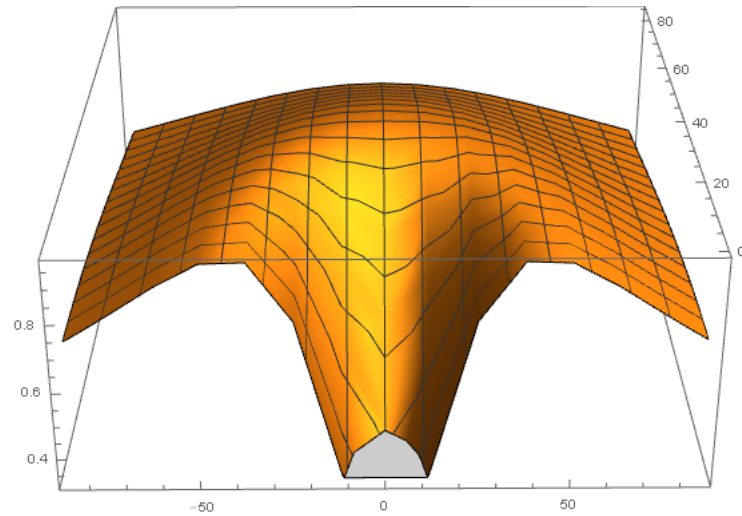


Figure 3.16: The "near Dirac point" Berry field computed from the analytic expression. Notice that the expression actually diverges and Mathematica cuts it off for the sake of representation.

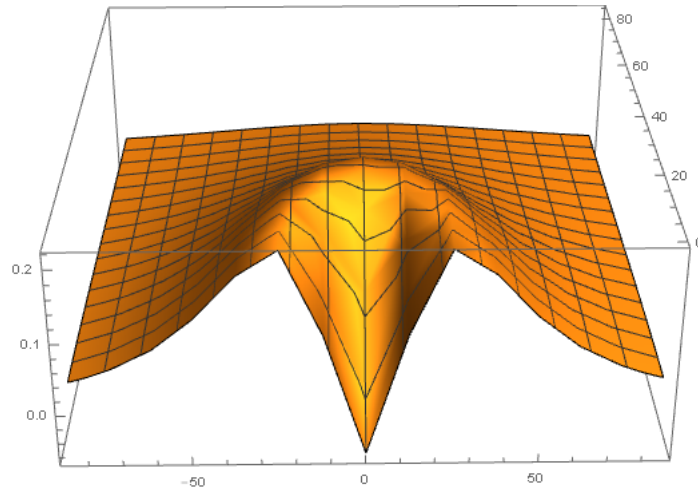


Figure 3.17: The "near Dirac point" Berry field computed by the machine. Notice that the expression converges instead and this is mostly due to the power series approximations.

efficient performance of the computer assisted verification procedure that drove me to directly use this technique as the first choice tool to break down and analyze the doubly kicked system independently. With the expressions becoming more and more complex, I was fortunate to have the procedures ready to be ported from the singly kicked case which ultimately led to the conclusion in the doubly kicked case too.

Chapter 4

Doubly Kicked Graphene

4.1 Clarifications

Before moving onto the doubly kicked system, it is prudent to understand what exactly does a Dirac train perturbation look like. For instance, in the case of the previous chapter, the Hamiltonian must have had the structure (not mathematically rigorous, but physically true) shown in Figure 4.1. I

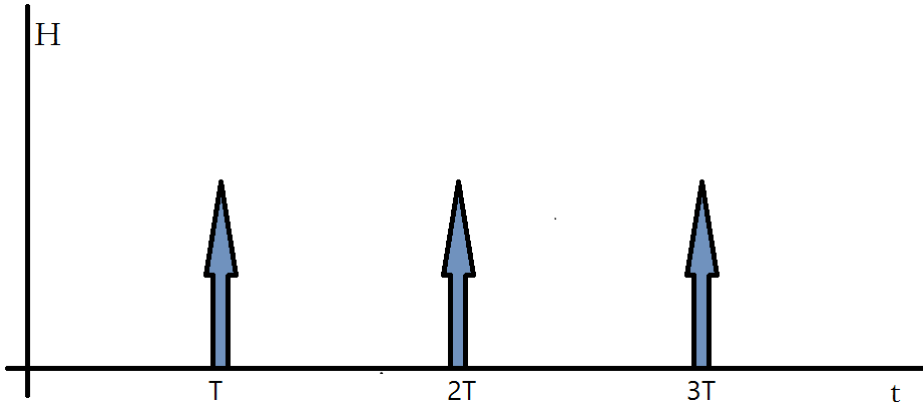


Figure 4.1: Singly kicked system. The arrows represent Dirac delta spikes normalized to $\bar{\alpha} \cdot \bar{\sigma}$.

have never actually found use for the full Hamiltonian of the doubly kicked system and I will use a much more qualitative discussion to compute the properties. Firstly, drawing an analogy to this graphical interpretation of the kicking Hamiltonian, the doubly kicked situation would look like the following, with two different kicking parameters $\bar{\alpha}_1$ and $\bar{\alpha}_2$ for two such kicks and the time interval between the kicks $\delta t < T$. There is a better upper bound to the value of δt too. This might not be apparent at a first glance, and it wasn't really obvious until I ran the simulation with a value of

4. DOUBLY KICKED GRAPHENE

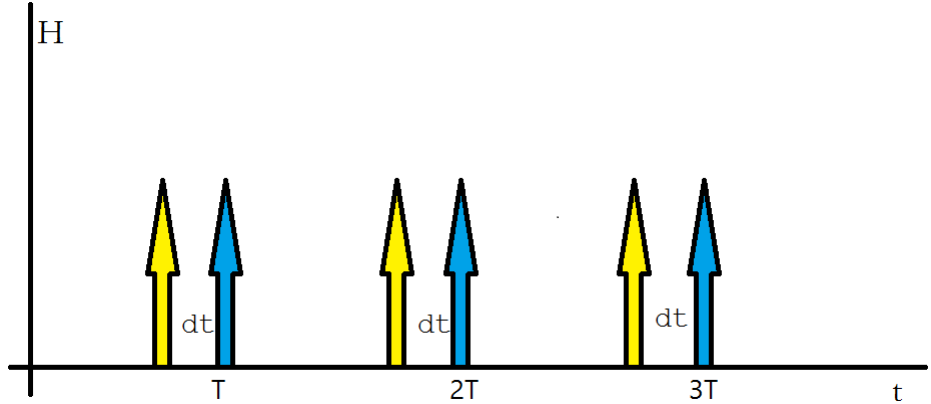


Figure 4.2: Doubly kicked system. The arrows represent Dirac delta spikes normalized to $\bar{\alpha}_1 \bar{\sigma}$ and $\bar{\alpha}_2 \bar{\sigma}$.

$\delta t > \frac{T}{2}$ when I figured that the bands actually cross each other, an unphysical picture for sure. The reason for δt to have this bound is quite simple. Let us say, on the contrary, that $\delta t = \frac{2T}{3}$. That is, the first kick happens after $\frac{T}{3}$ from the origin (which starts off with no kicks, clearly) and then the second kick arrives at T . The next kick is now scheduled to be $\frac{T}{3}$ time units away from this, but the new kicking pattern is not like the kicking pattern in the first cycle. That is, the Hamiltonian is no longer periodic, even physically (refer Figure 4.3). With the slight digression into this technical clarification

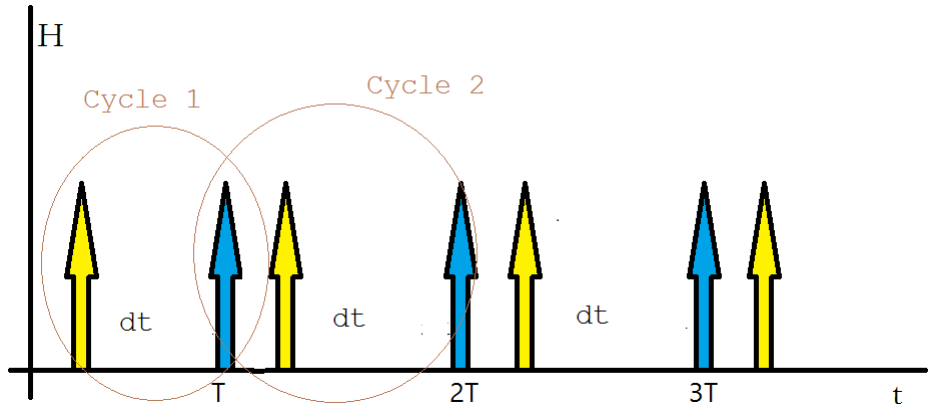


Figure 4.3: The anomalous case of double kicking no longer being periodic of $\delta t > \frac{T}{2}$. Note that the first cycle has a kick, gap, kick. The second cycle has kick, small gap, kick, large gap, kick. This is unlike Figure 4.2 where it was truly periodic.

complete, I will now resume the usual itinerary of analysis and simulation.

4.2 Analysis

The singly kicked case becomes a much better friend when I need to quantum mechanically describe the doubly kicked system so that I can start my analysis and derive the final $\hat{k} \cdot \vec{\sigma}$ as a function of $\alpha_{z,1}, \alpha_{z,2}$ and δt . Using the Floquet-Abel theorem directly, and referring to Fig. 4.2 as the kicking pattern, I can write the following description for the stroboscopic operator.

$$\mathcal{U}_{XYZ} = e^{-i\mathcal{H}_{XYZ}T} = e^{-\hat{\alpha}_2 \cdot \vec{\sigma}} e^{-i\mathcal{H}_k \delta t} e^{-i\hat{\alpha}_2 \cdot \vec{\sigma}} e^{-i\mathcal{H}_k(T-\delta t)}$$

The explanation to the structure is quite simple. There is the static Hamiltonian \mathcal{H}_k which operates for the time in the cycle when the first kick hasn't arrived yet, and this is equal to $T - \delta t$. When the first kick, quantified by $\hat{\alpha}_1$, arrives, the corresponding kick operator is used, and the static Hamiltonian exists for the inter-kick gap and then the second kick arrives, quantified by $\hat{\alpha}_2$. To reassure oneself, the parameter δt can be set to zero to see that it is nothing but the singly kicked case with a kicking amplitude of $\bar{\alpha} = \bar{\alpha}_1 + \bar{\alpha}_2$ and this makes sense graphically too as this just implies a superimposed Dirac spike at T intervals.

The next idea is to use the identity of the Pauli matrices

$$e^{ia(\hat{n} \cdot \vec{\sigma})} e^{ib(\hat{m} \cdot \vec{\sigma})} = e^{ic(\hat{k} \cdot \vec{\sigma})}$$

where

$$c = \text{ArcCos}(\text{Cos}(a)\text{Cos}(b) - \hat{n} \cdot \hat{m} \text{Sin}(a)\text{Sin}(b))$$

$$\hat{k} = \frac{1}{\text{Sin}(c)} (\hat{n} \text{Sin}(a)\text{Cos}(b) + \hat{m} \text{Sin}(b)\text{Cos}(a) - \hat{n} \times \hat{m} \text{Sin}(a)\text{Sin}(b))$$

In the singly kicked case, there were only two exponential functions which had to be collated using the identity but in this case I have four exponential functions. It should become obvious that the parenthesizing might be important for the collation. That is, the following question arises. Is the expression

$$\mathcal{U}_{XYZ,1} = e^{-i\mathcal{H}_{XYZ}T} = (e^{-\hat{\alpha}_2 \cdot \vec{\sigma}} e^{-i\mathcal{H}_k \delta t})(e^{-i\hat{\alpha}_2 \cdot \vec{\sigma}} e^{-i\mathcal{H}_k(T-\delta t)})$$

the same as this one?

$$\mathcal{U}_{XYZ,2} = e^{-i\mathcal{H}_{XYZ}T} = (e^{-\hat{\alpha}_2 \cdot \vec{\sigma}} (e^{-i\mathcal{H}_k \delta t} (e^{-i\hat{\alpha}_2 \cdot \vec{\sigma}} (e^{-i\mathcal{H}_k(T-\delta t)}))))$$

Again, for a first look it doesn't look like the order should matter as long as the multiplications are complying with the identity. But it is clear that the second way of parenthesizing is much more computationally resource consuming than the first one as in the $(A(B(C(D))))$ scheme, there is one term which keeps accumulating the resulting exponent iteratively and to

4. DOUBLY KICKED GRAPHENE

keep track of a symbolically complicated expression is harder than manipulating two smaller exponents with lesser number of symbols. For a personal benchmark the reader can run both the scripts `doubly-kicked-1.nb` and `doubly-kicked-2.nb` provided in the appendices for a practical perspective on this argument.

For the sake of completeness, I used the $(AB)(CD)$ type of parenthesizing for the computer assisted calculation while Tridev used the $(A(B(C(D))))$ type of parenthesizing for his analytical hand computations and comparisons were done with the outcomes. Due to the sheer size of the analytic calculation I only state the final result and the complete details can be worked out by the interested reader in the same spirit as the calculations done in Appendix A. Using the identity stated, I can reduce the first two and the last two parentheses into simpler exponentials in the Pauli basis. Rewriting the earlier expression

$$e^{-i\mathcal{H}_{XYZ}T} = (e^{-iA_2(\hat{\alpha}_2 \cdot \hat{\sigma})} e^{-iE(k)(\hat{\beta} \cdot \hat{\sigma})\delta t})(e^{-iA_1(\hat{\alpha}_1 \cdot \hat{\sigma})} e^{-iE(k)(\hat{\beta} \cdot \hat{\sigma})(T-\delta t)})$$

where the following correspondence can be made

$$A_2 \rightarrow -||\bar{\alpha}_2||$$

$$A_1 \rightarrow -||\bar{\alpha}_1||$$

$$B_2 \rightarrow E(k)\delta t$$

$$B_1 \rightarrow E(k)(T - \delta t)$$

$$\hat{\beta} \rightarrow \frac{(G(k), -H(k), 0)}{\sqrt{G(k)^2 + H(k)^2}}$$

These substitutions can be seen in the code snippet shown in Figure 4.4 and this should explain the simplicity of the computation of this style of parenthesizing when compared to the other style. Continuing from Fig 4.4, I can finally write the effective Hamiltonian for the doubly kicked system as the following

$$\mathcal{H}_{XYZ}(\alpha_1, \alpha_2, \delta t) = \frac{-c_0}{T} \times (\hat{k} \cdot \hat{\sigma})$$

where c_0, \hat{k} are the final components of the exponent after repeated usage of the Pauli identity. From here, it is the same old grind as the singly kicked case except that approximations need to be made multifold times and emphasis should be given on keeping the expressions simple so that further hand computations do not become messy. Before I get to the simulations and the results from the machine, I would like to state the approximate analytical functions for the mass term, which was the furthest we could get in terms of hand computed formulae. (Added to the size, the complication

4.2. Analysis

```

C2[{x_, y_}] = ArcCos[Cos[A2] * Cos[B2[{x, y}]] - (N2.m[{x, y}]) * Sin[A2] * Sin[B2[{x, y}]]];
khat2[{x_, y_}] = (1 / Sin[C2[{x, y}]]) * (Sin[A2] * Cos[B2[{x, y}]] * N2 +
Sin[B2[{x, y}]] * Cos[A2] * m[{x, y}] -
Sin[A2] * Sin[B2[{x, y}]] * Cross[N2, m[{x, y}]]);

C1[{x_, y_}] = ArcCos[Cos[A1] * Cos[B1[{x, y}]] - (N1.m[{x, y}]) * Sin[A1] * Sin[B1[{x, y}]]];
khat1[{x_, y_}] = (1 / Sin[C1[{x, y}]]) * (Sin[A1] * Cos[B1[{x, y}]] * N1 +
Sin[B1[{x, y}]] * Cos[A1] * m[{x, y}] -
Sin[A1] * Sin[B1[{x, y}]] * Cross[N1, m[{x, y}]]);

C0[{x_, y_}] = ArcCos[Cos[C2[{x, y}]] * Cos[C1[{x, y}]] - (khat2[{x, y}].khat1[{x, y}]) * Sin[C2[{x, y}]]];
khat[{x_, y_}] =
1 / (Sin[C0[{x, y}]]) *
(Sin[C2[{x, y}]] * Cos[C1[{x, y}]] * khat2[{x, y}] + Sin[C1[{x, y}]] * Cos[C2[{x, y}]] * khat1[{x, y}] -
Sin[C2[{x, y}]] * Sin[C1[{x, y}]] * Cross[khat2[{x, y}], khat1[{x, y}]]);

```

Figure 4.4: The Mathematica code snippet from the file doubly-kicked-1.nb provided in the appendices. Note: α_z^2 is not the square of α_z

with two α 's to handle along with a third parameter δt made writing down expressions even harder and confusing)

$$\begin{aligned} \Delta = \frac{1}{\sin \tilde{c}} & \left[-\frac{\sin^2 \alpha_z^1 \cos \alpha_z^2}{\sin(c)} - \frac{E(k)^2 T^2}{2} \left(\frac{\cos \alpha_z^2 \cos 2 \alpha_z^1}{\sin(c)} + \sin \alpha_z^2 \cos \alpha_z^1 \alpha_z^2 \right) + \right. \\ & \left. \delta t T E_k^2 \left(\frac{\cos \alpha_z^2 \cos 2 \alpha_z^1}{\sin(c)} - \frac{\alpha_z^1 \cos \alpha_z^2 \sin^2 \alpha_z^1}{\sin(c)} + \right. \right. \\ & \left. \left. \alpha_z^2 \sin \alpha_z^2 \cos \alpha_z^1 (1 - \sin \alpha_z^1) + \alpha_z^2 \sin \alpha_z^2 \cos \alpha_z^1 - \frac{\alpha_z^1 \cos \alpha_z^2 \delta t T^3 E(k)^4 \cos^2 \alpha_z^1}{2 \sin(c)} \right) \right] \end{aligned}$$

where \tilde{c} and c are such that

$$\begin{aligned} \cos \tilde{c} = \cos \alpha_z^2 \cos \alpha_z^1 & \left(1 - \frac{E(k)^2 T^2}{2} + E(k)^2 T^2 \delta t (1 - \sin \alpha_z^1) \right) - a_z^2 \left[-\frac{\sin \alpha_z^1 \sin \alpha_z^2}{\sin(c)} (\sin \alpha_z^1 + \right. \\ & \left. \frac{1}{2} E(k)^2 (T^2 - 2 T \delta t) \frac{\cos 2 \alpha_z^1}{\sin \alpha_z^1} - \right. \\ & \left. \frac{\sin \alpha_z^2 \alpha_z^1 \delta t T E(k)^2}{\sin(c)} (\sin^2 \alpha_z^1 + \frac{T^2 E(k)^2 \cos^2 \alpha_z^1}{2}) \right] \\ \sin(c) = \sqrt{1 - \cos^2 \alpha_z^1} & (1 - E(k)^2 T^2) \end{aligned}$$

4.3 Simulation and Computer Assisted Proof

In the same spirit as the discussion on the singly kicked system's properties, I start off with the band structures. It is assumed that $T = 1$ throughout and that $\delta t = \frac{T}{2.55} < \frac{T}{2}$. In addendum, I take both the kicks to be purely in z -direction and fix $\alpha_z^1 = \sqrt{3}$ and use α_z^2 as the modulating quantity along with δt to explore the nature of the doubly kicked system. Although the simulation is exploratory in nature, I will be mostly hunting for topological transition points and these points have characteristic behavior seen in the singly kicked case. These include the flipping of the Berry field, the closing of the band gap and the zeros of the mass term Δ , all of which will be demonstrated in this section.

In Figures 4.5 and 4.6 one can see the purely doubly z -kicked Graphene band structure for $\alpha_z^2 = 2\sqrt{3}$ and $\alpha_z^2 = 10\sqrt{3}$. A naive conclusion that can be drawn from these plots is that the band gap reduces with increasing α_z^2 .

However, testing the hypothesis with more α_z^2 samples shows that this

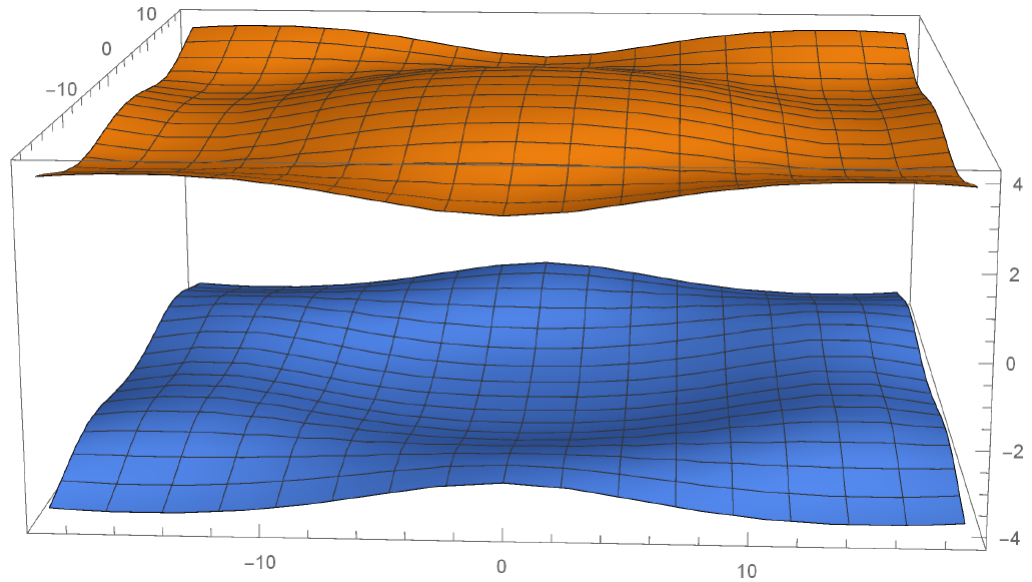


Figure 4.5: The band structure for purely doubly z -kicked Graphene for $\alpha_z^2 = 2\sqrt{3}$

might not be the case and that the band gap actually alternates with α_z^2 increasing. For instance, refer to Figures 4.7 and 4.8. This should give a hint as to the fact that the band gap and therefore the mass term both follow some oscillatory behavior, an encouraging sign. What is more encouraging is the fact that this oscillatory behavior leads to flips at exactly the same points the Berry field shows flipping. It can be seen that there is not one, but many

4.3. Simulation and Computer Assisted Proof

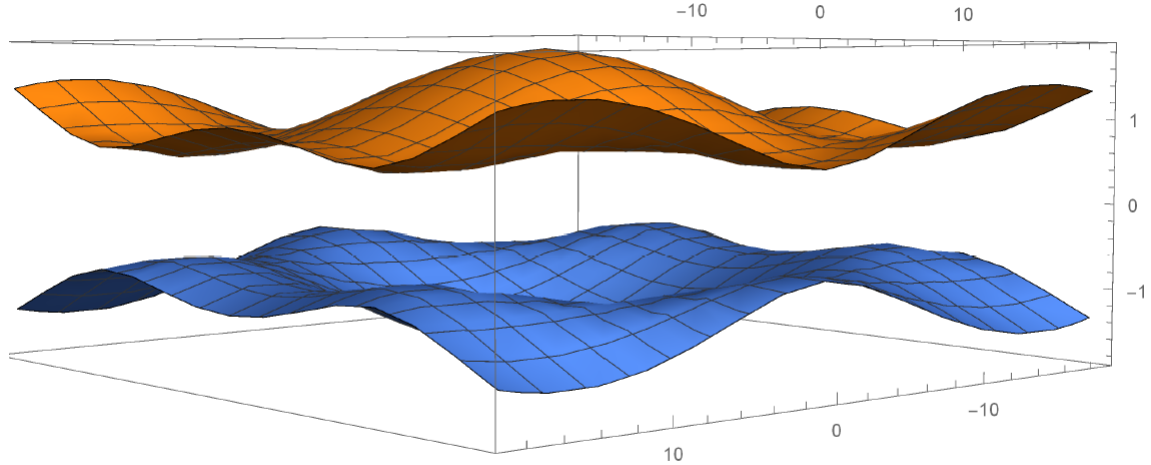


Figure 4.6: The band structure for purely doubly z-kicked Graphene for $\alpha_z^2 = 10\sqrt{3}$. Note the shift in the scale and the fact that the curvature becomes more prominent.

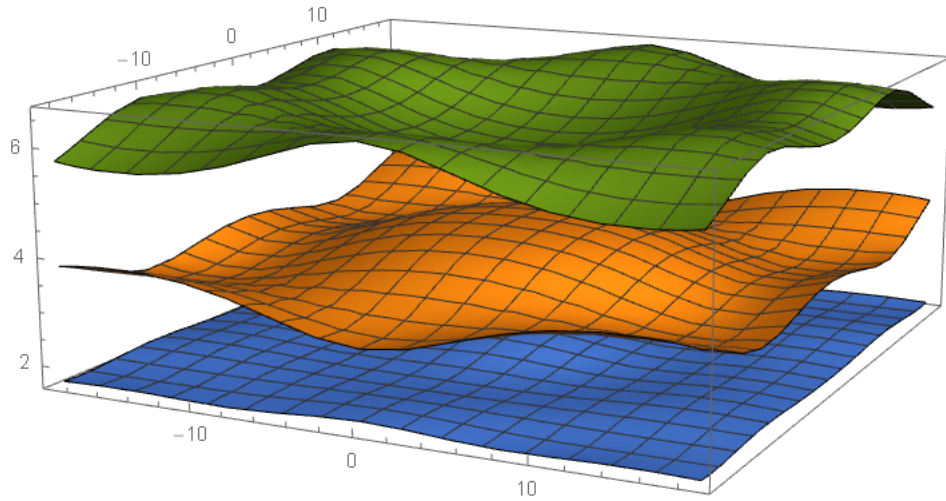


Figure 4.7: The upper half plane band structures for $\alpha_z^2 = 2\sqrt{3}$ in yellow, $\alpha_z^2 = 3\sqrt{3}$ in blue and $\alpha_z^2 = 4\sqrt{3}$ in red. The band comes close to the zero plane and then moves away.

points where the system goes through a topological transition and this is somewhat approximately tracked by the closing of the band gap. It will be seen later that this is exact near the Dirac points when one goes really close to these transition ranges. The next and the final task of the computer is to verify the analytic expressions for the mass term as a function of α_z^2 and δt . The calculations are done with the linear approximation in perspective and

4. DOUBLY KICKED GRAPHENE

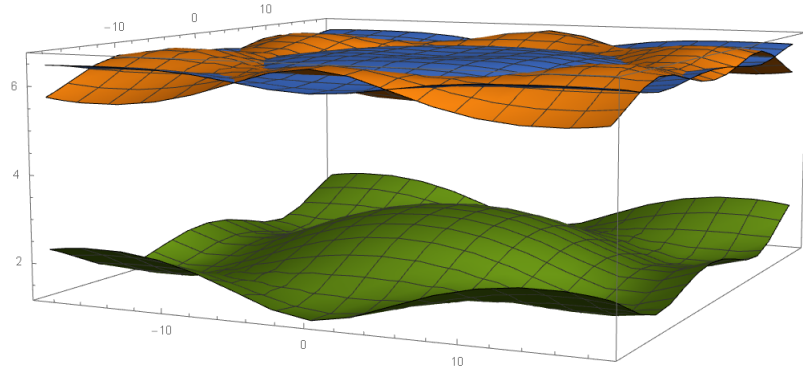


Figure 4.8: The upper half plane band structures for $\alpha_z^2 = 4\sqrt{3}$ in yellow, $\alpha_z^2 = 5\sqrt{3}$ in blue and $\alpha_z^2 = 6\sqrt{3}$ in green. The bands show reverse polarity before coming closer to the zero plane again.

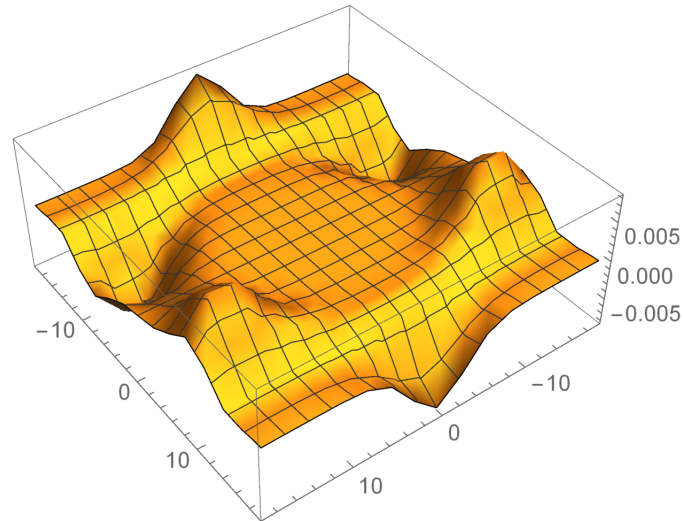


Figure 4.9: The Berry field for the purely doubly z-kicked Graphene when $\alpha_z^2 = \sqrt{3}$. This was taken as the base case for further comparisons. Note that the Lorentzian nature of the Dirac cones is very stark. Just as a reminder, the FWHM of the Lorentzian is a rule-of-thumb indicator of the band gap.

the comparisons are explained in the descriptions for each plot.

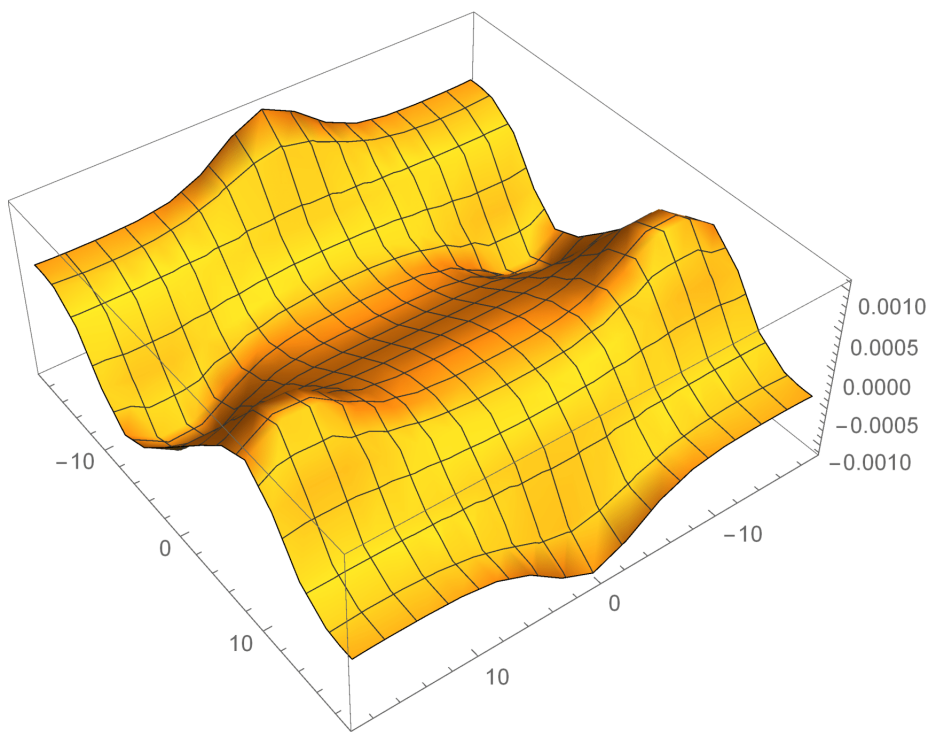


Figure 4.10: The Berry field for the purely doubly z-kicked Graphene when $\alpha_z^2 = 2\sqrt{3}$. The peaks and the valleys become smoother and the Lorentzian approximation turns out to be almost exact. So far there was no phase transition related to the Berry field flipping was noted.

4. DOUBLY KICKED GRAPHENE

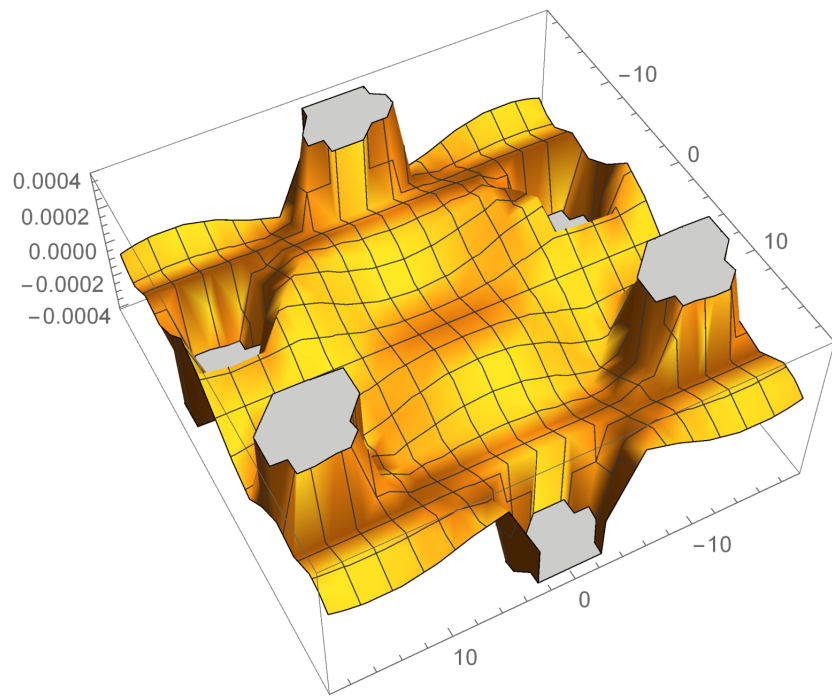


Figure 4.11: The Berry field for the purely doubly z-kicked Graphene when $\alpha_z^2 = 2.6\sqrt{3}$. The peaks and the valleys become sharp and distinct Dirac spikes start forming around the FBZ. This also implies the band gap lowering, refer Figure 4.7.

4.3. Simulation and Computer Assisted Proof

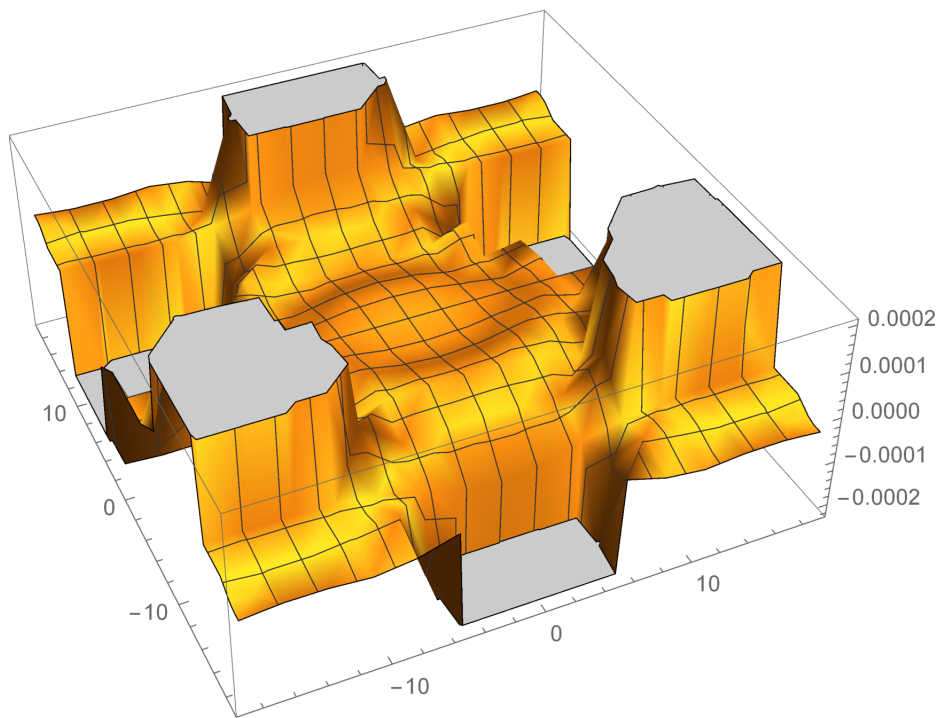


Figure 4.12: The Berry field for the purely doubly z-kicked Graphene when $\alpha_z^2 = 2.7\sqrt{3}$. The peaks and the valleys become wide and almost rectangular. This is probably the limit of the machine precision and it shows an incoming phase flip point.

4. DOUBLY KICKED GRAPHENE

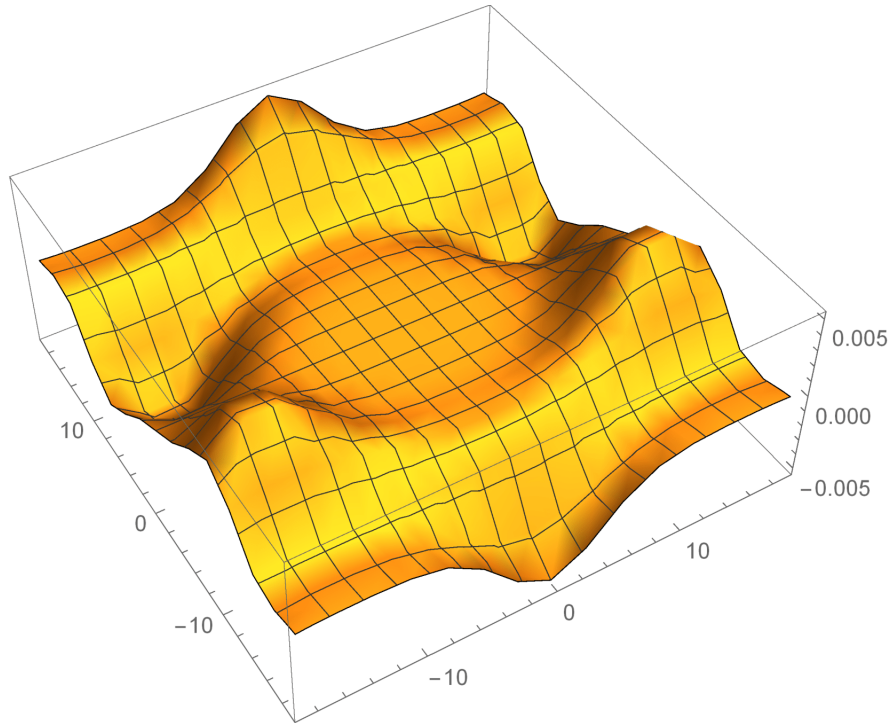


Figure 4.13: The Berry field for the purely doubly z-kicked Graphene when $\alpha_z^2 = 2.9\sqrt{3}$. The peaks and the valleys surprisingly become smooth once again. An initial naive guess would be that we already passed the phase transition point but the Berry field has hardly flipped.

4.3. Simulation and Computer Assisted Proof

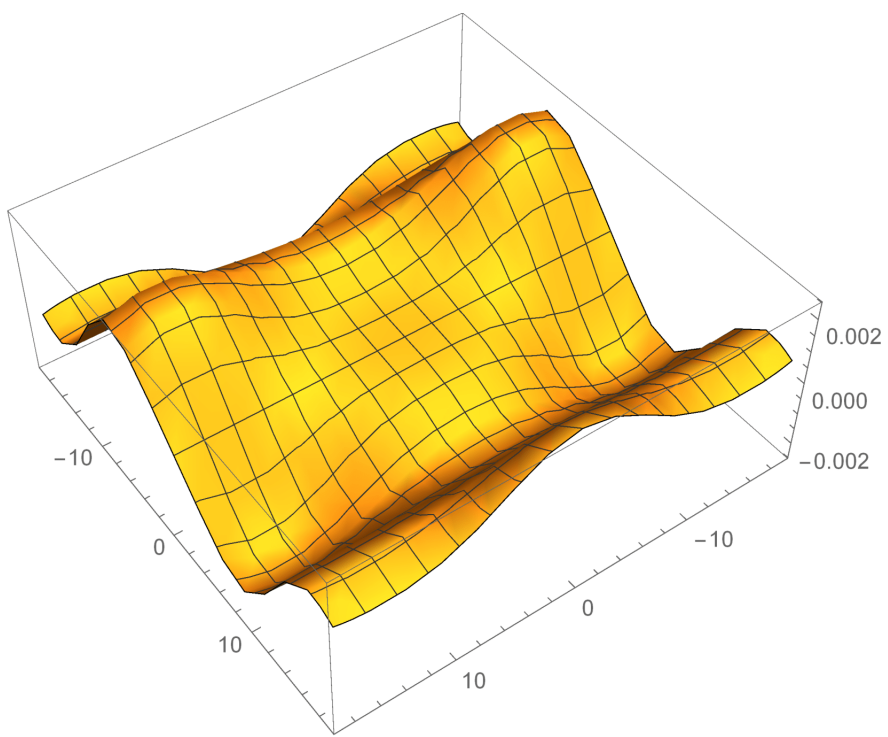


Figure 4.14: The Berry field for the purely doubly z-kicked Graphene when $\alpha_z^2 = 3\sqrt{3}$. The transition has occurred! The peaks and valleys have flipped completely.

4. DOUBLY KICKED GRAPHENE

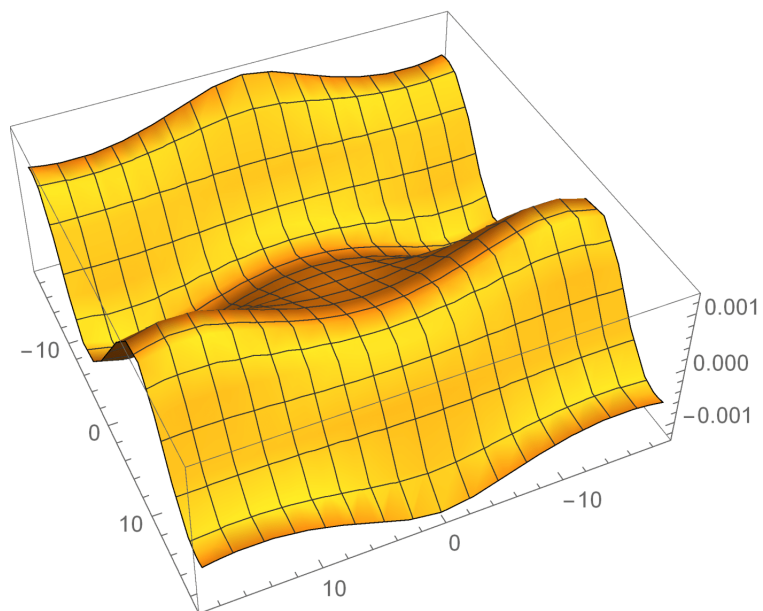


Figure 4.15: The Berry field for the purely doubly z-kicked Graphene when $\alpha_z^2 = 5\sqrt{3}$. Another transition has occurred! The peaks and valleys have flipped once again. Notice that this is similar to Figure 4.9 and the Lorentzian Dirac cones have resurfaced.

4.3. Simulation and Computer Assisted Proof

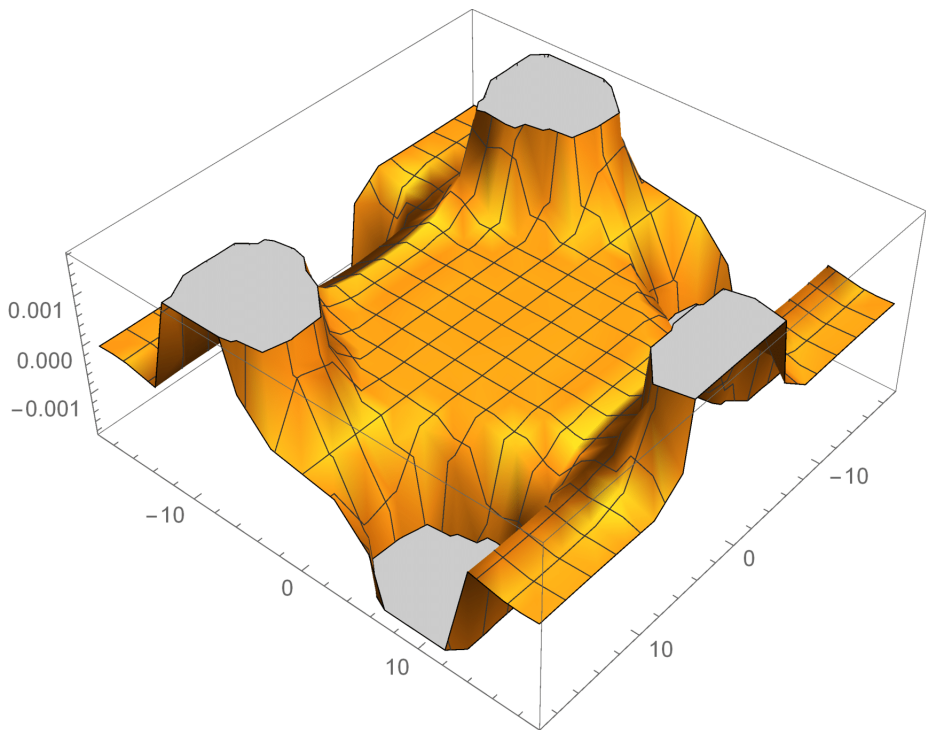


Figure 4.16: The Berry field for the purely doubly z-kicked Graphene when $\alpha_z^2 = 10\sqrt{3}$. This is a flip away from the previous image and thus the doubly kicked system has gone through another topological transition.

4. DOUBLY KICKED GRAPHENE

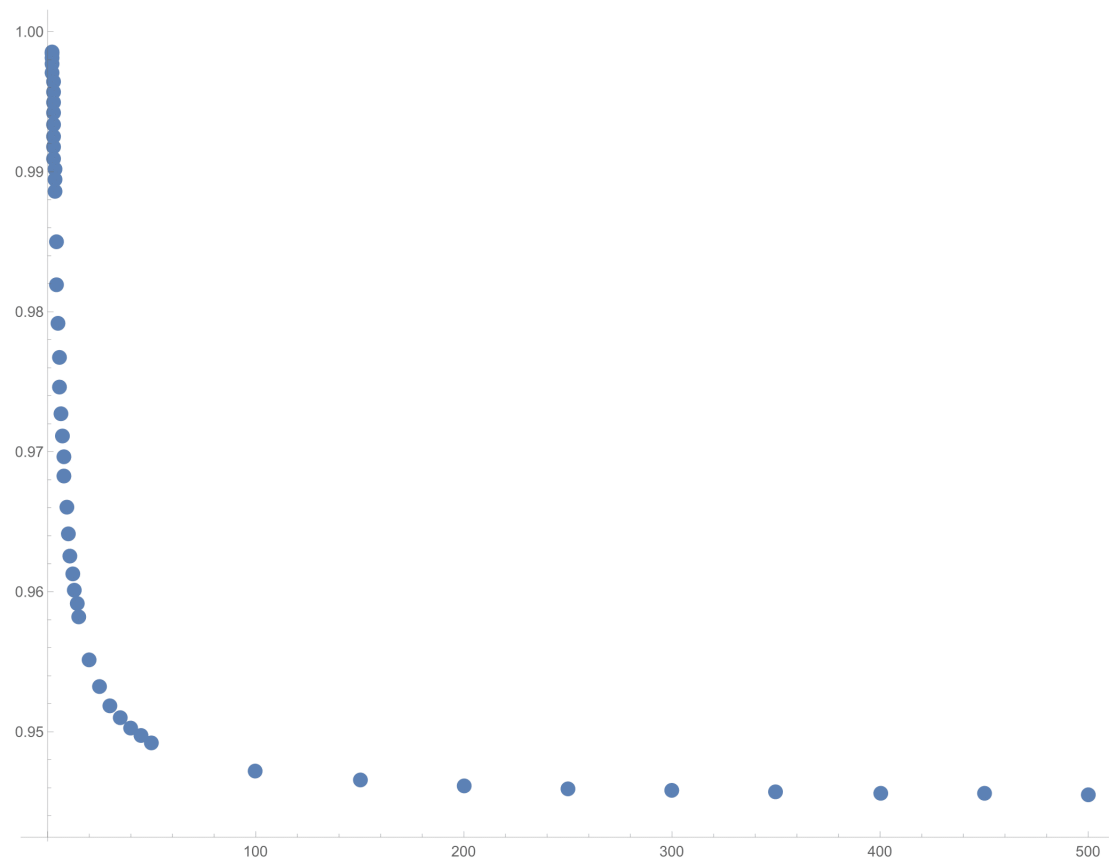


Figure 4.17: The variation of the mass term with δt when $\alpha_z^2 = 2\sqrt{3}$ as computed by the machine. Notice that it decreases for increasing δt but saturates at a value. It is to be seen as to how well this trend performs with the analytic expression stated in the text.

4.3. Simulation and Computer Assisted Proof



Figure 4.18: The variation of the mass term with δt when $\alpha_z^2 = 2\sqrt{3}$ as computed by the approximate analytic expression. Notice that it decreases for increasing δt but saturates at a different value than the machine, probably due to the same scaling issue encountered in singly kicked system. However it has remarkably the same behavior as the machine computed result.

4. DOUBLY KICKED GRAPHENE

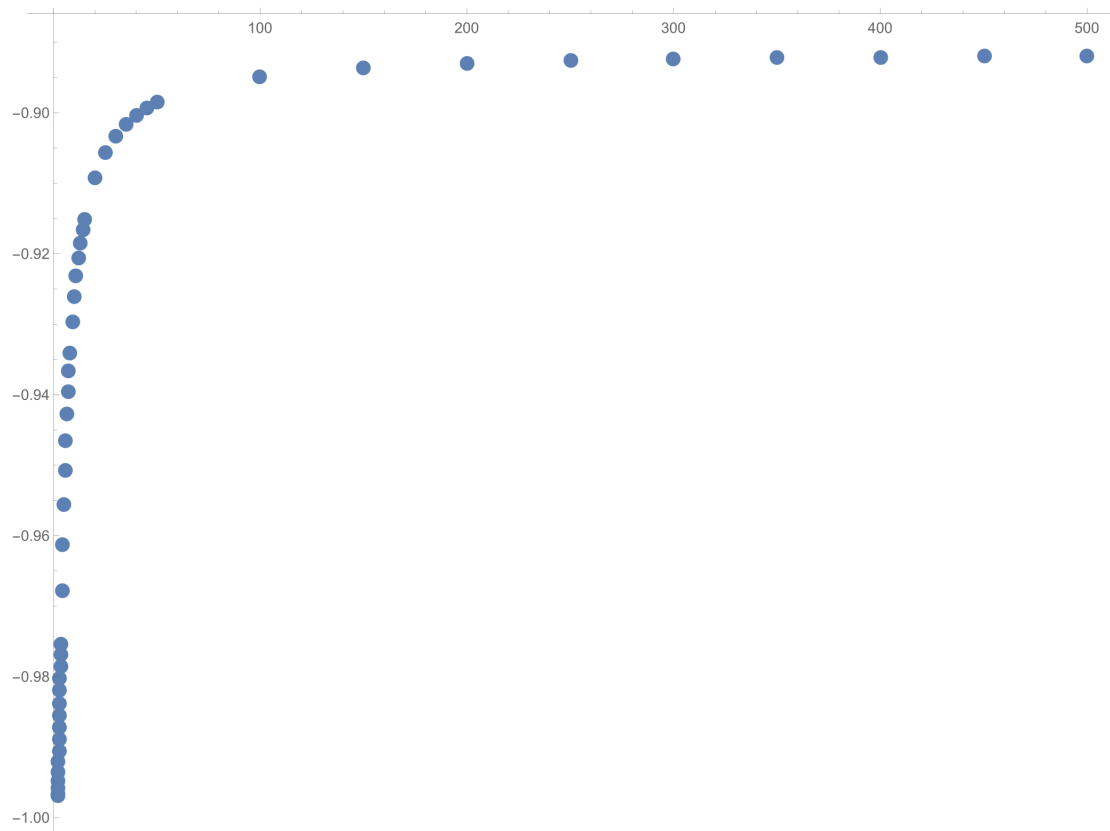


Figure 4.19: The variation of the mass term with δt when $\alpha_z^2 = 3\sqrt{3}$ as computed by the machine. Notice that it increases for increasing δt but saturates at a value. The transition has occurred signified by the change in the trend.

4.3. Simulation and Computer Assisted Proof

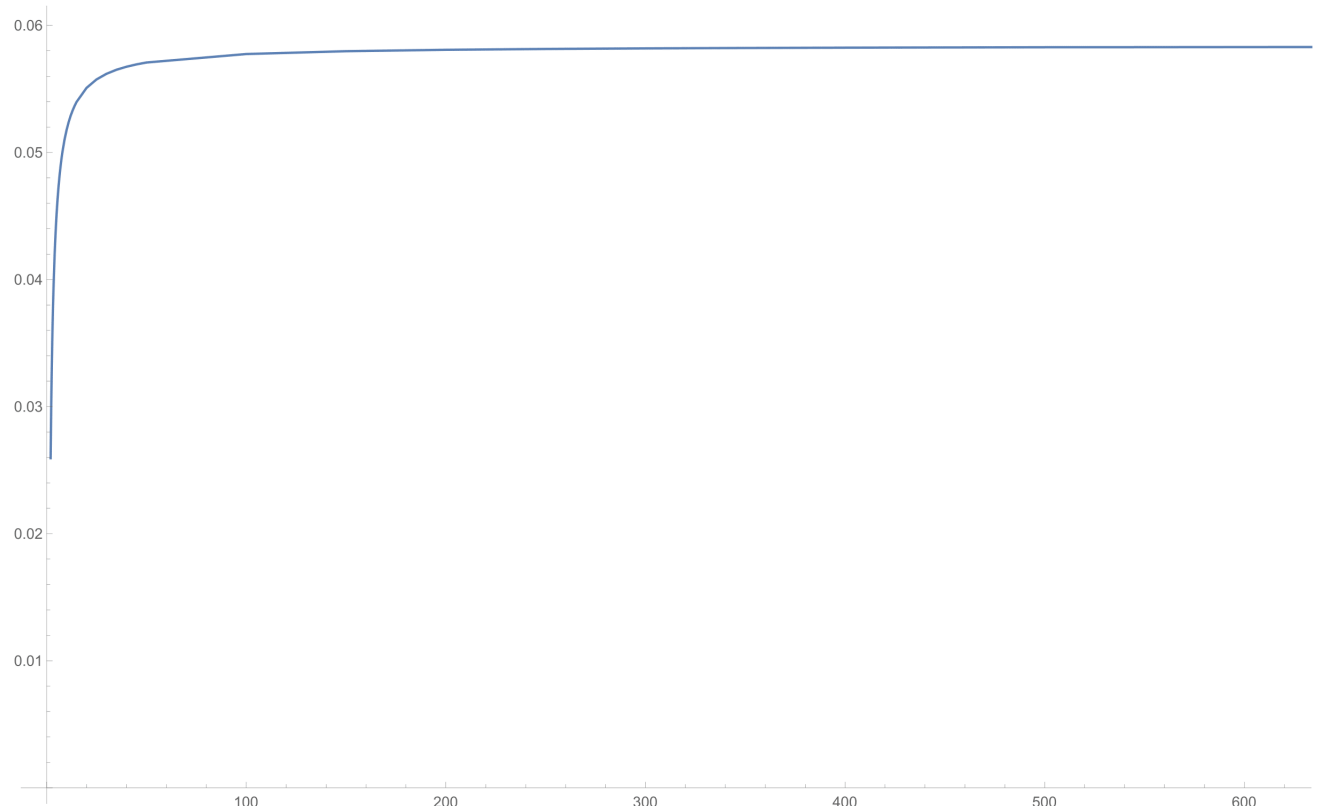


Figure 4.20: The variation of the mass term with δt when $\alpha_z^2 = 3\sqrt{3}$ as computed by the approximate analytic expression. Notice that it increases monotonically but saturates at a different value yet again. The transition has been verified by this.

4. DOUBLY KICKED GRAPHENE

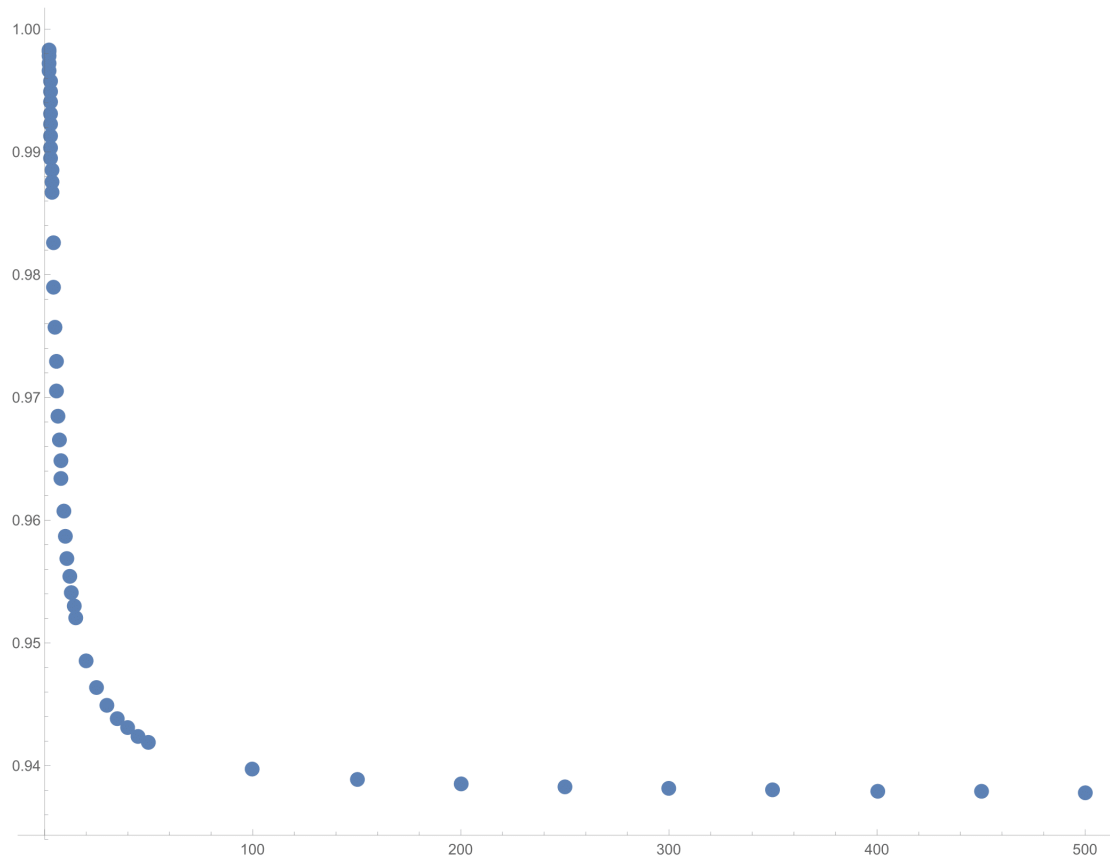


Figure 4.21: The variation of the mass term with δt when $\alpha_z^2 = 5\sqrt{3}$ as computed by the machine. Notice that it decreases once again for increasing δt but saturates at a value. The transition has occurred signified by the change in the trend once again.

4.3. Simulation and Computer Assisted Proof

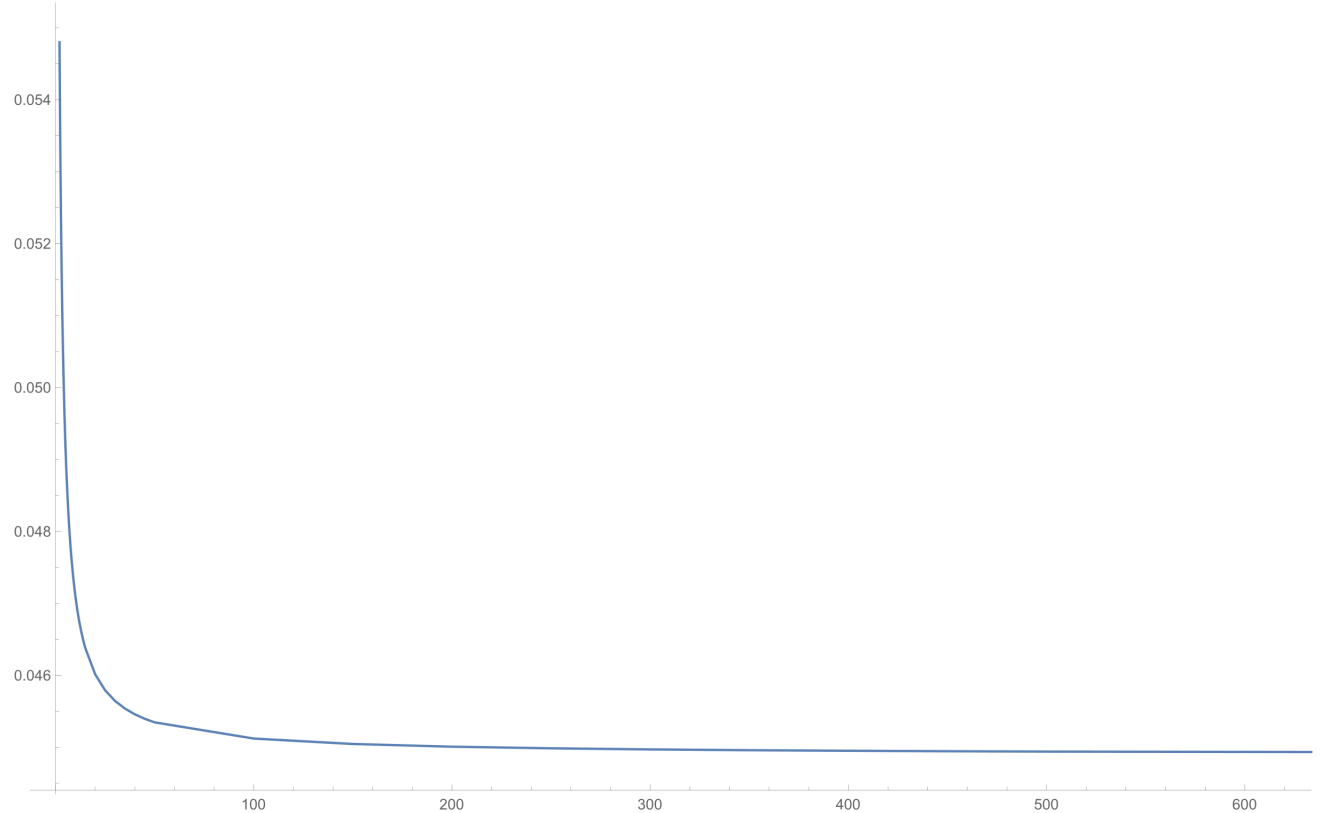


Figure 4.22: The variation of the mass term with δt when $\alpha_z^2 = 5\sqrt{3}$ as computed by the approximate analytic expression. Notice that it decreases monotonically. The transition has been verified yet again by this.

4. DOUBLY KICKED GRAPHENE

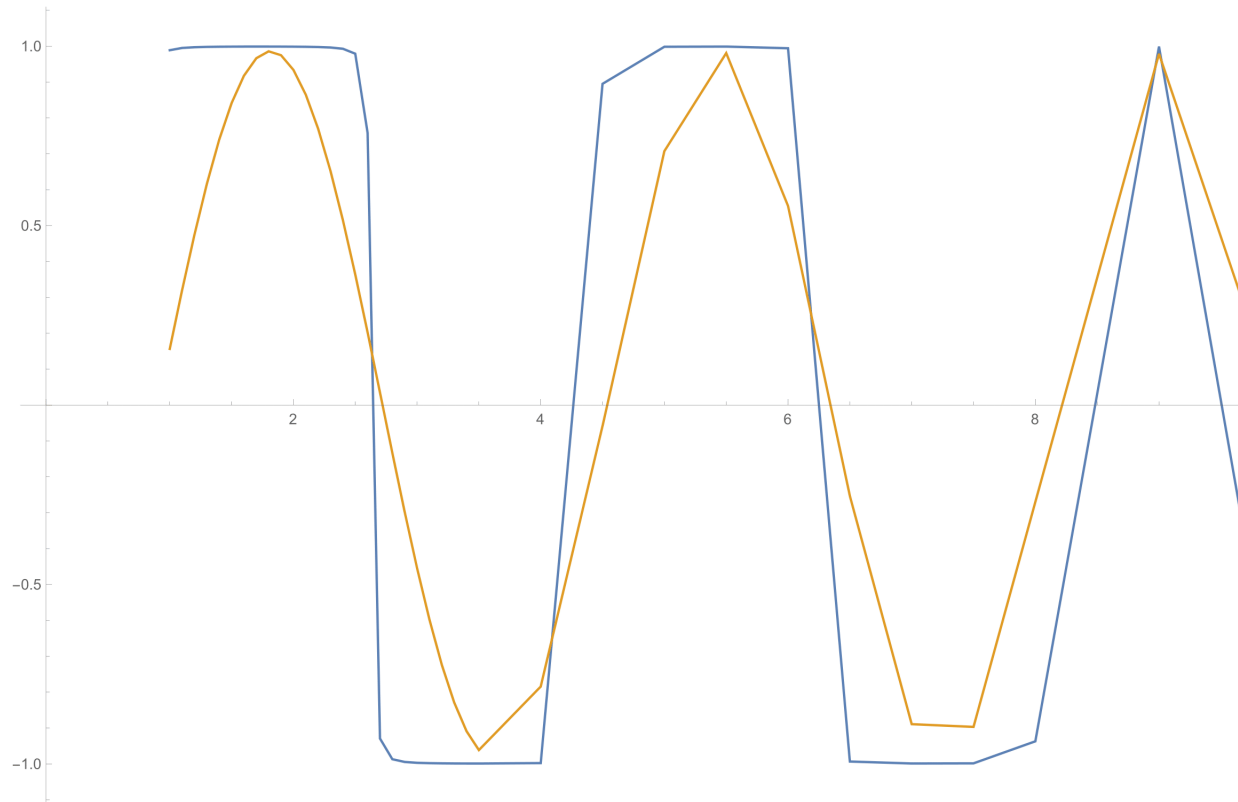


Figure 4.23: Probably the most decisive piece of evidence which shows the amount of correlation between the machine computed data, the analytic expression and the points of phase transition. This is the plot of the mass term with a fixed δt and α_z^2 increasing. The blue plot represents the machine computed result and the red plot represents the analytic expression. It can be seen that the mass term goes to zero and then changes sign at approximately $\alpha_z^2 = 3, 5, 7, 9$ and so on and it can be seen from the Berry field plots or from the δt variation plots to check that these are the points where there is a mirror flip in the trend. The analytic expression is a smoother sinusoid while the machine result shows a much more rectangular shape.

Chapter 5

Epilogue

With Figure 4.23, the thesis has come to an apparent end. The next few sections include the appendices, the data sets used for the plots and some bibliography. It had been a long journey, starting from the most basic unperturbed Graphene system to the restricted doubly kicked system. One common feature to the singly and doubly kicked system which was probably not exposed upon in the previous sections is the breaking of time reversal symmetry. Although theoretically speaking the Dirac delta train perturbation goes from negative time to positive time, the simulations and the analytic computations were done with the single sided Dirac train, that is, t was always positive. That is, the system is technically not symmetric about the y axis, and it is suspected that this is the underlying cause for observing the transitions and shows a link to the model worked on by F. Duncan Haldane which won him the Nobel Prize this year. However, the emphasis in the two sections of kicked Graphene was more on the amount of correlation between hand computation and the approximate machine result. This methodology was tested with the fully hand computed singly kicked case and it was then tested on the doubly kicked case. It is truly beautiful to see that it worked out well for the latter system and this leads to a vision in the future when physical scenarios can be automatically analyzed using pure symbolic manipulation. This ends up in saving the user some time for doing something more profitable than going through the drivel of routine calculations and committing mistakes en route to the conclusion. The topological point of view presented here now gives a viable way to identify the Chern insulators and their analysis becomes much more streamlined and organized. For a symbolic math problem, these two are a tad bit complex and Mathematica performs brilliantly even if it had walls and walls of symbols to crunch (kudos to the people at Wolfram Research). It is only to be seen as to how far this can be done and it would be an interesting exercise to construct such workflows for more general situations in modern physics.

Appendix A

Analytic derivation of the Singly Kicked Berry Field

As promised before, here is the full derivation of the compact analytic expression of the Berry field for a singly kicked Graphene system. It starts from the commutator formula for the Berry tensor from the density matrix and the subsequent reduction of the same into an expression involving the commutator of the derivatives of the matrix $\hat{k} \cdot \bar{\sigma}$. The two unique matrix elements are listed below once again for the sake of continuity

$$(\hat{k} \cdot \bar{\sigma})_{1,1} = \frac{1}{\sqrt{1 - (1 - T^2 \gamma^2 \frac{9a^2}{4} (k_x^2 + k_y^2)) \cos^2 \alpha_z}} - \sin \alpha_z (1 - T^2 \gamma^2 \frac{9a^2}{8} (k_x^2 + k_y^2))$$

$$(\hat{k} \cdot \bar{\sigma})_{1,2} = \frac{1}{\sqrt{1 - (1 - T^2 \gamma^2 \frac{9a^2}{4} (k_x^2 + k_y^2)) \cos^2 \alpha_z}} ((-\frac{3a\gamma T}{2} k_y \cos \alpha_z + \frac{3a}{2} \alpha_z k_x \gamma T \sin \alpha_z) + i(\frac{3a}{2} k_x \gamma T \cos \alpha_z + \frac{3a}{2} \gamma T k_y \alpha_z \sin \alpha_z))$$

It can be seen that the factor

$$\frac{3a\gamma T}{2\sqrt{1 - (1 - T^2 \gamma^2 \frac{9a^2}{4} (k_x^2 + k_y^2)) \cos^2 \alpha_z}}$$

is common for the matrix and on subsequent factorization, we obtain another matrix multiplied by the above constant, whose (1,1) element is the mass term which was stated in section 3.2 and is restated here for the sake of continuity

$$\Delta = -\sin \alpha_z (\frac{2}{3a\gamma T} - \frac{3a\gamma T}{4} (k_x^2 + k_y^2))$$

A. ANALYTIC DERIVATION OF THE SINGLY KICKED BERRY FIELD

I call this matrix \hat{A} . Calculating the partial derivatives which will be a part of the commutator eventually, we obtain the following

$$\begin{aligned}\partial_{k_x} \hat{k} \cdot \bar{\sigma} &= \frac{3a\gamma T}{4(1 - (1 - T^2\gamma^2 \frac{9a^2}{4}(k_x^2 + k_y^2))\cos^2\alpha_z)^{\frac{3}{2}}} \times T^2\gamma^2 \frac{9a^2}{2} k_x \cos^2\alpha_z \times A \\ &+ \frac{3a\gamma T}{2\sqrt{1 - (1 - T^2\gamma^2 \frac{9a^2}{4}(k_x^2 + k_y^2))\cos^2\alpha_z}} \begin{bmatrix} \sin\alpha_z \frac{3aT}{2} k_x & \alpha_z \sin\alpha_z + i\cos\alpha_z \\ \alpha_z \sin\alpha_z - i\cos\alpha_z & -\sin\alpha_z \frac{3aT}{2} k_x \end{bmatrix} \\ \partial_{k_y} \hat{k} \cdot \bar{\sigma} &= \frac{3a\gamma T}{4(1 - (1 - T^2\gamma^2 \frac{9a^2}{4}(k_x^2 + k_y^2))\cos^2\alpha_z)^{\frac{3}{2}}} \times T^2\gamma^2 \frac{9a^2}{2} k_y \cos^2\alpha_z \times A \\ &+ \frac{3a\gamma T}{2\sqrt{1 - (1 - T^2\gamma^2 \frac{9a^2}{4}(k_x^2 + k_y^2))\cos^2\alpha_z}} \begin{bmatrix} \sin\alpha_z \frac{3aT}{2} k_y & -\cos\alpha_z + i\alpha_z \sin\alpha_z \\ -\cos\alpha_z - i\alpha_z \sin\alpha_z & -\sin\alpha_z \frac{3aT}{2} k_y \end{bmatrix}\end{aligned}$$

It should become clear that if we start computing the commutator using these expressions the going will get rough, but the Pauli basis is here to the rescue yet again. The reason for using the Pauli basis is because I know the commutator relations for the individual Pauli matrices directly.

$$\begin{aligned}\partial_{k_x} \hat{k} \cdot \bar{\sigma} &= \frac{3a\gamma T}{2\sqrt{1 - (1 - T^2\gamma^2 \frac{9a^2}{4}(k_x^2 + k_y^2))\cos^2\alpha_z}} (\sin\alpha_z (\frac{3a\gamma T k_x}{2} - \\ &\quad k_x T^2 \gamma^2 9a^2 \cos^2\alpha_z [\frac{2}{3a\gamma T} - \frac{3a\gamma T}{4}(k_x^2 + k_y^2)]) \sigma_z + (\frac{\cos^2\alpha_z T^2 \gamma^2 \frac{9a^2}{4} k_x (\alpha_z k_x \sin\alpha_z - k_y \cos\alpha_z)}{1 - (1 - T^2\gamma^2 \frac{9a^2}{4}(k_x^2 + k_y^2))\cos^2\alpha_z} \\ &\quad + \alpha_z \sin\alpha_z) \sigma_x - (\frac{\cos^2\alpha_z T^2 \gamma^2 \frac{9a^2}{4} k_x (k_x \cos\alpha_z + k_y \alpha_z \sin\alpha_z)}{1 - (1 - T^2\gamma^2 \frac{9a^2}{4}(k_x^2 + k_y^2))\cos^2\alpha_z} + \cos\alpha_z) \sigma_y) \\ \partial_{k_y} \hat{k} \cdot \bar{\sigma} &= \frac{3a\gamma T}{2\sqrt{1 - (1 - T^2\gamma^2 \frac{9a^2}{4}(k_x^2 + k_y^2))\cos^2\alpha_z}} (\sin\alpha_z (\frac{3a\gamma T k_y}{2} - \\ &\quad k_y T^2 \gamma^2 9a^2 \cos^2\alpha_z [\frac{2}{3a\gamma T} - \frac{3a\gamma T}{4}(k_x^2 + k_y^2)]) \sigma_z + (\frac{\cos^2\alpha_z T^2 \gamma^2 \frac{9a^2}{4} k_y (\alpha_z k_x \sin\alpha_z - k_y \cos\alpha_z)}{1 - (1 - T^2\gamma^2 \frac{9a^2}{4}(k_x^2 + k_y^2))\cos^2\alpha_z} \\ &\quad + -\cos\alpha_z) \sigma_x - (\frac{\cos^2\alpha_z T^2 \gamma^2 \frac{9a^2}{4} k_y (k_x \cos\alpha_z + k_y \alpha_z \sin\alpha_z)}{1 - (1 - T^2\gamma^2 \frac{9a^2}{4}(k_x^2 + k_y^2))\cos^2\alpha_z} + \alpha_z \sin\alpha_z) \sigma_y)\end{aligned}$$

To recapitulate, the commutator relations between the Pauli matrices are given by

$$[\sigma_x, \sigma_y] = 2i\sigma_z$$

$$[\sigma_y, \sigma_z] = 2i\sigma_x$$

$$[\sigma_z, \sigma_x] = 2i\sigma_y$$

and with some useful notation

$$\omega = \frac{3a\gamma T}{2}$$

$$1 - (1 - T^2\gamma^2 \frac{9a^2}{4}(k_x^2 + k_y^2)) \cos^2 \alpha_z = \Omega$$

With these substitutions and simplifications, and after a little algebra, the terms cancel out due to the visible symmetry of the components of the derivatives and the Pauli commutator relations and I end up with the following two unique matrix elements for

$$[\partial_{k_x} \hat{k} \cdot \bar{\sigma}, \partial_{k_y} \hat{k} \cdot \bar{\sigma}]_{(1,1)} = \frac{-\omega^2 \cos^2 \alpha_z}{\Omega} [(k_x \cos \alpha_z + k_y \alpha_z \sin \alpha_z)^2 + (k_x \alpha_z \sin \alpha_z - k_y \cos \alpha_z)^2]$$

$$[\partial_{k_x} \hat{k} \cdot \bar{\sigma}, \partial_{k_y} \hat{k} \cdot \bar{\sigma}]_{(2,1)} = \sin \alpha_z (k_x \alpha_z \sin \alpha_z - k_y \cos \alpha_z) [\omega - \frac{\omega^2 \cos^2 \alpha_z}{\Omega} (\frac{1}{\omega} - \frac{\omega}{2}(k_x^2 + k_y^2))] +$$

$$i \sin \alpha_z (k_x \cos \alpha_z + k_y \alpha_z \sin \alpha_z) [-\omega + \frac{\omega^2 \cos^2 \alpha_z}{\Omega} (\frac{1}{\omega} - \frac{\omega}{2}(k_x^2 + k_y^2))]$$

The final expression which is sought then turns out to be

$$Tr(\hat{k} \cdot \bar{\sigma} [\partial_{k_x} \hat{k} \cdot \bar{\sigma}, \partial_{k_y} \hat{k} \cdot \bar{\sigma}]) = \frac{2i\omega^3}{\Omega^{\frac{3}{2}}} \left[\frac{2\omega^2 \sin \alpha_z \cos^2 \alpha_z}{\Omega} [(k_x \cos \alpha_z + k_y \alpha_z \sin \alpha_z)^2 + (k_x \alpha_z \sin \alpha_z - k_y \cos \alpha_z)^2] \right.$$

$$(\frac{1}{\omega} - \frac{\omega}{2}(k_x^2 + k_y^2)) + \sin \alpha_z (\omega - \frac{\omega^2 \cos^2 \alpha_z}{\Omega} (\frac{1}{\omega} - \frac{\omega}{2}(k_x^2 + k_y^2))) [(-k_y \cos \alpha_z + \alpha_z k_x \sin \alpha_z) +$$

$$i(k_x \cos \alpha_z + k_y \alpha_z \sin \alpha_z)] [(k_x \alpha_z \sin \alpha_z - k_y \cos \alpha_z) - i(k_x \cos \alpha_z + k_y \alpha_z \sin \alpha_z)]$$

$$+ \sin \alpha_z (\omega - \frac{\omega^2 \cos^2 \alpha_z}{\Omega} (\frac{1}{\omega} - \frac{\omega}{2}(k_x^2 + k_y^2))) [(-k_y \cos \alpha_z + \alpha_z k_x \sin \alpha_z) -$$

$$i(k_x \cos \alpha_z + k_y \alpha_z \sin \alpha_z)] [(k_x \alpha_z \sin \alpha_z - k_y \cos \alpha_z) + i(k_x \cos \alpha_z + k_y \alpha_z \sin \alpha_z)]]$$

Expanding the squares and evaluating the expression again it can be reduced to the following compact form with a few steps of manipulation

$$Tr(\hat{k} \cdot \bar{\sigma} [\partial_{k_x} \hat{k} \cdot \bar{\sigma}, \partial_{k_y} \hat{k} \cdot \bar{\sigma}]) = \frac{4i \sin \alpha_z \omega^4}{\Omega^{\frac{3}{2}}} [(k_x \cos \alpha_z + k_y \alpha_z \sin \alpha_z)^2 + (k_x \alpha_z \sin \alpha_z - k_y \cos \alpha_z)^2]$$

Expanding the final square terms and cancelling the cross terms, we reach our goal

$$\mathcal{F}_{k_x k_y} = -\frac{1}{2} \frac{\omega^4 \sin(\alpha_z) (k_x^2 + k_y^2) (\alpha_z^2 \sin^2(\alpha_z) + \cos^2(\alpha_z))}{(1 - [1 - \omega^2(k_x^2 + k_y^2)] \cos^2(\alpha_z))^{\frac{3}{2}}}$$

This ends the sketch of the derivation of the Berry field for the singly kicked Graphene system.

Appendix B

The Hall Effect

B.1 Classical Hall Effect

Edwin Herbert Hall discovered in 1879 that transverse voltages appear in electrical conductors when there is a current through them and an external magnetic field is switched on (it was his doctoral thesis at Johns Hopkins University in Baltimore, Maryland). The explanation of this (classical) Hall effect is not very difficult and a very simplified calculation can be done when the magnetic field is not very strong. Assuming the charge carriers are non interacting, we can compute the statistical motion as the motion of a single electron (this does not imply that the other electrons are not important, they define the plane in which motion takes place). Writing the Lorentz force law,

$$m \frac{d\vec{v}}{dt} = q\vec{v} \times \vec{B}$$

where q is the charge of the charge carrier in the field. The electric field which leads to the current can be cancelled out by moving in a frame in which it can be nulled, and this assumption is made for now (the magnetic field will be modified, but it can still be seen as a pure field as long as the frame is known). The solution to the Lorentz force equation is a circular trajectory given by the following parametrized equations

$$x = x_0 - r \sin(\omega_B t + \alpha)$$

$$y = y_0 - r \cos(\omega_B t + \alpha)$$

where the term ω_B is the *cyclotron frequency*, given by

$$\omega_B = \frac{eB}{m}$$

That is all there is to Hall's discovery. It was a discovery that came well before its time, as it was done nearly two decades before the electron was actually discovered by Thomson, and it was a purely experimental fact which

B. THE HALL EFFECT

he noted as the ideas of charge carriers et cetera came much more later. One might choose to use the laboratory frame to analyse the problem, and also include an extra term to the Lorentz force law to account for a non ideal two dimensional electron system.

$$m \frac{d\vec{v}}{dt} = -e\vec{E} - e\vec{v} \times \vec{B} - \frac{m\vec{v}}{\tau}$$

Here, τ is known as the scattering time. The term does not contribute when $\tau \rightarrow \infty$ and becomes more prominent when the scattering time is smaller. Hence, it somehow encapsulates the lattice effects as the average time between collisions, and this is known as the *Drude model* of electronic conduction. If one can recall correctly, the Ohm law for conduction (which is usually derived in the absence of an external magnetic field) is given by

$$\bar{J} = \sigma \bar{E}$$

However, in the Drude model, and in the presence of an external magnetic field, the conductivity is no longer a scalar as there is a transverse motion of the charge carriers and this can be accounted for in the Ohm law by extending σ to be a tensor σ_{ij} .

That is, σ_{xx} accounts for the pure conduction due to the electric field and σ_{xy} accounts for the Hall conduction. Since a constantly maintained magnetic field can bend the carriers in only one direction, you have

$$\sigma_{xy} = -\sigma_{yx}$$

A simple calculation from the Drude model suffices to see that the conductivity tensor can be written down in terms of the cyclotron frequency and the scattering time

$$\sigma = \frac{ne^2\tau}{m(1 + \omega_B^2\tau)} \hat{\sigma}$$

where $\hat{\sigma}$ is given by

$$\begin{pmatrix} 1 & -\omega_B\tau \\ \omega_B\tau & 1 \end{pmatrix}$$

The inverse of this matrix gives the resistivity tensor, and the only two components which are of interest to us for the Hall effect are the terms ρ_{xx} and ρ_{xy} , and in the current system it can also be seen that the resistivity and the *Hall resistance* turn out to be the same in *magnitude*,

$$R_{xy} = \frac{V_y}{I_x} = \frac{E_y}{J_x} = -\rho_{xy}$$

The resistivity tensor for the Drude model gives the following components for the longitudinal and Hall resistivities:

$$\rho_{xx} = \frac{m}{ne^2\tau}$$

$$\rho_{xy} = \frac{B}{ne}$$

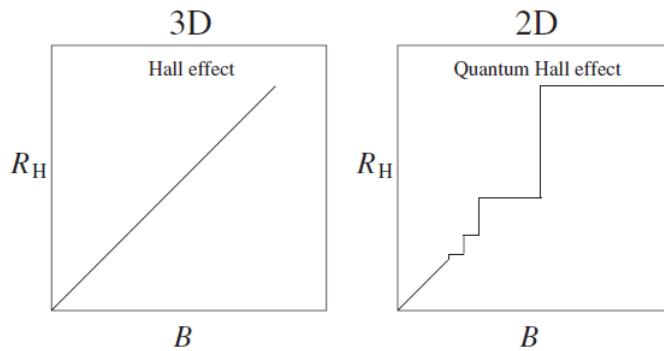
If the magnetic field intensity is increased, it is seen that ρ_{xx} is more or less independent while ρ_{xy} increases linearly and we would expect the same to happen even at higher magnetic field intensities. But something else seems to happen at around 3 Tesla (and low temperatures) for *two dimensional* material conduction.

B.2 Quantum Hall Effect

B.2.1 Introduction

Klaus von Klitzing, G. Dorda and M. Pepper discovered that for two dimensional materials placed in a strong perpendicular field at low temperatures, the Hall resistivity becomes *quantized*. That is, for a given range of magnetic field intensities it occupies a well defined resistivity and then *jumps* to a higher value. When you fit the data to match the quantization, it is seen that the Hall resistivity gets quantized following the rule below

$$\rho_{xy} = \frac{2\pi\hbar}{e^2} \times \frac{1}{v}$$



where v is an integer. This is (somewhat wrongly) known as the *Integer Quantum Hall Effect*. It turns out that if you make the sample cleaner, that is, you *decrease disorder* in your two dimensional material, you get much more exotic scenarios where v could also be a rational number, and this is rightly known as the *Fractional Quantum Hall Effect*. This was discovered by D.C. Tsui, H. Stormer, and A. Gossard in 1982. The FQHE is the most comprehensive description of the generic phenomenon of the QHE and it involves the idea that fermions behave as composite quasiparticles with non spin half, non integer spins (and are called anyons, hence). The explanation to the FQHE and many of the intricacies of the IQHE was given by Robert

B. THE HALL EFFECT

Laughlin who was awarded the Nobel Prize for the same reason. In this document, only the IQHE shall be discussed in detail.

B.2.2 The Landau Problem (Landau Gauge)

The title of the section relates to the scenario of a sheet of electrons in a magnetic field and the subsequent quantum mechanical analysis of the distribution of energies in the electrons when the field is on and off. To be more pedantic, we are dealing with a two dimensional electron gas in a magnetic field. The problem was solved in its full glory first by Lev Landau.

If recollected correctly, the zero magnetic field case Hamiltonian for a two dimensional electron gas is given by the standard form

$$\epsilon(\vec{p}) = \frac{p_x^2}{2m} + \frac{p_y^2}{2m}$$

However, when there is a magnetic field applied, say in the direction perpendicular to the two dimensional sheet of electrons, we must modify the canonical quantities p_x and p_y into the corresponding electrodynamic counterparts, $p_x - \frac{eA_x}{c}$ and $p_y - \frac{eA_y}{c}$. It is clear that we must know the vector potential in order to construct these terms. We can choose one of the two commonly used vector potential forms for a given magnetic field. This process of fixing a form for \vec{A} is called choosing a 'gauge'. The two standard gauges available to us are the **symmetric gauge**

$$\vec{A}_s = \frac{B}{2}(-y, x, 0)$$

and the commonly used gauge for the current situation, the **Landau gauge**

$$\vec{A}_l = -B(y, 0, 0)$$

Choosing the latter case, and setting $c = 1$, we get the following new Hamiltonian for the Landau problem

$$\mathcal{H} = \frac{1}{2m}(-i\hbar\partial_x + eBy)^2 + \frac{\hbar^2}{2m}(-i\hbar\partial_y)^2$$

Solving the Schrodinger equation with this as the Hamiltonian gives us the eigenvalues or the energy levels which are none other than the famously known **Landau levels**. A simple way out to solve the Schrodinger equation is to observe that it is nothing but a superposition of the free particle motion in the x direction and of a shifted harmonic oscillator like motion in the y

direction. We go with the *ansatz* that the solution looks like

$$\psi(x, y) = e^{ikx} \varphi(y)$$

To simplify matters, let us assume a periodic boundary condition in the x direction, say

$$\begin{aligned}\psi(x, y) &= \psi(x + L_x, y) \\ \implies e^{ikL_x} &= 1 \\ \implies k &= \frac{2\pi}{L_x} n_x\end{aligned}$$

Now, we have our reduced, purely y dependent hamiltonian

$$\mathcal{H}_y(k) = \frac{1}{2m}(\hbar k + eBy)^2 + \frac{\hbar^2}{2m}(-i\partial_y)^2$$

The y motion, as described before is a shifted harmonic oscillator motion which is the reason for the occurrence for the quantized Landau levels. To find the frequency of oscillation, we just compare the quadratic y coefficient to the standard harmonic oscillator quadratic coefficient $\frac{1}{2}m\omega_c^2$. Doing so, we see that

$$\omega_c = \frac{eB}{m}$$

and the Landau levels are given by

$$\varepsilon_{n,L} = (n + \frac{1}{2})\hbar\omega_c$$

The c in the subscript of the angular frequency is due to the fact that this is the same frequency of electrons in a *cyclotron*. Now, enumerating the combined density of states function is easy, as there are quantized levels and no other energies accessible in between,

$$g(\varepsilon) = \sum_n g_n \delta(\varepsilon - (n + \frac{1}{2})\hbar\omega_c)$$

From the diagram and also from the idea of a harmonic oscillator, we can see that the maximum amplitude of oscillation when started from origin is given by

$$|y_{max}| = \frac{L_y}{2}$$

B. THE HALL EFFECT

$$\begin{aligned}\frac{\hbar k}{eB} &= \frac{L_y}{2} \\ \frac{\hbar}{eB} \left(\frac{2\pi}{L_x} n_x \right) &= \frac{L_y}{2} \\ g_n = 2n_x = L_x L_y \frac{eB}{\hbar} &= (L_x L_y B) \frac{1}{\frac{\hbar}{e}}\end{aligned}$$

Notice that $\frac{\hbar}{e}$ is the quantum elementary flux value a field can have and the first bracket represents the total flux through the sheet. Hence, we come to the startling conclusion that the flux through the sheet is quantized for every Landau level.

$$\begin{aligned}g_n &= \frac{\Phi}{\Phi_e} \\ g(\varepsilon) &= \sum_n g_n \delta(\varepsilon - (n + \frac{1}{2})\hbar\omega_c) = \frac{\Phi}{\Phi_e} \sum_n \delta(\varepsilon - (n + \frac{1}{2})\hbar\omega_c)\end{aligned}$$

It can also be seen that the wavefunctions look like the following

$$\psi_{n,k}(x, y) = C e^{ikx} H_n(y + kl_B^2) e^{-\frac{(y + kl_B^2)^2}{2l_B^2}}$$

where C is the normalization constant, H_n is the usual Hermite polynomial which enters as the quantum harmonic oscillator solution, and l_B is the characteristic *magnetic length scale*

$$l_B = \sqrt{\frac{\hbar}{eB}}$$

Thus, we can see that the energy spectrum has the degeneracy which looks like $\frac{\Phi}{\Phi_e}$ number of flux tubes for each Landau level, and this fact is also apparent from the fact that the energy spectrum is dependent *purely on n*.

However the degeneracy can be lifted in the presence of an external electric field. We continue working in the rectangular two dimensional sheet geometry and now choose the Landau gauge and the electric field with

$$\bar{A}_I = -B(0, x, 0)$$

$$\varphi = -Ex$$

The Hamiltonian now looks like the following

$$\mathcal{H} = \frac{1}{2m} (\hat{p}_x^2 + (\hat{p}_y + e\hat{x}B)^2) - e\hat{x}E$$

The harmonic oscillator ansatz comes into play again and we have another shifted oscillator, the eigenfunctions of this Hamiltonian can be written in terms of the non electric field wavefunctions as follows

$$\xi(x, y) = \psi_{n,k}(x - \frac{mE}{eB^2}, y)$$

The energy spectrum now shows the dependence of k and thence the lifting of the degeneracy

$$E_{n,k} = \hbar\omega_B(n + \frac{1}{2}) + eE(kl_B^2 - \frac{eE}{m\omega_B^2}) + \frac{mE^2}{2B^2}$$

The velocity expectation value in the y direction also gives us a hint as to what exactly is happening here

$$\langle v_y \rangle = \frac{1}{\hbar} \frac{\partial E}{\partial k} = \frac{E}{B}$$

This is simply the drift of the cyclotron orbit centers which were initially stationary, and they drift in the direction of $\vec{E} \times \vec{B}$ with a velocity $\frac{E}{B}$.

B.2.3 The Landau Problem (Symmetric Gauge)

The symmetric gauge which we have avoided so far can also be used to derive similar expressions albeit the computation for the rectangular geometry using this gauge choice just complicates the calculations, however it is a peach of a gauge to use when dealing with rotationally symmetric geometries, and also has the nice property that the gauge in itself is rotationally invariant, thereby leading to the angular momentum being diagonalized (via the Noether theorem), and the degeneracies become the eigenvalues of the angular momentum operator. This leads to a nice representation of the lowest Landau level (and hence all subsequent levels).

Since the calculation for the wavefunctions for the Landau problem involved the harmonic oscillator, it is also viable to represent the entire procedure using the Dirac ladder operator representation. Define the creators and annihilators as follows

$$\begin{aligned}\hat{a} &= \frac{1}{\sqrt{2e\hbar B}}(\pi_x - i\pi_y) \\ \hat{a}^\dagger &= \frac{1}{\sqrt{2e\hbar B}}(\pi_x + i\pi_y)\end{aligned}$$

where

$$\pi_x = p_x + eA_x$$

$$\pi_y = p_y + eA_y$$

B. THE HALL EFFECT

Now, we invent fancy fake (non gauge invariant) momenta to do a little magic trick

$$\tilde{\pi}_x = p_x - eA_x$$

$$\tilde{\pi}_y = p_y - eA_y$$

and we define some new operators as follows

$$\hat{b} = \frac{1}{\sqrt{2e\hbar B}}(\tilde{\pi}_x + i\tilde{\pi}_y)$$

$$\hat{b}^\dagger = \frac{1}{\sqrt{2e\hbar B}}(\tilde{\pi}_x - i\tilde{\pi}_y)$$

The reason for doing all this is that in the symmetric gauge it can be seen that

$$[\pi_i, \tilde{\pi}_j] = 0$$

and hence, we can simultaneously diagonalize the Hamiltonian *twice*, and hence we have uncovered another quantum number and this (should) hopefully return the information regarding the degeneracy in the system. Labelling the degeneracies for a given Landau level n with the index m , we have

$$|n, m\rangle = \frac{\hat{a}^{\dagger n} \hat{b}^{\dagger m}}{\sqrt{n!m!}} |0, 0\rangle$$

where

$$a|0, 0\rangle = b|0, 0\rangle = 0$$

It should be kept in mind that the Landau levels are still purely dependent on n and not on m in the absence of any degeneracy lifting mechanism. The structure of the lowest Landau level in this system can be worked out by switching to the complex plane and esoterically defining

$$z = x - iy, \bar{z} = x + iy$$

and the so called "holomorphic" and "anti-holomorphic" derivatives as follows

$$\partial = \frac{1}{2}\left(\frac{\partial}{\partial x} + i\frac{\partial}{\partial y}\right)$$

$$\bar{\partial} = \frac{1}{2}\left(\frac{\partial}{\partial x} - i\frac{\partial}{\partial y}\right)$$

With the nomenclature clarified, we have the creators and annihilators which look like the following

$$\hat{a} = -i\sqrt{2}(l_B \bar{\partial} + \frac{z}{4l_B})$$

$$\hat{a}^\dagger = -i\sqrt{2}(l_B \partial - \frac{\bar{z}}{4l_B})$$

Now, we need to solve for $|0,0\rangle = \psi(z, \bar{z})$ and doing so, we have $\hat{a}\psi(z, \bar{z}) = 0$, thence

$$|0,0\rangle = Ae^{\frac{-zz}{4l_B^2}}$$

Since in this gauge we can also count for the degeneracies in the wavefunction itself, we redefine the operators \hat{b} and \hat{b}^\dagger in the complex plane and hit the wavefunction with \hat{b} and set it to zero. The final lowest Landau level wavefunction $|0,m\rangle$ can be seen to look like

$$|0,m\rangle = C\left(\frac{z}{l_B}\right)^m e^{\frac{-zz}{4l_B^2}}$$

The angular momentum operator can also be written in the complex plane as follows

$$\hat{J} = i\hbar(x\frac{\partial}{\partial y} - y\frac{\partial}{\partial x}) = \hbar(z\partial - \bar{z}\bar{\partial})$$

It can be seen that the operator has m as the eigenvalue, and the wavefunction $|0,m\rangle$ is an eigenfunction due to the rotational symmetry of the gauge choice as explained before. The symmetric gauge has the advantage that rotationally invariant configurations become easier to handle. The degeneracy can be counted by dividing the total area of the circular disk of radius R divided by the area occupied by the quantum of flux, which is nothing but $\pi \times r^2$ where r is the radius at which the first Landau level occurs, and can be seen as being numerically equal to $\sqrt{2}l_B$ from the wavefunction. Thus

$$g_n = \frac{\pi \times R^2}{\pi \times r^2} = \frac{A}{2\pi l_B^2} = \frac{\Phi}{\Phi_0}$$

B.2.4 The Landau Problem (Center Of Mass Coordinates)

If one can recollect, the equations of motion for the cyclotron orbits are written as follows

$$\begin{aligned} x &= x_0 - r \sin(\omega_B t + \alpha) \\ y &= y_0 - r \cos(\omega_B t + \alpha) \end{aligned}$$

where x_0 and y_0 are constants in the parametrization representing the center of mass coordinates. You can represent the above in a different way,

$$\begin{aligned} x_0 &= x - \frac{\dot{y}}{\omega_B} = x - \frac{\pi y}{m\omega_B} \\ y_0 &= y + \frac{\dot{x}}{\omega_B} = y + \frac{\pi x}{m\omega_B} \end{aligned}$$

It can be seen that if we treat x_0, y_0 as \hat{x}_0, \hat{y}_0 , that is, promote them to quantum mechanical operators, then we have the following relations, substituting the appropriate position and momentum operators,

$$\hat{x}_0 = -\frac{\tilde{\pi}_y}{eB}$$

B. THE HALL EFFECT

$$\hat{y}_0 = \frac{\tilde{\pi}_x}{eB}$$

where we have already defined $\tilde{\pi}$ observables as the non gauge invariant momentum like quantities in the previous section. It turns out that

$$[\hat{x}_0, \hat{y}_0] = il_B^2$$

and this implies, from Heisenberg principle,

$$\Delta x_0 \Delta y_0 = 2\pi l_B^2$$

Now, the degeneracy can be seen quite simply as the area of the given geometry divided by the area occupied by an uncertain region where the flux tube exists, given by $\Delta x_0 \Delta y_0$. This implies

$$g_n = \frac{A}{\Delta x_0 \Delta y_0} = \frac{A}{2\pi l_B^2} = \frac{\Phi}{\Phi_0}$$

B.3 The Phenomenon

B.3.1 Spectral Flow

For understanding the actual nature of the quantized Hall plateaus and their apparent robustness to changing magnetic field intensities, and also to the extremely peculiar *enhancement* of the effect when the disorder in the system is moderately increased, we need to study about the idea of spectral flow.

In the process of understanding spectral flow, we shall also provide a preliminary explanation to the Aharonov-Bohm effect. Classically, we do not expect the magnetic vector potential \vec{A} to play any physical role in defining the dynamics of a charged particle in an electromagnetic configuration. In quantum mechanics, however, the vector potential enters into the phase of the wavefunction and this leads to *physically observable* effects such as interference et cetera, and this is the core idea behind the Aharonov-Bohm effect.

Firstly, let us constrain a charged particle to move in a circular path *around* a solenoid which fixes the magnetic field intensity *inside it*. Clearly, since the particle's orbit is outside the solenoid, there is no way the magnetic field is going to affect its dynamics if the solenoid is ideal (and we assume it is). But a null magnetic field does *not* imply that the vector potential is zero too, and in fact it is given by the following (the first equality is from Stokes' theorem)

$$\oint \vec{A} \cdot d\vec{r} = \int \vec{B} \cdot d\vec{S} = \Phi \implies A_\varphi = \frac{\Phi}{2\pi r}$$

Now, we do the usual stuff, convert the mechanical momentum to the canonical one, $\pi_\varphi = p_\varphi + eA_\varphi$, and then write the Hamiltonian as follows

$$\mathcal{H} = \frac{\pi_\varphi^2}{2m} = \frac{1}{2mr^2} \left(-i\hbar \frac{\partial}{\partial \varphi} + \frac{e\Phi}{2\pi} \right)^2$$

This is an old friend of ours, except that it is shifted by a constant flux through the center. Thus, the wavefunctions would not look very different, but the energy spectrum gets shifted by the same amount

$$\therefore E_n = \frac{1}{2mr^2} \left(\hbar n + \frac{e\Phi}{2\pi} \right)^2 = \frac{\hbar^2}{2mr^2} \left(n + \frac{\Phi}{\Phi_0} \right)^2$$

where n is an integer, the quantum number defining the energy level. Now comes the essential concept. If you increase Φ in the center slowly, unlike the classical picture, in which case you would say there would be no difference, the spectrum would go on a parabola for a given n and then the moment Φ hits Φ_0 (at this time obviously $\frac{\Phi}{\Phi_0} = 1$) the energy term becomes

$$E_n = \frac{\hbar^2}{2mr^2} (n+1)^2 = \frac{\hbar^2}{2mr^2} \left(n+1 + \frac{0}{\Phi_0} \right)^2$$

B. THE HALL EFFECT

This is equivalent to (as the second equality demonstrates) the fact that the spectrum now shifts to the next level $n + 1$ and Φ will again wait till it hits $2\Phi_0$ and then it will *jump* to $n + 2$ and so on. This is exactly how the jumps take place in the actual plot, but there is something more to be explained in the actual Hall configuration, such as the effect of the disorder. However, this is the basis of much of the discussion to come and the terminology of "spectral flow" is hopefully clear, as the system jumps through the spectrum when the flux is increased.

B.3.2 Conduction

Now, we come to handling the actual issue of the Integer Quantum Hall Effect in moderate detail, and we will do a calculation which gives us the conductivity from a quantum mechanical perspective. Before we get into the computation, we need to find out when given the concentration of electrons in the system (in units of number per unit area, for we are dealing with two dimensional materials) and the magnetic field intensity, the number of Landau levels that are filled. Denoting this by ν we have the following

$$\begin{aligned} g_n &= \frac{\Phi}{\Phi_0} = \frac{BA}{\Phi_0} \\ \implies \frac{g_n}{A} &= \frac{B}{\Phi_0} \end{aligned}$$

Now, the density of states is simply the number of electrons in the Landau level n . Assuming, ν Landau levels are filled, we have

$$\frac{g_n}{A} = \frac{n}{\nu} \implies \nu = \left[\frac{n\Phi_0}{B} \right]$$

where the square brackets denote the floor function. Thus, given both B and n for the system we can calculate the number of filled Landau levels which would exist (and this turns out to be huge for classical values of n and B , as expected). Now, we proceed to the calculation of the quantum mechanical current and thence the conductivity from the Landau levels we have derived so far. The current is defined as (a vector, but this is debatable)

$$\bar{I} = -e\dot{\bar{x}}$$

and

$$\dot{\bar{x}} = \frac{\bar{p} + e\bar{A}}{m}$$

Now, we would like to find out the expectation value of the classical expression for the current and derive the quantum mechanical result (a la Ehrenfest)

$$\bar{I} = -\frac{e}{m} \sum_{LL} \langle \psi_{n,k} | -i\hbar\nabla + e\bar{A} | \psi_{n,k} \rangle$$

Now, we fix the gauge to be the Landau gauge and thereby $\bar{A} = B(0, x, 0)$. If there are ν Landau levels filled then we can split the summation over the two quantum numbers n and k giving us

$$\bar{I} = -\frac{e}{m} \sum_{n=1}^{\nu} \sum_{k,D} < \psi_{n,k} | -i\hbar\nabla + eB(0, x, 0) | \psi_{n,k} >$$

It is to be understood that n here is the quantum number and not the electron concentration per unit area, and also that D in the k summation was to denote the degeneracy involved in the scenario. The x component for the current is simply the expectation value of the momentum in the x direction since the component of \bar{A} is zero in that direction. From experience with the standard QHO problem, we know that (or one can verify by switching to the Dirac representation of the momentum) the expectation value is zero and thus $I_x = 0$. However, I_y contains the potential term entering the picture and we have

$$I_y = -\frac{e}{m} \sum_{n=1}^{nu} \sum_{k,D} < \psi_{n,k} | -i\hbar \frac{\partial}{\partial y} + e\hat{x}B | \psi_{n,k} > = -\frac{e}{m} \sum_{n=1}^{nu} \sum_{k,D} < \psi_{n,k} | \hbar k + e\hat{x}B | \psi_{n,k} >$$

The expectation value of the position operator is zero for a pure two dimensional system but if we introduce an electric field in the x direction with magnitude E , we have a shifted oscillator with the expectation value

$$< \hat{x} > = -\frac{\hbar k}{eB} + \frac{mE}{eB^2}$$

This now leaves us with the following summation over k , with the summation over n done to remove all expectation values inside

$$I_y = -e\nu \sum_{k,D} \frac{E}{B}$$

Now, we see that the summand is a constant and hence can be pulled out thereby leaving 1 inside and that summed over k, D times gives you the degeneracy count of that level, which is nothing but the number of flux tubes $\frac{\Phi}{Phi_0} = \frac{BA}{\Phi_0}$. Plugging this in the expression above, we see that

$$I_y = -e\nu \frac{E}{B} \times \frac{BA}{\Phi_0}$$

We know that $\frac{I_y}{A} = J_y$ and $J_y = \sigma_{xy}E_x$, thereby letting us conclude that

$$\sigma_{xy} = \frac{e\nu}{\Phi_0} \implies \rho_{xy} = \frac{\Phi_0}{e\nu} = \frac{2\pi\hbar}{e^2\nu}$$

which is what von Klitzing concluded by fitting data to his experimental Hall plateaus

B.3.3 Conduction Revisited

The expectation value of the current calculation gives us the exact quantization of the plateaus but it does not really help understand the way things physically happen. The complete description is quite complicated and comes under the name of *Anderson localization* and there is a similarity that is drawn between the phenomenon of QHE and the behaviour of the so called *Abrikosov vortices* in type II superconductors.

The finite size of the two dimensional material in itself a way of breaking the translational symmetry and this leads to a feature of conduction called *edge modes*. Edge modes can be visualized simply as states at the edges of the material where there exists a nearly infinite potential wall (in a real scenario the wall won't be infinitely high, probably as high as the work function, but for the sake of argument we assume it is). Now, from the Schrodinger equation for an infinite potential wall, we know that there would be complete reflection and no tunnelling. Imagine a particle sitting at the left corner of your rectangular two dimensional material. When the magnetic field is applied, it moves in a circular orbit, but not a complete one, for after π radians it would encounter the infinite potential wall. This would lead to a perfect reflection, which implies that the particle would come back in the same direction it approached the wall (and this is tangential to the circular orbit). Thus, it would start another round of cyclotron motion until it hits the wall again. In this way, the particle would essentially move upwards or downwards depending on whether you are at the right or the left edge of the material.

To be a bit more technical, we can assume the infinite potential well configuration as a potential $V(x)$ which is zero inside the bulk but becomes infinite at both edges. Now, the slope depends on which edge you are at. It is negative at the left edge and positive at the right edge, but the slope is almost infinite either ways in magnitude. From the expectation value of the velocity, we can see that

$$v = \frac{-1}{eB} \frac{\partial V}{\partial x}$$

As explained before, the only places where the slope is non zero is at the edges and this complies with our previous classical heuristic on edge conduction. But the question is can we use this heuristic to also explain the current expression we derived in the previous section? Yes.

$$I_y = -ev_y = -e \int \frac{dk}{2\pi} v_y(k)$$

Now, observe that from a change of variable in the Fourier transform

$$dkv_y(k) = \frac{dx}{l_B^2} v_y(x)$$

Plugging this back, we have,

$$I_y = \frac{e}{2\pi l_B^2} \int dx \frac{1}{eB} \frac{\partial V}{\partial x} = \frac{e}{2\pi \hbar} \int dV$$

The integral over dV will just give me the potential difference across the two edges, the Hall voltage multiplied by the charge of the charge carrier, which we might as well call the chemical potential difference $\Delta\mu$. The net result is that we have established the same fact that we got in the last section, that is, the conductivity for a single Landau level is

$$\sigma_{xy} = \frac{e^2}{2\pi \hbar}$$

The potential inside the bulk need not really be flat, but it could be any random shape as long as it does not exceed the potential of the maximum filled edge state. The physics is the same when the internal hills and valleys are bounded above and below by the edge states, but if it does deviate, then we would essentially have two or more hills/valleys where we could have tunnelling and inter-valley transport too, and this leads to exotic conduction modes and possibly new techniques to modulate channel currents.

B.4 The Landau Problem in Graphene with an Electric Field

As done with a normal 2DEG, I solve the Landau problem with Graphene. To generalize the procedure, I also include an external electric potential. Again, I solved the problem as a mathematical one than as a problem in physics i.e., work out the matrix equations, end up with a differential equation and then solve it. Professor Vijay Shenoy, IISc, on the other hand, worked out the same problem completely using a standard technique in mechanical and civil engineering known as the *Finite Element Method*. My mathematical solution ultimately ended up in using a FEM package to solve my PDE(*FreeFEM++*, a C++ extension), although I used with absolutely no idea as to what FEM was. I thank Professor Shenoy for enlightening me about the same, and I have included the discussion in this section.

B.4.1 Mathematical Solution

The standard Dirac Hamiltonian is given by the following 4x4 matrix:

$$\begin{pmatrix} -\bar{\sigma}^* \cdot \vec{p} & 0 \\ 0 & \bar{\sigma} \cdot \vec{p} \end{pmatrix}$$

B. THE HALL EFFECT

where $\bar{\sigma}$ is the Pauli spin matrix vector and \bar{p} is the canonical momentum. As the usual procedure goes, replace \bar{p} with $\bar{\pi}$ and add a potential term, which is the scalar potential multiplied by the 4x4 identity element.

$$\begin{pmatrix} -\bar{\sigma}^* \cdot \bar{\pi} + V(x) \mathbb{I}_2 & 0 \\ 0 & \bar{\sigma} \cdot \bar{\pi} + V(x) \mathbb{I}_2 \end{pmatrix} \Psi = \varepsilon \Psi$$

As stated before, Ψ is a four component wave function. Now as to what each component means, I shall explain later, but for now, since I'm focusing on solving the problem mathematically, I state that we can group the four components into two groups of two components each(each component belonging to a sublattice).

$$\begin{aligned} \Psi &= \begin{pmatrix} \tilde{\varphi}^1 \\ \tilde{\varphi}^2 \end{pmatrix} \\ \tilde{\varphi}^j &= \begin{pmatrix} \varphi_A^j \\ \varphi_B^j \end{pmatrix} \\ \implies \begin{pmatrix} -\bar{\sigma}^* \cdot \bar{\pi} + V(x) \mathbb{I}_2 & 0 \\ 0 & \bar{\sigma} \cdot \bar{\pi} + V(x) \mathbb{I}_2 \end{pmatrix} \begin{pmatrix} \tilde{\varphi}^1 \\ \tilde{\varphi}^2 \end{pmatrix} &= \varepsilon \begin{pmatrix} \tilde{\varphi}^1 \\ \tilde{\varphi}^2 \end{pmatrix} \\ [-\bar{\sigma}^* \cdot \bar{\pi} + V(x) \mathbb{I}_2] \tilde{\varphi}^1 &= \varepsilon \tilde{\varphi}^1 \\ [\bar{\sigma} \cdot \bar{\pi} + V(x) \mathbb{I}_2] \tilde{\varphi}^2 &= \varepsilon \tilde{\varphi}^2 \end{aligned}$$

We need only the first two components of the Pauli spin matrix vector

$$\bar{\sigma}^* = [\begin{pmatrix} 0 & 1 \\ 1 & 0 \end{pmatrix}, \begin{pmatrix} 0 & -i \\ +i & 0 \end{pmatrix}]$$

I use the symmetric gauge, and writing the first matrix equation in its full expanded form, we see that

$$-[\begin{pmatrix} 0 & 1 \\ 1 & 0 \end{pmatrix} (\hat{p}_x + \frac{eB\hat{y}}{2c})] + \begin{pmatrix} 0 & -i \\ i & 0 \end{pmatrix} (\hat{p}_y - \frac{eB\hat{x}}{2c}) + \begin{pmatrix} V(x) & 0 \\ 0 & V(x) \end{pmatrix} \begin{pmatrix} \varphi_A^1 \\ \varphi_B^1 \end{pmatrix} = \varepsilon \begin{pmatrix} \varphi_A^1 \\ \varphi_B^1 \end{pmatrix}$$

Or, adding up the 2x2 matrices, we end up with

$$\begin{pmatrix} V(x) & -[\hat{p}_x - i\hat{p}_y + \frac{eB}{2c}(\hat{y} + i\hat{x})] \\ -[\hat{p}_x + i\hat{p}_y + \frac{eB}{2c}(\hat{y} - i\hat{x})] & V(x) \end{pmatrix} \begin{pmatrix} \varphi_A^1 \\ \varphi_B^1 \end{pmatrix} = \varepsilon \begin{pmatrix} \varphi_A^1 \\ \varphi_B^1 \end{pmatrix}$$

Again, writing the equations separately, we see that

$$V(x)\varphi_A^1 - (\hat{p}_x - i\hat{p}_y + \frac{eB}{2c}(\hat{y} + i\hat{x}))\varphi_B^1 = \varepsilon\varphi_A^1$$

$$V(x)\varphi_B^1 - (\hat{p}_x + i\hat{p}_y + \frac{eB}{2c}(\hat{y} - i\hat{x}))\varphi_A^1 = \varepsilon\varphi_B^1$$

The equations look symmetric and as is suggested, I proceed by elimination, substituting for φ_A^1 ,

$$[\hat{p}_x + i\hat{p}_y + \frac{eB}{2c}(\hat{y} - i\hat{x})][\hat{p}_x - i\hat{p}_y + \frac{eB}{2c}(\hat{y} + i\hat{x})]\varphi_B^1 = (V(x) - \varepsilon)^2\varphi_B^1$$

$$\implies (\hat{p}_x + \frac{eB\hat{y}}{2c})^2 + (\hat{p}_y - \frac{eB\hat{x}}{2c})^2 + i[\hat{p}_y - \frac{eB\hat{x}}{2c}, \hat{p}_x + \frac{eB\hat{y}}{2c}]\varphi_B^1 = (V(x) - \varepsilon)^2\varphi_B^1$$

where $[,]$ are the standard commutation brackets. Simplifying further

$$(\hat{p}_x^2 + \hat{p}_y^2 + \frac{e^2B^2}{2c}(\hat{x}^2 + \hat{y}^2) + \frac{eB}{c}(\hat{y}\hat{p}_x - \hat{x}\hat{p}_y) + i[\hat{p}_y - \frac{eB\hat{x}}{2c}, \hat{p}_x + \frac{eB\hat{y}}{2c}])\varphi_B^1 = (V(x) - \varepsilon)^2\varphi_B^1$$

Using the canonical commutation relations,

$$(\hat{p}_x^2 + \hat{p}_y^2 + \frac{eB}{c}(\hat{y}\hat{p}_x - \hat{x}\hat{p}_y) + (\hat{x}^2 + \hat{y}^2)\frac{e^2B^2}{2c} + \frac{\hbar eB}{c})\varphi_B^1 = (V(x) - \varepsilon)^2\varphi_B^1$$

This is the (eigenvalue) partial differential equation which we have to solve. I substitute $\hat{p}_x = -i\hbar\partial_x$ and $\hat{p}_y = -i\hbar\partial_y$. Also, using the natural units in which we set $e = c = \hbar = 1$, we see that the differential equation is much simplified to

$$(-(\partial_x^2 + \partial_y^2) + B(y(-i\partial_x) - x(-i\partial_y)) + \frac{x^2 + y^2}{2}B^2 + B)\varphi_B^1 = (V(x) - \varepsilon)^2\varphi_B^1$$

My first attempt at trying to find out the structure of $\varphi_B^1(x, y)$ was to use a polynomial series expansion upto quadratic order and figure out the initial coefficients. That is

$$\varphi_B^1(x, y) = \lambda + A_1x + B_1y + \mu_1xy + A_2x^2 + B_2y^2$$

This is **wrong** as it leads to senseless conclusions from the relationships between various coefficients. According to technical mathematical documentation, I am officially dealing with a **complex elliptic partial differential equation**, and every elliptic PDE can be written in the form of

$$\sum_{i,j} a^{ij} \varphi_{ij} + \sum_i b^i \varphi_i + c\varphi = \lambda\varphi$$

In this case, we can configure these coefficients:

$$a^{ij} = -\delta^{ij}$$

$$b^i = (-iBx_2, iBx_1)$$

$$c = c(x_1, x_2) = \frac{x_1^2 + x_2^2}{2}B^2 + B$$

FreeFEM++ is a C++-like programming language used to solve partial differential equations using the finite element method. One does not need explicit knowledge of FEM to use the language, but one must know how to reduce a partial differential equation into its so called *weak form*. How does one do that? Let v be a smooth function in the same domain of definition as φ . Note the following transformations

$$\sum_{i,j} a^{ij} \varphi_{ij} + \sum_i b^i \varphi_i + c\varphi = \lambda\varphi$$

$$\int_{\mathcal{T}} \sum_{i,j} a^{ij} \varphi_{ij} v + \sum_i b^i \varphi_i v + c\varphi v = \int_{\mathcal{T}} \lambda\varphi v$$

Using integration by parts on the first term, we see that this can be reduced to the following, with appropriate boundary conditions

$$\int_{\mathcal{T}} \sum_{i,j} a^{ij} \varphi_i v_j + \sum_i b^i \varphi_i v + c\varphi v = \int_{\mathcal{T}} \lambda\varphi v$$

This is supposedly the weak form of the elliptic PDE. The FreeFEM++ PDE solver works on this weak form and hence, we should convert our PDE to this form and then feed it into FreeFEM++. I once again notify that none of this is relevant to how FEM happens(which is the subject for the next section). Before any of this, the above theory applies to real elliptic PDEs and not complex ones. Hence, taking the modulus of the PDE on both sides, we get the following eigenvalue equation for the **modulus** of the wavefunction. Also, the eigenvalues are, from comparison, $(V(x) - \varepsilon)^2$.

$$(-(\partial_x^2 + \partial_y^2) - B(y(\partial_x) - x(\partial_y)) + \frac{x^2 + y^2}{2} B^2 + B) |\varphi_B^1| = (V(x) - \varepsilon)^2 |\varphi_B^1|$$

The FreeFEM++ simulation computes the first twenty eigenvalues from the ground state, with candidate value of $B = 1T$ on a square domain. The color plots are those of $|\varphi_B^1|$.

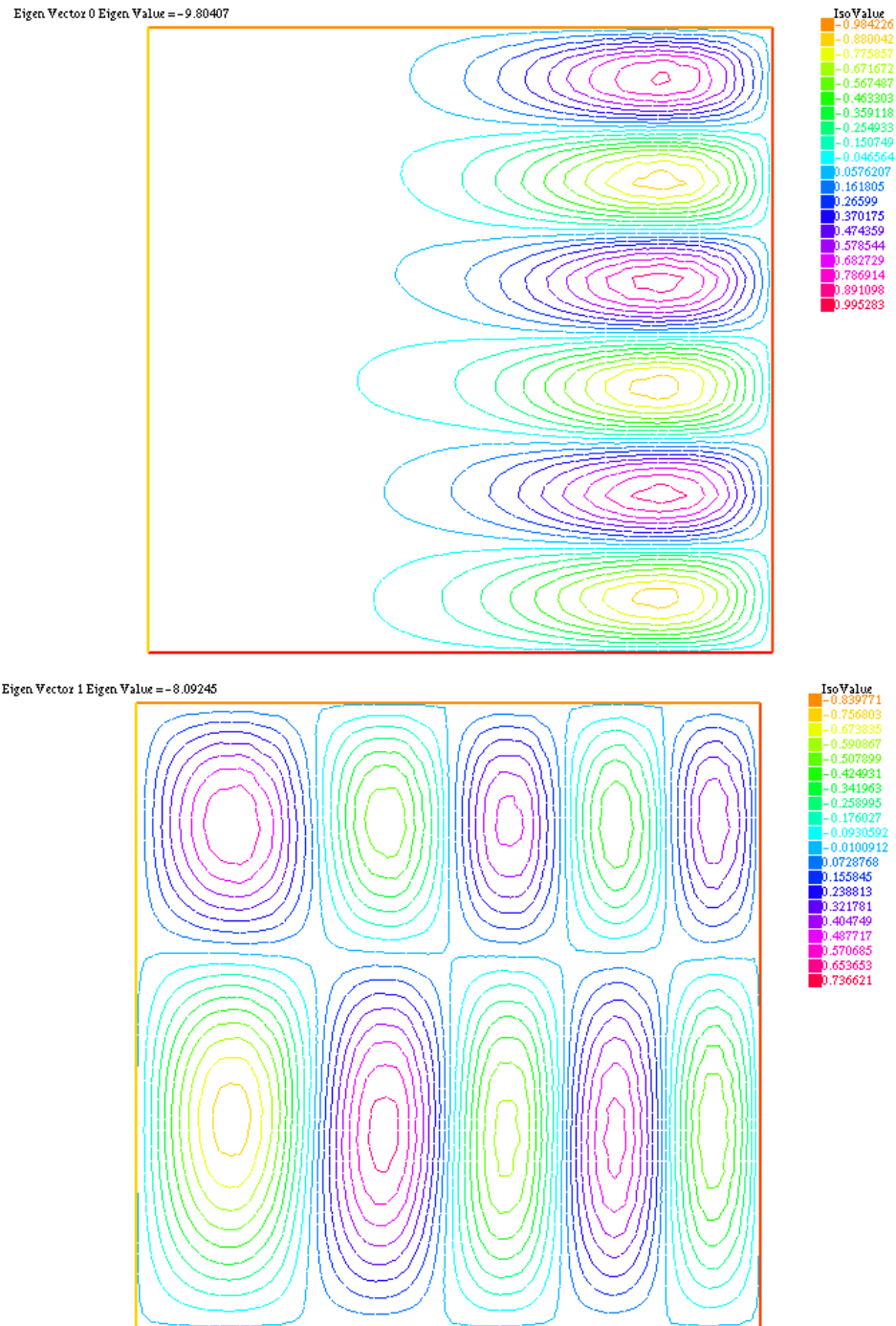
```
verbosity=10;
mesh Th=square(20,20,[pi*x,pi*y]);
fespace Vh(Th,P2);
Vh u1,u2;
func f=sin(x*y);
real sigma = 20; // value of the shift

varf op(u1,u2)= int2d(Th)( - dx(u1)*dx(u2) - dy(u1)*dy(u2) - y*dx(u1)
- sigma*u1*u2 )+ on(1,2,3,4,u1=0) ; // Boundary condition
varf b([u1],[u2]) = int2d(Th)( u1*u2 )
```

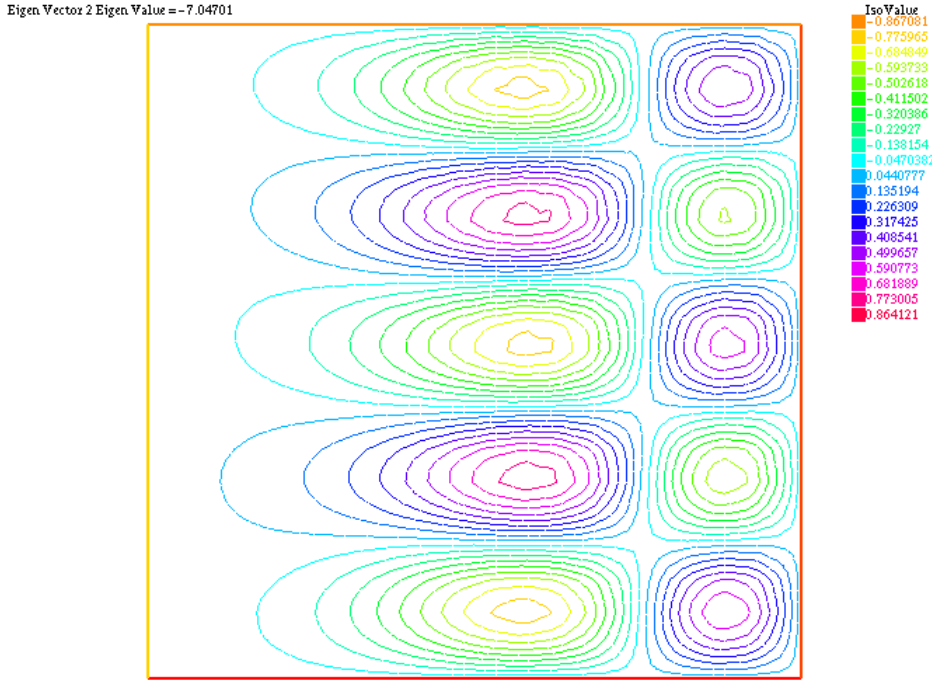
B.4. The Landau Problem in Graphene with an Electric Field

```
matrix OP= op(Vh,Vh,solver=Crout,factorize=1);
matrix B= b(Vh,Vh,solver=CG,eps=1e-20);
int nev=20; // number of computed eigen value close to sigma
real[int] ev(nev); // to store the nev eigenvalue
Vh[int] eV(nev); // to store the nev eigenvector
int k=EigenValue(OP,B,sym=true,sigma=sigma,value=ev,vector=eV,
tol=1e-10,maxit=0,ncv=0);
```

B. THE HALL EFFECT



B.4. The Landau Problem in Graphene with an Electric Field



The procedure for identifying the exact structure of the eigenfunctions for the complex PDE is done iteratively rather, for we are now hunting the real and imaginary parts of the wavefunction using one connecting equation. Let us say

$$\varphi_B^1 = \varphi = \varphi_R + i\varphi_I$$

Substituting this,

$$(-(\partial_x^2 + \partial_y^2) + (\frac{x^2 + y^2}{2}B^2 + B))\varphi_R + (B(y(\partial_x) - x(\partial_y)))\varphi_I = \lambda\varphi_R$$

$$(-(\partial_x^2 + \partial_y^2) + (\frac{x^2 + y^2}{2}B^2 + B))\varphi_I - (B(y(\partial_x) - x(\partial_y)))\varphi_R = \lambda\varphi_I$$

Direct solution of simultaneous eigenvalue elliptic partial differential equations did not look like it was solvable by FreeFEM++, however, the iterative procedure can be seen by setting φ_I to be zero initially and running the first equation as a pure eigenvalue equation in φ_R and then to solve the second equation for φ_I using this first order approximation for φ_R .

From numerous technical documents available on Graphene, one can verify that the eigenvalues vary as the square root of the Landau level number n . From our simulation data above, we can see that the curve fitting generates the same solution. We take the absolute values of the negative eigenvalues and plot from quantum number $n = 0$ to $n = 100$. The first image is the smooth fit and the second one shows the actual interpolation. We get

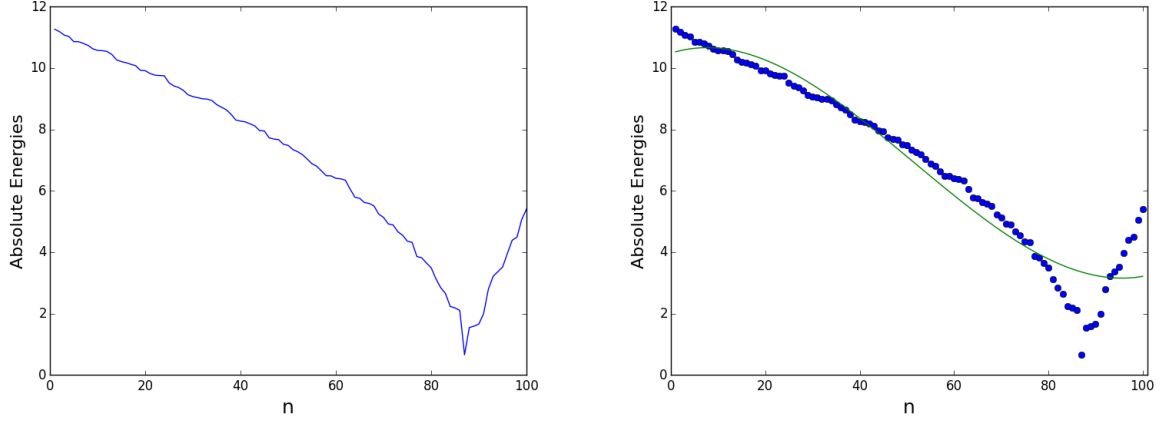
B. THE HALL EFFECT

negative eigenvalues because FreeFEM++ does not know we're working on a physics problem.

B.4. The Landau Problem in Graphene with an Electric Field

```
[ 11.26578892  11.18762709  11.07348184  11.02769242
10.86043277
 10.85822269  10.80476747  10.73769063  10.62746442
10.57511229
 10.56584119  10.5399241   10.44332323  10.26542741
10.20950537
 10.17388815  10.12151174  10.07754931  9.9259055
9.91359168
 9.82456615   9.76935515  9.75583928  9.74982564
9.51821412
 9.41844467   9.36682444  9.27351605  9.12630265
9.06996692
 9.03639309   8.99840541  8.98783066  8.94223686
8.80872863
 8.72476361   8.64164915  8.49601671  8.30800818
8.27047157
 8.2452168    8.18213297  8.11343331  7.96170836
7.94917606
 7.72657104   7.68709958  7.66630289  7.51521124
7.47990642
 7.34198202   7.2722555   7.17713035  7.03386096
6.8805741
 6.80077201   6.64456169  6.49077807  6.48689448
6.40595816
 6.39264421   6.34394987  6.05446942  5.78968047
5.75438094
 5.61728582   5.58835396  5.50764923  5.23946562
5.13415037
 4.92089423   4.89024539  4.66682976  4.5542288
4.35985091
 4.32050923   3.86011658  3.81865159  3.64953422
3.49200515
 3.13114516   2.84472319  2.6546205   2.23233286
2.18468991
 2.10464249   0.65718034  1.54434776  1.59089283
1.65793546
 1.99626902   2.79268688  3.21540044  3.36616993
3.51992898
 3.96378607   4.38943049  4.48912018  5.06374367
5.40705095]
```

B. THE HALL EFFECT



B.4.2 The Finite Element Method

The above computation which I have done, is based on this method. In this aspect, FreeFEM++ is a very good package for end users as one does not need to know what FEM does, and it has inbuilt routines to compute eigenvalues for comparatively large grid sizes. Before I dive into what the method actually is, a few technicalities. Our Hamiltonian, or atleast an element looks like

$$\hbar \tilde{v}_F \bar{\sigma} \cdot \bar{\pi} + \mathcal{V}(x) \mathbb{I}$$

where the constant \tilde{v}_F is the Fermi velocity. Using the Landau gauge, we see that

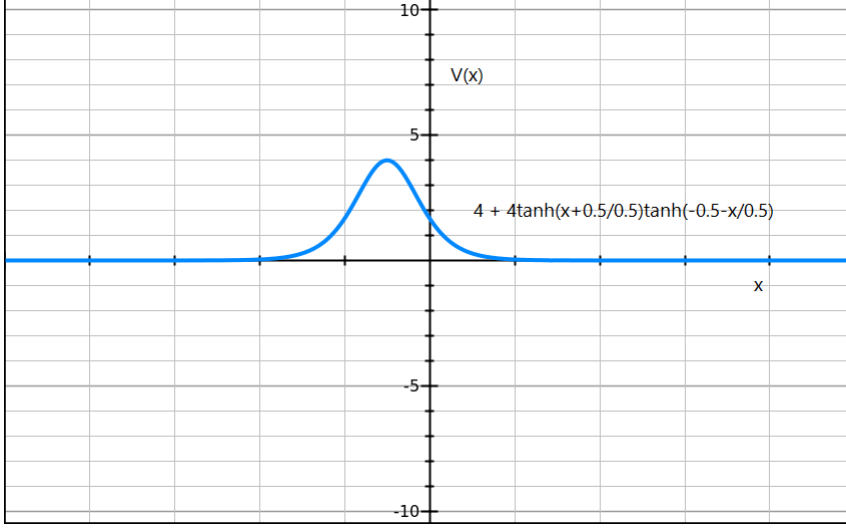
$$[\hbar \tilde{v}_F \bar{\sigma} \cdot (-i\bar{\partial} - eB\hat{y}\hat{e}_x) + \mathcal{V}(x) \mathbb{I}] \Psi = E \Psi$$

Here Ψ is the two component wavefunction and **not** the scalar one. Note that it is a 2X2 system on both sides. The next technicality involves the structure of $\mathcal{V}(x)$ as a modulated step function.

$$\mathcal{V}(x) = \frac{V_0}{2} + \frac{V_0}{2} \left(\tanh\left(\frac{x + L_G}{\zeta_0}\right) \tanh\left(\frac{L_G - x}{\zeta_0}\right) \right)$$

B.4. The Landau Problem in Graphene with an Electric Field

With specimen values, it looks somewhat like



I define a new equivalent potential term

$$\mathbb{V}_B(x) = -\hbar \tilde{v}_F e B y \sigma_x + \mathcal{V}(x) \mathbb{I}$$

Now, our effective hamiltonian looks like

$$\mathcal{H}\Psi = [\hbar \tilde{v}_F \bar{\sigma} \cdot (-i\bar{\partial}) + \mathbb{V}_B(\bar{r})] \Psi = \lambda \Psi$$

This is a field equation(the Dirac field). If recalled correctly, given a Lagrangian density one can construct the field equations by minimizing the effective action. The resulting equations are known as the Euler-Lagrange equations corresponding to the density. The idea here is to work backwards instead, and take this field equation as your Euler-Lagrange equation and look for a suitable Lagrangian density. This process won't assure a unique density, for, from a standard theorem, if I add the gradient of a smooth scalar function to a given L density, the resulting Euler-Lagrange equations would be invariant. Luckily, we can construct the density, and hence the action for the Dirac field.

$$\epsilon[\Psi^*, \Psi; \lambda] = \int_{\Omega} d^2\bar{r} \Psi^*(\bar{r}) [\mathcal{H}(\bar{r})] \Psi(\bar{r}) - \lambda \Psi^*(\bar{r}) \Psi(\bar{r})$$

If I extremize this, I would get back the original field equation. For simplicity, I relabel

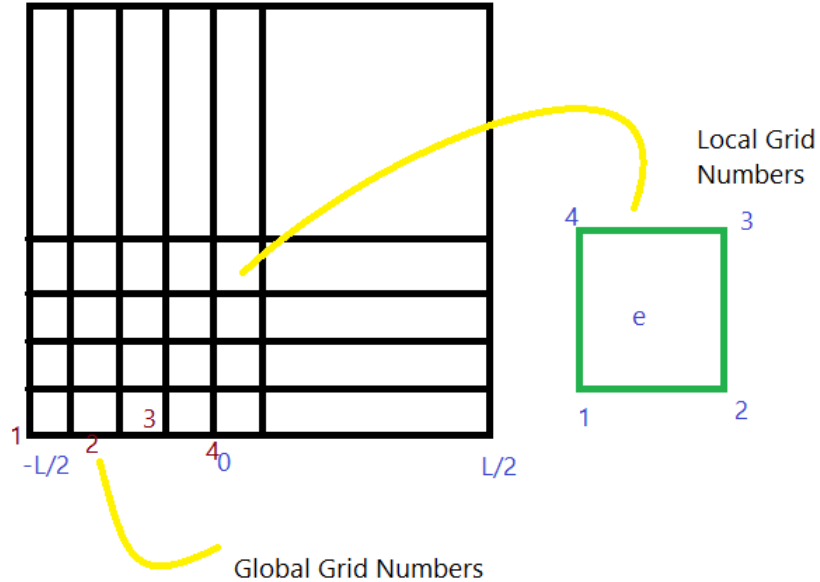
$$\mathcal{H}(\bar{r}) - \lambda \mathbb{I} = \tilde{\mathcal{H}}(\bar{r})$$

$$\epsilon[\Psi^*, \Psi; \lambda] = \int_{\Omega} d^2\bar{r} \Psi^*(\bar{r}) \tilde{\mathcal{H}}(\bar{r}) \Psi(\bar{r})$$

With these apparent technicalities out of the way, let us look at the domain which we are working on. It is a square domain with a square mesh on it.

B. THE HALL EFFECT

Each element in the square mesh is the "finite element" in the finite element



method.

The nodes in the square domain are numbered using a **global numbering** scheme. Each square element has a separate indexing for its nodes known as the **local numbering** scheme. It is straightforward to see, that for a given element e , and a given local node number, one can easily compute the global node number of the corresponding node. We symbolize this with the help of

$$j = gn(e, i)$$

where gn is known as the **connectivity matrix**. The advantage of the finite element method is the following: *given an element, and the values of the wavefunction at the four corners, I can calculate the value of the wavefunction at any other point inside the element.* Mathematically

$$\Psi^e(\vec{r}) = \sum_{i \in e} \Psi_i^e(\vec{r}) N_i^e(\vec{r})$$

The new functions $N_i^e(\vec{r})$ are standard weighting functions known as **shape functions** which are completely mesh dependent and are different for different local nodes. I will show the exact structure of these functions in a while. Getting back to our action functional, we can write the action for the entire domain as the sum of these finite element actions:

$$\mathcal{S}[\Psi^*, \Psi; \lambda] = \sum_e \int_{\Omega_e} d^2\vec{r} \Psi^{e*}(\vec{r}) \tilde{H}(\vec{r}) \Psi^e(\vec{r})$$

B.4. The Landau Problem in Graphene with an Electric Field

$$\begin{aligned}
&= \int_{\Omega} \sum_e d^2\bar{r} \Psi^{e*}(\bar{r}) \tilde{H}(\bar{r}) \Psi^e(\bar{r}) \\
&= \int_{\Omega} \sum_e d^2\bar{r} \sum_{i \in e} \Psi_i^{e*}(\bar{r}) N_i^e(\bar{r}) \tilde{H}(\bar{r}) \sum_{i' \in e} \Psi_{i'}^e(\bar{r}) N_{i'}^e(\bar{r}) \\
&= \sum_e \sum_{ii'} \int d^2\bar{r} \Psi_i^{e*}(\bar{r}) N_i^e(\bar{r}) \tilde{H}(\bar{r}) N_{i'}^e(\bar{r}) \Psi_{i'}^e(\bar{r})
\end{aligned}$$

We group the central term under the new notation

$$N_i^e(\bar{r}) \tilde{H}(\bar{r}) N_{i'}^e(\bar{r}) = \tilde{H}_{ii'}^e$$

The right hand side is more commonly known in the engineering sciences as the element of the stress matrix.

$$\varepsilon[\Psi^*, \Psi; \lambda] = \sum_e \sum_{ii'} \int d^2\bar{r} \Psi_i^{e*}(\bar{r}) \tilde{H}_{ii'}^e \Psi_i^e(\bar{r})$$

To get things back to physics, we are still solving an eigenvalue equation, but now the same eigenvalue equation has been reduced to a smaller, localized domain. Extremizing this form of the action(the finite element form), we see that we have to solve the following

$$(\mathcal{H} - \lambda \mathcal{M} \mathbb{I}) \Psi = 0$$

where the matrix \mathcal{M} is seen to be

$$\mathcal{M}_{ii'} = \mathbb{I} \int d^2\bar{r} N_{gn(e,i)}^e(x, y) N_{gn(e,i')}^e(x, y)$$

How do I work out what \mathcal{H} matrix is for the larger square domain? Once again, the connectivity matrix comes to our rescue.

$$\begin{aligned}
\mathcal{H}_{gn(e,i), gn(e,i')} &= \mathcal{H}_{i,i'}^e \\
H_{i,i'}^e &= \int d\bar{r} N_i^e(\bar{r}) [\hbar \bar{\sigma} \cdot (-i\bar{\partial}) + \mathbb{V}_B(\bar{r})] N_{i'}^e(\bar{r}) \\
&= \hbar \tilde{v}_F \bar{\sigma} \left[\int d^2\bar{r} N_i^e(\bar{r}) (-i\bar{\partial}) N_{i'}^e(\bar{r}) \right] + \sum_k \mathbb{V}_k^e \int d^2\bar{r} N_i^e(\bar{r}) N_k^e(\bar{r}) N_{i'}^e(\bar{r})
\end{aligned}$$

where \mathbb{V}_k^e is the value of the modified potential on the elemental nodes. As far as the shape functions are concerned, they are completely mesh shape dependent and are well tabulated. For a square mesh with edge coordinates $(0, 0), (0, b), (a, 0), (a, b)$, the nodal shape functions are given by

$$\begin{aligned}
N_1(x) &= \frac{(x-a)(y-b)}{ab} \\
N_2(x) &= \frac{-x(y-b)}{ab}
\end{aligned}$$

B. THE HALL EFFECT

$$N_3(x) = \frac{-(x-a)y}{ab}$$

$$N_4(x) = \frac{xy}{ab}$$

Another advantage of the finite element scheme is apparent. All we need to construct the eigenvalue equation are integrals of these polynomial expressions which can be done by hand easily or by Mathematica routines. I thank Professor Shenoy for taking his time and explaining the procedure to me.

VARIATION OF CHERN NUMBER WITH ALPHA_Z FOR SINGLY KICKED GRAPHENE

ALPHA_Z CHERN

-8.1	38.2074
-8	77.8718
-7.9	155.444
-7.8	145.269
-7.7	67.7715
-7.6	31.8957
-7.5	16.9966
-7.4	9.99941
-7.3	6.30836
-7.2	4.1781
-7.1	2.86168
-7	2.00456
-6.9	1.42377
-6.8	1.01845
-6.7	0.73046
-6.6	0.52644
-6.5	0.39275
-6.4	0.35938
-6.3	1.57982
-6.2	-0.4049
-6.1	-0.342
-6	-0.4123
-5.9	-0.5292
-5.8	-0.6868
-5.7	-0.8945
-5.6	-1.1723
-5.5	-1.5547
-5.4	-2.1028
-5.3	-2.9298
-5.2	-4.2617
-5.1	-6.5945
-5	-11.146
-4.9	-21.22
-4.8	-44.115
-4.7	-61.573
-4.6	-33.571
-4.5	-14.928
-4.4	-7.4393
-4.3	-4.15
-4.2	-2.5131
-4.1	-1.6133
-4	-1.0804
-3.9	-0.7469
-3.8	-0.5298
-3.7	-0.3852
-3.6	-0.2888
-3.5	-0.2278

-3.4 -0.1992
-3.3 -0.2197
-3.2 -0.4683
-3.1 0.6444
-3 0.22614
-2.9 0.1766
-2.8 0.17341
-2.7 0.18773
-2.6 0.2135
-2.5 0.25031
-2.4 0.30068
-2.3 0.37021
-2.2 0.46953
-2.1 0.61908
-2 0.86102
-1.95 1.04271
-1.9 1.29116
-1.8 2.15099
-1.7 4.03796
-1.6 6.84739
-1.5 4.85517
-1.4 1.99521
-1.3 0.87321
-1.2 0.4379
-1.1 0.24717
-1 0.15505
-0.9 0.10786
-0.8 0.08338
-0.7 0.07159
-0.6 0.06783
-0.5 0.07024
-0.4 0.0791
-0.3 0.0978
-0.2 0.13878
-0.1 0.26706
0 0

BERRY FIELD VERSUS ALPHA_Z

ALPHAZ	BERRY_MACHINE	BERRY_ANALYTIC
-8.1	-0.374857	-0.126664
-8	-0.367431	-0.124154
-7.9	-0.359119	-0.121346
-7.8	-0.350052	-0.118282
-7.7	-0.340303	-0.114988
-7.6	-0.329886	-0.111468
-7.5	-0.318762	-0.107709
-7.4	-0.306831	-0.103678
-7.3	-0.293914	-0.0993131
-7.2	-0.279729	-0.0945201
-7.1	-0.263843	-0.0891521
-7	-0.245598	-0.0829873
-6.9	-0.224017	-0.0756949
-6.8	-0.197689	-0.0667988
-6.7	-0.164804	-0.055687
-6.6	-0.123864	-0.0418535
-6.5	-0.076491	-0.0258462
-6.4	-0.032442	-0.0109621
-6.3	-0.0037186	-0.00125651
-6.2	0.0207191	0.00700094
-6.1	0.0566165	0.0191306
-6	0.094334	0.0318753
-5.9	0.123038	0.0415743
-5.8	0.14139	0.0477756
-5.7	0.151813	0.0512974
-5.6	0.156842	0.0529967
-5.5	0.158319	0.0534956
-5.4	0.157456	0.0532043
-5.3	0.155039	0.0523876
-5.2	0.15175	0.0512171
-5.1	0.1474	0.0498063
-5	0.142738	0.048231
-4.9	0.137742	0.0465429
-4.8	0.132518	0.0447777
-4.7	0.12714	0.0429603
-4.6	0.121657	0.0411077
-4.5	0.116104	0.0392312
-4.4	0.1105	0.0373379
-4.3	0.104856	0.0354309
-4.2	0.0991698	0.0335093
-4.1	0.0934265	0.0315687
-4	0.0875974	0.029599
-3.9	0.0816321	0.0275834
-3.8	0.075448	0.0254938
-3.7	0.0689088	0.0232842
-3.6	0.0617839	0.0208767
-3.5	0.0536608	0.0181319

-3.4	0.0437599	0.0147864
-3.3	0.0306386	0.0103527
-3.2	0.0125308	0.00424429
-3.1	-0.00902934	-0.003051
-3	-0.0271471	-0.009173
-2.9	-0.0372808	-0.0125971
-2.8	-0.0409813	-0.0138475
-2.7	-0.0411116	-0.0138916
-2.6	-0.0395178	-0.013353
-2.5	-0.0371417	-0.0125501
-2.4	-0.0344441	-0.0116376
-2.3	-0.0316418	-0.0106917
-2.2	-0.0288602	-0.00975181
-2.1	-0.0261583	-0.00883884
-2	-0.0235717	-0.00796486
-1.95	-0.0223289	-0.0075449
-1.9	-0.0211225	-0.00713726
-1.8	-0.0188257	-0.00636118
-1.7	-0.0166936	-0.00564073
-1.6	-0.0147376	-0.00497981
-1.5	-0.0129704	-0.00438269
-1.4	-0.0114073	-0.0038545
-1.3	-0.0100677	-0.00340187
-1.2	-0.00897789	-0.00303362
-1.1	-0.00817354	-0.00276183
-1	-0.0077045	-0.00260334
-0.9	-0.00764111	-0.00258192
-0.8	-0.00808318	-0.0027313
-0.7	-0.00917073	-0.00309878
-0.6	-0.0110908	-0.00374757
-0.5	-0.0140541	-0.00474888
-0.4	-0.0181472	-0.00613193
-0.3	-0.0227726	-0.00769483
-0.2	-0.0251377	-0.00849398
-0.1	-0.0187488	-0.0063352
0	0	0

VARIATION OF MASS TERM WITH DT

DOUBLY KICKED SYSTEM

ANALYTIC RESULT

1,1 -> alphaz_! = 1, alphaz_2 = 1.

1,1,	1,2	1,3	1,5				
dt	DELTA	dt	DELTA	dt	DELTA	dt	DELTA
2	0.154827	2	8.9183	2	0.0259414	2	0.0548
2.1	0.152127	2.1	7.30525	2.1	0.0274474	2.1	0.05438
2.2	0.14964	2.2	6.41959	2.2	0.0288198	2.2	0.054
2.3	0.14734	2.3	5.84726	2.3	0.0300758	2.3	0.05365
2.4	0.145208	2.4	5.44229	2.4	0.0312295	2.4	0.05333
2.5	0.143226	2.5	5.13853	2.5	0.032293	2.5	0.05303
2.6	0.141378	2.6	4.90119	2.6	0.0332764	2.6	0.05274
2.7	0.139651	2.7	4.71004	2.7	0.0341884	2.7	0.05248
2.8	0.138034	2.8	4.55246	2.8	0.0350366	2.8	0.05224
2.9	0.136516	2.9	4.42011	2.9	0.0358273	2.9	0.05201
3	0.135088	3	4.30724	3	0.0365664	3	0.05179
3.1	0.133744	3.1	4.20975	3.1	0.0372586	3.1	0.05159
3.2	0.132475	3.2	4.12463	3.2	0.0379083	3.2	0.0514
3.3	0.131275	3.3	4.04964	3.3	0.0385192	3.3	0.05122
3.4	0.130139	3.4	3.98302	3.4	0.0390948	3.4	0.05104
3.5	0.129062	3.5	3.92344	3.5	0.0396381	3.5	0.05088
4	0.124419	4	3.69978	4	0.0419525	4	0.05019
4.5	0.12073	4.5	3.55267	4.5	0.043759	4.5	0.04963
5	0.117731	5	3.44831	5	0.0452082	5	0.04919
5.5	0.115243	5.5	3.37035	5.5	0.0463966	5.5	0.04882
6	0.113145	6	3.30986	6	0.0473888	6	0.0485
6.5	0.111353	6.5	3.26152	6.5	0.0482296	6.5	0.04824
7	0.109805	7	3.22201	7	0.0489513	7	0.04801
7.5	0.108453	7.5	3.1891	7.5	0.0495774	7.5	0.04781
8	0.107262	8	3.16126	8	0.0501259	8	0.04763
9	0.105263	9	3.11671	9	0.0510411	9	0.04734
10	0.103649	10	3.08265	10	0.0517743	10	0.0471
11	0.102318	11	3.05575	11	0.0523748	11	0.04691
12	0.101203	12	3.03397	12	0.0528758	12	0.04674
13	0.100255	13	3.01597	13	0.0533	13	0.0466
14	0.0994385	14	3.00085	14	0.0536638	14	0.04648
15	0.0987283	15	2.98796	15	0.0539793	15	0.04638
20	0.0962229	20	2.9444	20	0.0550849	20	0.04601
25	0.0947049	25	2.91935	25	0.0557493	25	0.04579
30	0.0936866	30	2.90308	30	0.0561926	30	0.04565
35	0.092956	35	2.89166	35	0.0565095	35	0.04554
40	0.0924065	40	2.8832	40	0.0567473	40	0.04546
45	0.0919781	45	2.87669	45	0.0569322	45	0.0454
50	0.0916347	50	2.87152	50	0.0570803	50	0.04535
100	0.0900822	100	2.84866	100	0.0577469	100	0.04512
150	0.0895621	150	2.84119	150	0.0579693	150	0.04505
200	0.0893016	200	2.83749	200	0.0580805	200	0.04501
250	0.0891451	250	2.83527	250	0.0581472	250	0.04499
300	0.0890407	300	2.8338	300	0.0581917	300	0.04497

350	0.0889661	350	2.83275	350	0.0582235	350	0.04496
400	0.0889102	400	2.83196	400	0.0582473	400	0.04495
450	0.0888666	450	2.83135	450	0.0582659	450	0.04495
500	0.0888318	500	2.83086	500	0.0582807	500	0.04494
1000	0.0886749	1000	2.82866	1000	0.0583475	1000	0.04492
1500	0.0886226	1500	2.82793	1500	0.0583697	1500	0.04491
2000	0.0885965	2000	2.82757	2000	0.0583809	2000	0.04491
10000	0.0885337	10000	2.82669	10000	0.0584076	10000	0.0449

VARIATION OF MASS TERM WITH DT

DOUBLY KICKED SYSTEM

MACHINE COMPUTED

1,1,	1,2		1,3		1,5		
dt	DELTA	dt	DELTA	dt	DELTA	dt	DELTA
2	0.98871	2	0.9986	2	-0.9969	2	0.99836
2.1	0.98773	2.1	0.99848	2.1	-0.9966	2.1	0.99821
2.2	0.98515	2.2	0.99815	2.2	-0.9959	2.2	0.99783
2.3	0.98143	2.3	0.99768	2.3	-0.9949	2.3	0.99727
2.4	0.9769	2.4	0.99709	2.4	-0.9936	2.4	0.99658
2.5	0.97184	2.5	0.99643	2.5	-0.9921	2.5	0.99581
2.6	0.96643	2.6	0.99571	2.6	-0.9905	2.6	0.99496
2.7	0.96083	2.7	0.99495	2.7	-0.9889	2.7	0.99407
2.8	0.95514	2.8	0.99416	2.8	-0.9872	2.8	0.99316
2.9	0.94945	2.9	0.99337	2.9	-0.9855	2.9	0.99223
3	0.94382	3	0.99256	3	-0.9837	3	0.99129
3.1	0.93828	3.1	0.99176	3.1	-0.982	3.1	0.99036
3.2	0.93286	3.2	0.99096	3.2	-0.9803	3.2	0.98943
3.3	0.92759	3.3	0.99018	3.3	-0.9786	3.3	0.98851
3.4	0.92248	3.4	0.9894	3.4	-0.977	3.4	0.98761
3.5	0.91753	3.5	0.98863	3.5	-0.9753	3.5	0.98672
4	0.89528	4	0.98505	4	-0.9678	4	0.98257
4.5	0.87686	4.5	0.98189	4.5	-0.9613	4.5	0.97892
5	0.86161	5	0.97913	5	-0.9556	5	0.97574
5.5	0.84887	5.5	0.97671	5.5	-0.9508	5.5	0.97297
6	0.83812	6	0.9746	6	-0.9465	6	0.97055
6.5	0.82896	6.5	0.97273	6.5	-0.9428	6.5	0.96841
7	0.82107	7	0.97108	7	-0.9396	7	0.96653
7.5	0.81421	7.5	0.9696	7.5	-0.9367	7.5	0.96485
8	0.8082	8	0.96828	8	-0.9341	8	0.96335
9	0.79818	9	0.96602	9	-0.9297	9	0.96079
10	0.79016	10	0.96415	10	-0.9262	10	0.95867
11	0.78361	11	0.96259	11	-0.9232	11	0.9569
12	0.77816	12	0.96126	12	-0.9207	12	0.95541
13	0.77356	13	0.96012	13	-0.9185	13	0.95412
14	0.76963	14	0.95912	14	-0.9167	14	0.953
15	0.76622	15	0.95825	15	-0.915	15	0.95202
20	0.75435	20	0.95513	20	-0.9093	20	0.94852
25	0.74727	25	0.95321	25	-0.9057	25	0.94637
30	0.74258	30	0.95191	30	-0.9034	30	0.94491
35	0.73923	35	0.95096	35	-0.9017	35	0.94386
40	0.73673	40	0.95025	40	-0.9004	40	0.94307
45	0.73479	45	0.94969	45	-0.8994	45	0.94244
50	0.73324	50	0.94924	50	-0.8985	50	0.94194
100	0.72629	100	0.9472	100	-0.8949	100	0.93967
150	0.72398	150	0.94651	150	-0.8937	150	0.93891
200	0.72283	200	0.94616	200	-0.893	200	0.93852
250	0.72214	250	0.94596	250	-0.8927	250	0.93829
300	0.72168	300	0.94582	300	-0.8924	300	0.93814
350	0.72135	350	0.94572	350	-0.8922	350	0.93803

400	0.7211	400	0.94564	400	-0.8921	400	0.93794
450	0.72091	450	0.94558	450	-0.892	450	0.93788
500	0.72076	500	0.94554	500	-0.8919	500	0.93783
1000	0.72007	1000	0.94533	1000	-0.8916	1000	0.9376
1500	0.71984	1500	0.94526	1500	-0.8914	1500	0.93752
2000	0.71973	2000	0.94522	2000	-0.8914	2000	0.93748
10000	0.71945	10000	0.94514	10000	-0.8912	10000	0.93739

VARIATION OF MASS TERM WITH ALPHAZ

DOUBLY KICKED SYSTEM

ANALYTIC RESULT

alphaz1 = 1, dt alphaz1 = 1, dt = T/3

alphaz2 DELTA alphaz2 DELTA

1	0.15647	1	0.15647
1.1	0.32022	1.1	0.32022
1.2	0.47495	1.2	0.47495
1.3	0.61615	1.3	0.61615
1.4	0.73953	1.4	0.73953
1.5	0.84116	1.5	0.84116
1.6	0.91767	1.6	0.91767
1.7	0.96641	1.7	0.96641
1.8	0.98566	1.8	0.98566
1.9	0.97472	1.9	0.97472
2	0.93399	2	0.93398
2.1	0.86491	2.1	0.86491
2.2	0.7699	2.2	0.7699
2.3	0.65216	2.3	0.65216
2.4	0.51546	2.4	0.51546
2.5	0.36402	2.5	0.36402
2.6	0.2023	2.6	0.2023
2.7	0.03492	2.7	0.03492
2.8	-0.1334	2.8	-0.1334
2.9	-0.2981	2.9	-0.2981
3	-0.4543	3	-0.4543
3.1	-0.5976	3.1	-0.5976
3.2	-0.7237	3.2	-0.7237
3.3	-0.8286	3.3	-0.8286
3.4	-0.9087	3.4	-0.9087
3.5	-0.9614	3.5	-0.9614
4	-0.7844	4	-0.7844
4.5	-0.0582	4.5	-0.0582
5	0.70749	5	0.70749
5.5	0.98076	5.5	0.98075
6	0.55484	6	0.55484
6.5	-0.2533	6.5	-0.2533
7	-0.8892	7	-0.8892
7.5	-0.8968	7.5	-0.8968
8	-0.2702	8	-0.2702
9	0.97875	9	0.97875
10	-0.0407	10	-0.0407
11	-0.9652	11	-0.9652
12	0.34761	12	0.34761
13	0.85033	13	0.85033
14	-0.6207	14	-0.6207
15	-0.6478	15	-0.6478
20	0.98244	20	0.98243
25	-0.7624	25	-0.7624

30	0.12173	30	0.12173
35	0.58371	35	0.58371
40	-0.9719	40	-0.9719
45	0.81202	45	0.81201
50	-0.202	50	-0.202
100	0.89949	100	0.89948
150	0.57333	150	0.57333
200	-0.6574	200	-0.6574
250	-0.8495	250	-0.8495
300	0.30529	300	0.30529
350	0.9799	350	0.97989
400	0.09644	400	0.09644
450	-0.9385	450	-0.9385
500	-0.4826	500	-0.4826
1000	0.50039	1000	0.50039
1500	0.98573	1500	0.98573
2000	0.46466	2000	0.46466
10000	0.60235	10000	0.60235

VARIATION OF MASS TERM WITH ALPHAZ

DOUBLY KICKED SYSTEM

MACHINE COMPUTED

alphaz1 = 1, dt alphaz1 = 1, dt alphaz1 = 1. dt = T/4

alphaz2 DELTA alphaz2 DELTA alphaz2 DELTA

1	0.98871	1	0.94382	1	0.89528
1.1	0.99502	1.1	0.97421	1.1	0.94975
1.2	0.99709	1.2	0.98469	1.2	0.96968
1.3	0.99799	1.3	0.9894	1.3	0.97884
1.4	0.99846	1.4	0.99182	1.4	0.98361
1.5	0.99871	1.5	0.99315	1.5	0.98623
1.6	0.99884	1.6	0.99384	1.6	0.98761
1.7	0.99889	1.7	0.99411	1.7	0.98814
1.8	0.99888	1.8	0.99402	1.8	0.98796
1.9	0.99879	1.9	0.99355	1.9	0.98701
2	0.9986	2	0.99256	2	0.98505
2.1	0.99826	2.1	0.99076	2.1	0.98147
2.2	0.99762	2.2	0.98739	2.2	0.97482
2.3	0.99627	2.3	0.98045	2.3	0.96133
2.4	0.99282	2.4	0.96311	2.4	0.92875
2.5	0.97902	2.5	0.90028	2.5	0.82232
2.6	0.75834	2.6	0.44402	2.6	0.32328
2.7	-0.9291	2.7	-0.7374	2.7	-0.6111
2.8	-0.9869	2.8	-0.9355	2.8	-0.8811
2.9	-0.9945	2.9	-0.9718	2.9	-0.9453
3	-0.9969	3	-0.9837	3	-0.9678
3.1	-0.9979	3.1	-0.9889	3.1	-0.9779
3.2	-0.9984	3.2	-0.9916	3.2	-0.9831
3.3	-0.9987	3.3	-0.993	3.3	-0.986
3.4	-0.9988	3.4	-0.9938	3.4	-0.9875
3.5	-0.9989	3.5	-0.9941	3.5	-0.9881
4	-0.9977	4	-0.988	4	-0.976
4.5	0.89507	4.5	0.65794	4.5	0.52635
5	0.99836	5	0.99129	5	0.98257
5.5	0.99882	5.5	0.99372	5.5	0.98736
6	0.99418	6	0.96984	6	0.94121
6.5	-0.9933	6.5	-0.9658	6.5	-0.9342
7	-0.9988	7	-0.9936	7	-0.9872
7.5	-0.9984	7.5	-0.9916	7.5	-0.9832
8	-0.937	8	-0.7549	8	-0.6255
9	0.99889	9	0.99411	9	0.98815
10	-0.9721	10	-0.8736	10	-0.7846
11	-0.9987	11	-0.9933	11	-0.9865
12	0.99553	12	0.97675	12	0.95454
13	0.99818	13	0.99032	13	0.9806
14	-0.998	14	-0.9895	14	-0.9791
15	-0.9962	15	-0.9801	15	-0.9607
20	0.99883	20	0.99378	20	0.98747
25	-0.9985	25	-0.9922	25	-0.9843
30	0.98578	30	0.93048	30	0.87276

35 0.99495	35 0.9737	35 0.94847
40 -0.9988	40 -0.9935	40 -0.9869
45 0.99865	45 0.99282	45 0.98558
50 -0.9913	50 -0.9562	50 -0.9169
100 0.99844	100 0.99171	100 0.98335
150 0.99777	150 0.98825	150 0.9766
200 -0.9964	200 -0.9809	200 -0.9621
250 -0.9987	250 -0.9932	250 -0.9864
300 0.96093	300 0.83077	300 0.72123
350 0.99889	350 0.99411	350 0.98814
400 0.98286	400 0.91763	400 0.85177
450 -0.9986	450 -0.9927	450 -0.9853
500 -0.9972	500 -0.985	500 -0.9703
1000 0.99218	1000 0.95996	1000 0.923
1500 0.99888	1500 0.99402	1500 0.98795
2000 0.99699	2000 0.98422	2000 0.96877
10000 0.99537	10000 0.97583	10000 0.95251

Appendix C

Mathematica Notebooks

The following pages contain the Mathematica notebooks which were used for simulating and visualizing the singly and doubly kicked Graphene system. The following files are appended and their descriptions are given for the sake of clarity.

`band.nb` Probably the most basic notebook in the series. Shows how the basic Graphene band structure can be computed and plotted.

`singly-kicked.nb` The main script for the singly kicked Graphene system, from the $\hat{k} \cdot \vec{\sigma}$ to the Chern number.

`doubly-kicked-1.nb` The main script for the doubly kicked Graphene system, in the $(AB)(CD)$ style parenthesizing. This is computationally superior to the next script.

`doubly-kicked-2.nb` The main script for the doubly kicked Graphene system, in the $(A(B(C(D))))$ style of parenthesizing. Slower than the previous script.

```

In[28024]:= M1 = 3 a/2 * {1, 1/Sqrt[3]}
M2 = 3 a/2 * {1, -1/Sqrt[3]}
G[x_, y_] = 1 + Cos[{x, y}.M1] + Cos[{x, y}.M2]
H[x_, y_] = Sin[{x, y}.M1] + Sin[{x, y}.M2]
e0[x_, y_] = -gamma * Simplify[Sqrt[G[x, y]^2 + H[x, y]^2]]
Plot3D[{e0[x, y], -e0[x, y]}, {x, -6 Pi, 6 Pi}, {y, -6 Pi, 6 Pi}]

Out[28024]= {0.21, 0.121244}

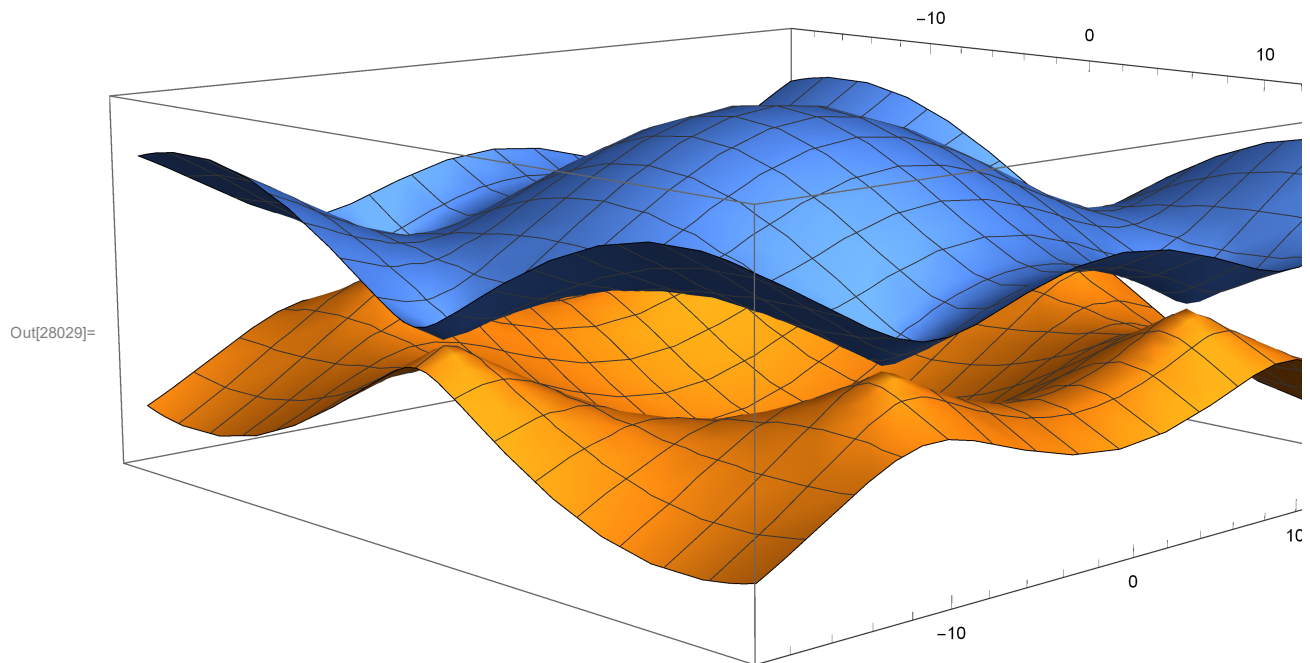
Out[28025]= {0.21, -0.121244}

Out[28026]= 1 + Cos[0.21 x - 0.121244 y] + Cos[0.21 x + 0.121244 y]

Out[28027]= Sin[0.21 x - 0.121244 y] + Sin[0.21 x + 0.121244 y]

Out[28028]= -2.8 Sqrt[3 + 4 Cos[(0.21 + 0. I) x] Cos[(0.121244 + 0. I) y] +
2 Cos[(0.121244 + 0. I) y]^2 - 2 Sin[(0.121244 + 0. I) y]^2]

```



```

In[1]:= a = 0.14;
k = {k_x, k_y};
M1 = 3 a/2 * {1, 1/Sqrt[3]};
M2 = 3 a/2 * {1, -1/Sqrt[3]};
SZ = {{1, 0}, {0, -1}};
SX = {{0, 1}, {1, 0}};
SY = {{0, -I}, {I, 0}};

H0[{x_, y_}] := {{0, 1 + Exp[I x y].M1} + Exp[I x y].M2},
{1 + Exp[I x y].M1} + Exp[I x y].M2, 0}};

G[{x_, y_}] = 1 + Cos[{x, y}.M1] + Cos[{x, y}.M2];
H[{x_, y_}] = Sin[{x, y}.M1] + Sin[{x, y}.M2];

h0[{x_, y_}] = -gamma * (G[{x, y}].SX - H[{x, y}].SY);
e0[{x_, y_}] = Simplify[gamma * Sqrt[G[{x, y}]^2 + H[{x, y}]^2]];

gamma = 2.8;
t0 = 1/gamma;

alpha = {alphax, alphay, alphaz};
alphax = 0;
alphay = 0;
alphaz = Sqrt[3];
sigma = {SX, SY, SZ};
beta[{x_, y_}] = {G[{x, y}], -H[{x, y}], 0};
n = alpha/Sqrt[alpha.alphaz];
m[{x_, y_}] = beta[{x, y}]/Sqrt[beta[{x, y}].beta[{x, y}]];
a1 = -Sqrt[alpha.alphaz];
b[{x_, y_}] = e0[{x, y}] * t0;

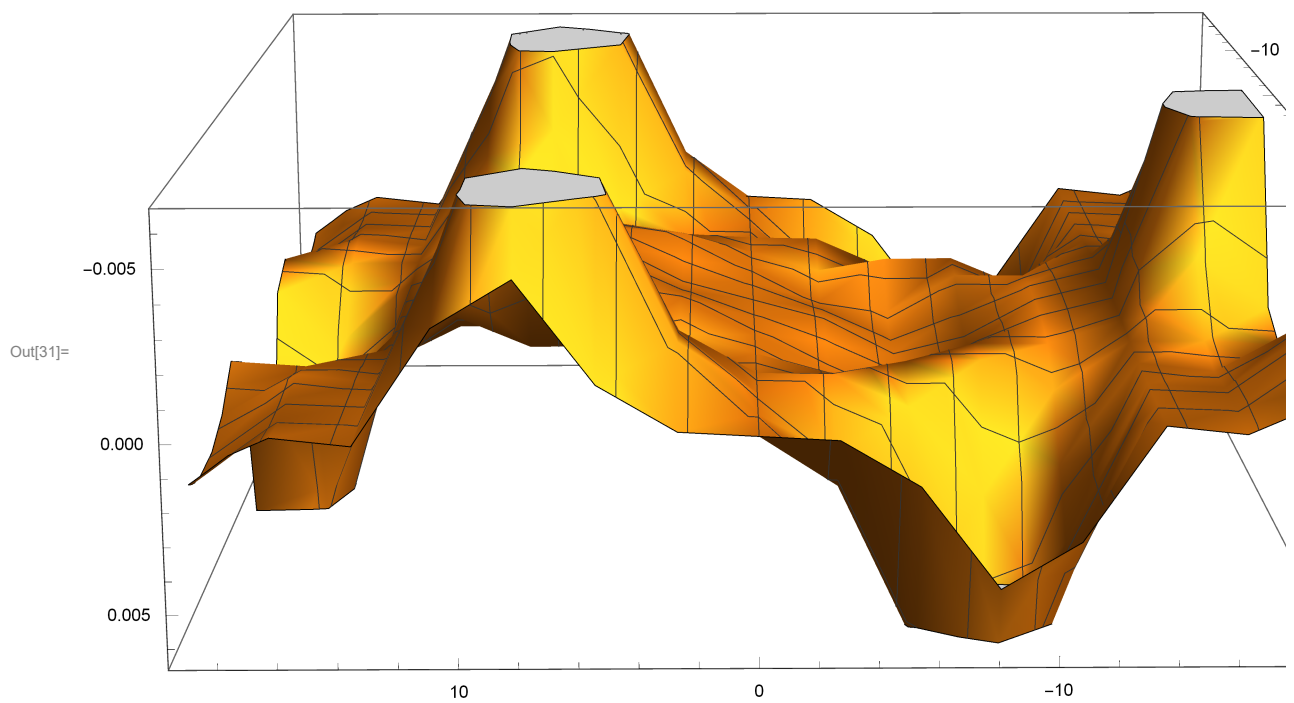
c[{x_, y_}] =
ArcCos[Cos[a1] * Cos[b[{x, y}]] - (n.m[{x, y}]) * Sin[a1] * Sin[b[{x, y}]]];
khat[{x_, y_}] = (1/Sin[c[{x, y}]]) *
((Sin[a1] * Cos[b[{x, y}]]) * n + (Sin[b[{x, y}]] * Cos[a1]) * m[{x, y}] -
(Sin[a1] * Sin[b[{x, y}]])) * Cross[n, m[{x, y}]]);

HXYZ[{x_, y_}] = -c[{x, y}]/t0 * (khat[{x, y}].sigma);
Eigenvalues[FullSimplify[HXYZ[{x, y}]]]
rho[{x_, y_}] = (1 - khat[{x, y}].sigma)/2;
BerryTensor[{x_, y_}] =
(1/(2*I)) * Tr[rho[{x, y}] * (D[rho[{x, y}], x].D[rho[{x, y}], y] -
D[rho[{x, y}], y].D[rho[{x, y}], x])];

```

```
Plot3D[BerryTensor[{x, y}], {x, -6*Pi, 6*Pi}, {y, -6*Pi, 6*Pi}]  
  
(NIntegrate[TransformedField["Cartesian" → "Polar", BerryTensor[{x, y}],  
{x, y} → {r, θ}], {r, 0, 15}, {θ, 0, 2*Pi}, AccuracyGoal → 6] / (2*Pi)  
(* NIntegrate[BerryTensor[{x,y}],{x,-6*Pi,6*Pi},{y,-6*Pi,6*Pi}] *)
```

$$\begin{aligned}
\text{Out}[28]= & \left\{ - \left(1. \text{ArcCos} \left[\frac{\cos[\sqrt{3}] \cos[1. \sqrt{3 + 4 \cos[0.21 x] \cos[0.121244 y]} + 2 \cos[0.242487 y]]}{\sqrt{(22.9137 \cos[1. \sqrt{3 + 4 \cos[0.21 x] \cos[0.121244 y]} + 2 \cos[0.242487 y])^2 + 30.5516 \cos[0.21 x] \cos[0.121244 y]}} \right. \right. \right. \\
& \left. \left. \left. \cos[1. \sqrt{3 + 4 \cos[0.21 x] \cos[0.121244 y]} + 2 \cos[0.242487 y]]^2 + 15.2758 \cos[0.242487 y] \cos[1. \sqrt{3 + 4 \cos[0.21 x] \cos[0.121244 y]} + 2 \cos[0.242487 y]]^2 + 7.84 \sin[1. \sqrt{3 + 4 \cos[0.21 x] \cos[0.121244 y]} + 2 \cos[0.242487 y]]^2 + 31.36 \cos[0.21 x] \cos[0.121244 y] \sin[1. \sqrt{3 + 4 \cos[0.21 x] \cos[0.121244 y]} + 2 \cos[0.242487 y]]^2 + 31.36 \cos[0.21 x]^2 \cos[0.121244 y]^2 \sin[1. \sqrt{3 + 4 \cos[0.21 x] \cos[0.121244 y]} + 2 \cos[0.242487 y]]^2 + 31.36 \cos[0.121244 y]^2 \sin[0.21 x]^2 \sin[1. \sqrt{3 + 4 \cos[0.21 x] \cos[0.121244 y]} + 2 \cos[0.242487 y]]^2 \right) \right) \right. \\
& \left. \left(\sqrt{3 + 4 \cos[0.21 x] \cos[0.121244 y]} + 2 \cos[0.242487 y] \right)^2 \right. \\
& \left. \left. \left(\sqrt{1 - \cos[\sqrt{3}]^2} \cos[1. \sqrt{3 + 4 \cos[0.21 x] \cos[0.121244 y]} + 2 \cos[0.242487 y]]^2 \right. \right. \right. \\
& \left. \left. \left. \right), \left(1. \text{ArcCos} [\cos[\sqrt{3}] \cos[1. \sqrt{3 + 4 \cos[0.21 x] \cos[0.121244 y]} + 2 \cos[0.242487 y]]] \right. \right. \right. \\
& \left. \left. \left. \sqrt{(22.9137 \cos[1. \sqrt{3 + 4 \cos[0.21 x] \cos[0.121244 y]} + 2 \cos[0.242487 y])^2 + 30.5516 \cos[0.21 x] \cos[0.121244 y]}} \right. \right. \right. \\
& \left. \left. \left. \cos[1. \sqrt{3 + 4 \cos[0.21 x] \cos[0.121244 y]} + 2 \cos[0.242487 y]]^2 + 15.2758 \cos[0.242487 y] \cos[1. \sqrt{3 + 4 \cos[0.21 x] \cos[0.121244 y]} + 2 \cos[0.242487 y]]^2 + 7.84 \sin[1. \sqrt{3 + 4 \cos[0.21 x] \cos[0.121244 y]} + 2 \cos[0.242487 y]]^2 + 31.36 \cos[0.21 x] \cos[0.121244 y] \sin[1. \sqrt{3 + 4 \cos[0.21 x] \cos[0.121244 y]} + 2 \cos[0.242487 y]]^2 + 31.36 \cos[0.21 x]^2 \cos[0.121244 y]^2 \sin[1. \sqrt{3 + 4 \cos[0.21 x] \cos[0.121244 y]} + 2 \cos[0.242487 y]]^2 + 31.36 \cos[0.121244 y]^2 \sin[0.21 x]^2 \sin[1. \sqrt{3 + 4 \cos[0.21 x] \cos[0.121244 y]} + 2 \cos[0.242487 y]]^2 \right) \right) \right) \right. \\
& \left. \left(\sqrt{3 + 4 \cos[0.21 x] \cos[0.121244 y]} + 2 \cos[0.242487 y] \right)^2 \right) \}
\end{aligned}$$



Out[32]= $1.36373 \times 10^{-17} + 0.$ i

In[33]:=

In[34]:=

In[35]:=

In[36]:=

In[37]:=

In[38]:=

In[39]:=

```

a = 0.14;
k = {k_x, k_y};
M1 = 3 a/2 * {1, 1/Sqrt[3]};
M2 = 3 a/2 * {1, -1/Sqrt[3]};
SZ = {{1, 0}, {0, -1}};
SX = {{0, 1}, {1, 0}};
SY = {{0, -I}, {I, 0}};

H0[{x_, y_}] := {{0, 1 + Exp[I x y].M1} + Exp[I x y].M2},
{1 + Exp[I x y].M1} + Exp[I x y].M2, 0}};

G[{x_, y_}] = 1 + Cos[{x, y}.M1] + Cos[{x, y}.M2];
H[{x_, y_}] = Sin[{x, y}.M1] + Sin[{x, y}.M2];

h0[{x_, y_}] = -gamma * (G[{x, y}].SX - H[{x, y}].SY);
e0[{x_, y_}] = Simplify[gamma * Sqrt[G[{x, y}]^2 + H[{x, y}]^2]];

gamma = 2.8;
t0 = 1/gamma;
dt = 1/(2.55*gamma);
sigma = {SX, SY, SZ};
alphax1 = 0;
alphay1 = 0;
alphaz1 = Sqrt[3];
alphax2 = 0;
alphay2 = 0;
alphaz2 = 3 Sqrt[3];
alpha1 = {alphax1, alphay1, alphaz1};
alpha2 = {alphax2, alphay2, alphaz2};
A1 = -Sqrt[alpha1.alpha1];
A2 = -Sqrt[alpha2.alpha2];
N1 = alpha1/(-A1);
N2 = alpha2/(-A2);
B1[{x_, y_}] = e0[{x, y}] * (t0 - dt);
B2[{x_, y_}] = e0[{x, y}] * dt;
beta[{x_, y_}] = {G[{x, y}], -H[{x, y}], 0};
m[{x_, y_}] = beta[{x, y}]/Sqrt[beta[{x, y}].beta[{x, y}]];
C2[{x_, y_}] =
ArcCos[Cos[A2]*Cos[B2[{x, y}]] - (N2.m[{x, y}])*Sin[A2]*Sin[B2[{x, y}]]];
khat2[{x_, y_}] = (1/Sin[C2[{x, y}]])*(Sin[A2]*Cos[B2[{x, y}]]*N2 +
Sin[B2[{x, y}]]*Cos[A2]*m[{x, y}] -
Sin[A2]*Sin[B2[{x, y}]]*Cross[N2, m[{x, y}]]);

C1[{x_, y_}] = ArcCos[Cos[A1]*Cos[B1[{x, y}]] -

```

```

(N1.m[{x, y}]) * Sin[A1] * Sin[B1[{x, y}]]];
khat1[{x_, y_}] = (1/Sin[C1[{x, y}]]) * (Sin[A1] * Cos[B1[{x, y}]] * N1 +
Sin[B1[{x, y}]] * Cos[A1] * m[{x, y}] -
Sin[A1] * Sin[B1[{x, y}]] * Cross[N1, m[{x, y}]]) ;

C0[{x_, y_}] = ArcCos[Cos[C2[{x, y}]] * Cos[C1[{x, y}]] - 
(khat2[{x, y}].khat1[{x, y}]) * Sin[C2[{x, y}]] * Sin[C1[{x, y}]]];
khat[{x_, y_}] = 1/(Sin[C0[{x, y}]]) * (Sin[C2[{x, y}]] * Cos[C1[{x, y}]] *
khat2[{x, y}] + Sin[C1[{x, y}]] * Cos[C2[{x, y}]] * khat1[{x, y}] - 
Sin[C2[{x, y}]] * Sin[C1[{x, y}]] * Cross[khat2[{x, y}], khat1[{x, y}]]);

HXYZ[{x_, y_}] = -C0[{x, y}] / t0 * (khat[{x, y}].sigma);
Simplify[HXYZ[{1, 1}]];
Eigenvalues[FullSimplify[HXYZ[{4.5, 4.5}]]];
rho[{x_, y_}] = (1 - khat[{x, y}].sigma) / 2;
BerryTensor[{x_, y_}] =
(1/(2*ii)) * Tr[rho[{x, y}] * (D[rho[{x, y}], x].D[rho[{x, y}], y] -
D[rho[{x, y}], y].D[rho[{x, y}], x])];
Plot3D[BerryTensor[{x, y}], {x, -6*Pi, 6*Pi}, {y, -6*Pi, 6*Pi}]

```

$\{ \{ 0.691184 + 0.i, -1.65623 + 0.681278 i \}, \{ -1.65623 - 0.681278 i, -0.691184 + 0.i \} \}$
 $\{ -1.74102, 1.74102 \}$

```

a = 0.14;
k = {k_x, k_y};
M1 = 3 a/2 * {1, 1/\sqrt{3}};
M2 = 3 a/2 * {1, -1/\sqrt{3}};
SZ = {{1, 0}, {0, -1}};
SX = {{0, 1}, {1, 0}};
SY = {{0, -i}, {i, 0}};

H0[{x_, y_}] := {{0, 1 + Exp[i * {x, y}.M1] + Exp[i * {x, y}.M2]}, 
{1 + Exp[i * {x, y}.M1] + Exp[i * {x, y}.M2], 0}};

G[{x_, y_}] = 1 + Cos[{x, y}.M1] + Cos[{x, y}.M2];
H[{x_, y_}] = Sin[{x, y}.M1] + Sin[{x, y}.M2];

h0[{x_, y_}] = -gamma * (G[{x, y}].SX - H[{x, y}].SY);
e0[{x_, y_}] = Simplify[gamma * Sqrt[G[{x, y}]^2 + H[{x, y}]^2]];

gamma = 2.8;
t0 = 1/gamma;
dt = 1/(1.5 * gamma) These
sigma = {SX, SY, SZ};
alphax1 = 0;
alphay1 = 0;
alphaz1 = \sqrt{3};
alphax2 = 0;
alphay2 = 0;
alphaz2 = \sqrt{3};
alpha1 = {alphax1, alphay1, alphaz1};
alpha2 = {alphax2, alphay2, alphaz2};
A1 = -Sqrt[alpha1.alpha1];
A2 = -Sqrt[alpha2.alpha2];
N1 = alpha1 / (-A1);
N2 = alpha2 / (-A2);
B1[{x_, y_}] = -e0[{x, y}] * (t0 - dt);
B2[{x_, y_}] = -e0[{x, y}] * dt;
beta[{x_, y_}] = {G[{x, y}], -H[{x, y}], 0};
m[{x_, y_}] = beta[{x, y}] / Sqrt[beta[{x, y}].beta[{x, y}]];
C1[{x_, y_}] = Simplify[
ArcCos[Cos[A1] * Cos[B1[{x, y}]] - (N1.m[{x, y}]) * Sin[A1] * Sin[B1[{x, y}]]]];
khat1[{x_, y_}] = Simplify[(1/Sin[C1[{x, y}])] *
(Sin[A1] * Cos[B1[{x, y}]] * N1 + Sin[B1[{x, y}]] * Cos[A1] * m[{x, y}] -
Sin[A1] * Sin[B1[{x, y}]] * Cross[N1, m[{x, y}]])];
C2[{x_, y_}] = Simplify[ArcCos[Cos[B2[{x, y}]] * Cos[C1[{x, y}]] -
m[{x, y}].khat1[{x, y}] * Sin[B2[{x, y}]] * Sin[C1[{x, y}]]];
khat2[{x_, y_}] = Simplify[(1/Sin[C2[{x, y}])] *

```

```

(sin[B2[{x, y}]] * Cos[C1[{x, y}]] * m[{x, y}] +
 Sin[C1[{x, y}]] * Cos[B2[{x, y}]] * khat1[{x, y}] -
 Cross[m[{x, y}], khat1[{x, y}]] * Sin[B2[{x, y}]] * Sin[C1[{x, y}]]);

C3[{x_, y_}] = Simplify[ArcCos[Cos[A2] * Cos[C2[{x, y}]]] -
 N2.khat2[{x, y}] * Sin[A2] * Sin[C2[{x, y}]]];

khat3[{x_, y_}] = Simplify[(1 / Sin[C3[{x, y}]]) *
 (sin[A2] * Cos[C2[{x, y}]] * N2 + Sin[C2[{x, y}]] * Cos[A2] * khat2[{x, y}] -
 Cross[N2, khat2[{x, y}]] * Sin[A2] * Sin[C2[{x, y}]]);

HXYZ[{x_, y_}] = -C3[{x, y}] / t0 * (khat3[{x, y}].sigma);

Eigenvalues[FullSimplify[HXYZ[{x, y}]]]

rho[{x_, y_}] = (1 - khat3[{x, y}].sigma) / 2;

BerryTensor[{x_, y_}] = (1 / (2 * i)) * Tr[rho[{x, y}] * (D[rho[{x, y}], x] *
 D[rho[{x, y}], y] - D[rho[{x, y}], y].D[rho[{x, y}], x])];

Plot3D[BerryTensor[{x, y}], {x, -6 * Pi, 6 * Pi}, {y, -6 * Pi, 6 * Pi}]

```

Bibliography

The bibliography is alphabetically sorted and indexed. It enables for easier searching of the occurrence of the reference in the text of the thesis. All one has to do is Ctrl+F along with the search term and your PDF reader should navigate you further.

- AGA** Adhip Agarwala, Utso Bhattacharya, Amit Dutta, and Diptiman Sen, *Effects of periodic kicking on dispersion and wave packet dynamics in Graphene*, Phys. Rev. B 93, 174301, May 2016.
- AHA** Yakir Aharonov, David Bohm, *Significance of Electromagnetic Potentials in the Quantum Theory*, Phys. Rev. 115, 1959.
- AHA1** Y. Aharonov, J. Anandan, *Phase Change During A Cyclic Quantum Evolution*, Phys. Rev. Lett. 58, 1987, pp. 1593-1596.
- ARM** M. A. Armstrong, *Basic Topology*, pp. 8, Undergraduate Texts In Mathematics, Springer, 1983.
- BAR** Valentin Bargmann, *Note on Wigner's Theorem on Symmetry Operations*, Journal on Mathematical Physics, Vol. 5, No. 7, July 1964.
- BER** Michael V. Berry, *The Adiabatic Phase and Pancharatnam's Phase for Polarized Light*, J. Mod. Optics 34, 1987, pp. 1401-1407.
- COL** Sidney R. Coleman, *There are no Goldstone bosons in two dimensions*, Comm. Math. Phys., 31, 259, 1973.
- CHE** Shiing-Shen Chern, *A Simple Intrinsic Proof Of The Gauss-Bonnet Formula For Closed Riemann Manifolds*, Annals Of Mathematics, Vol. 45, No. 4, October 1944.
- DAL** J. Dalibard, N. Goldman, *Periodically Driven Quantum Systems : Effective Hamiltonians and Engineered Gauge Fields*, arXiv: 1404.4373v2, May 2014.

BIBLIOGRAPHY

- ECK** Andre Eckardt, E. Anisimovas, *High Frequency Approximation for Periodically Driven Quantum Systems from a Floquet space perspective*, New. J. Phys 17, 2015, 093039.
- FEY** Richard Feynman, Robert Leighton, *The Feynman Lectures On Physics: Vol III*, Chapter 13, Pearson India, 2011.
- GAU** Carl Friedrich Gauss, *Disquisitiones generales circa superficies curvas*, Typis Dieterichianis, 1828.
- GEI** Andre K Geim, Konstantin S Novoselov, *The Rise Of Graphene*, Nature Materials, 6, pp. 183-191, 2007.
- HAZ** Michiel Hazewinkel ed., *Encyclopedia of Mathematics*, Springer, 2001.
- HOH** Pierre C. Hohenberg, *Existence Of Long Range Order In One and Two Dimensions*, Phys. Rev. Lett., 158, 383, 1967.
- KOB** Shoshichi Kobayashi, Katsumi Nomizu, *Foundations Of Differential Geometry*, John Wiley and Sons, 1996.
- LAK** Imre Lakatos, *Proofs and Refutations: The Logic Of Mathematical Discovery*, Cambridge Univeristy Press, 1976.
- LEG** Anthony J. Leggett, *Graphene: Electronic Band Structures and Dirac Fermions*, Selected Topics in Condensed Matter Physics, Univ. Of Waterloo, 2010.
- LEO** Francois Leonard, *Physics Of Carbon Nanotube Devices*, Elsevier, September 2008.
- MER** N. David Mermin, Herbert Wagner, *Absence of Ferromagnetism or Antiferromagnetism in One or Two-Dimensional Isotropic Heisenberg Models*, Phys. Rev. Lett. 17, 1966, pp. 1133-1136.
- MUK** Narasimhiengar Mukunda, *Geometric Phases*, Lecture series at IISER, Mohali, February 2015.
- PAN** S. Pancharatnam, *Generalized Theory Of Interference and its Applications*, Collected Works of S. Pancharatnam, Oxford University Press, UK, 1975.
- SAM** J. Samuel, R. Bhandari, *General Setting for Berry's Phase*, Phys. Rev. Lett. 60, 1988, pp. 2339-2342.
- SIM** B. Simon, *Holonomy, the Quantum Adiabatic Theorem, and Berry's Phase*, Phys. Rev. Lett. 51, 1983, pp. 2167-2170.
- SHA** Rajath Shashidhara, *Hall conductivity of Aubry-André system driven by rapidly oscillating magnetic field*, Unpublished Master Thesis at BITS Pilani, 2016.
- SHI** Jon H. Shirley, *Solution Of The Schrodinger Equation With A Hamiltonian Periodic In Time*, Phys. Rev. 138, 4B, May 1965.

SPI Michael Spivak, *A Comprehensive Introduction To Differential Geometry, Vols: I-V*, Publish Or Perish Incorporated, 1975.

STR Dirk Struik, *Lectures On Classical Differential Geometry*, 2nd Edition, Dover Publications, New York, 1988.

TGS Tapomoy G. Sarkar, J. N. Bandyopadhyay, Tridev Mishra, *Effective Time Independent Analysis for Floquet Systems*, Unpublished note, August 2014.

TON David Tong, *Lectures On The Quantum Hall Effect*, TIFR Bombay Infosys Lectures, January 2016.

WAL P. R. Wallace, *The Band Theory Of Graphite*, Phys. Rev. 71, 622, May 1947.